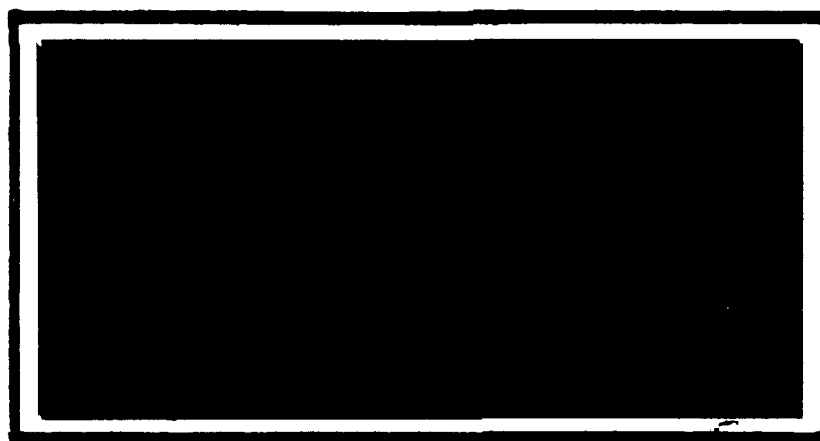


AD-A230 459



DTIC
S ELECTE D
JAN 09 1991
E

DEPARTMENT OF THE AIR FORCE
AIR UNIVERSITY

AIR FORCE INSTITUTE OF TECHNOLOGY

Wright-Patterson Air Force Base, Ohio

DISTRIBUTION STATEMENT A

Approved for public release
Distribution Unlimited

91 1 3 088

AFIT/GAE/ENY/90D-3

EFFECTS OF SPECIFIC HEAT RATIO ON A
SIMULATED CHEMICAL LASER CAVITY FLOW

THESIS

Curt DeWayne Botts, Captain, USAF

AFIT/GAE/ENY/90D-3



Approved for public release; distribution unlimited

**EFFECTS OF SPECIFIC HEAT RATIO ON A
SIMULATED CHEMICAL LASER CAVITY FLOW**

THESIS

Presented to the Faculty of the School of Engineering
of the Air Force Institute of Technology

Air University

In Partial Fulfillment of the
Requirements for the Degree of

Master of Science in Aeronautical Engineering

Curt DeWayne Botts, B.S.

Captain, USAF

December 1990

Accession For	
NTIS GRA&I	<input checked="checked" type="checkbox"/>
DTIC TAB	<input type="checkbox"/>
Unannounced	<input type="checkbox"/>
Justification	
By _____	
Distribution/	
Availability Codes	
Dist	Avail and/or Special
A-1	

Approved for public release; distribution unlimited



Table of Contents

	Page
Acknowledgements	ii
List of Figures	iii
List of Tables	vii
List of Symbols	viii
Abstract	x
I. Introduction	1-1
Background	1-1
Scope	1-3
II. Theory	2-1
Mixture Specific Heat Ratio	2-1
Nozzle Flow	2-3
III. Experimental Apparatus	3-1
Flow System	3-1
Compressed Air System	3-1
Orifice Meter	3-2
Horizontal Stilling Chamber	3-2
Helium Supply System	3-2
Venturi Flow Meter	3-5
Mixer	3-5
Variable Supersonic Diffuser	3-7
Vacuum System	3-8
Nozzle/Cavity Test Section	3-9
Data Acquisition System	3-12
Piezoresistive Pressure Transducers	3-12
Signal Conditioning Units/Power Supplies	3-15
Nicolet System 500	3-16
Schlieren Optical System	3-17

	Page
IV. Experimental Procedures	4-1
Pressure Transducer Calibration	4-1
Schlieren Photographic Techniques	4-2
Data Acquisition and Reduction	4-2
V. Results and Discussion	5-1
Test Equipment Performance	5-1
Schlieren Photography Observations	5-3
Pressure Data Analysis	5-7
VI. Conclusions	6-1
VII. Recommendations	7-1
Appendix A. Pressure Transducer Calibration Curves . .	A-1
Appendix B. Data Acquisition Software	B-1
Bibliography	BIB-1
Vita	VITA-1

Acknowledgements

I would like to express my appreciation to the many people who were very much a part of this endeavor.

Many, many thanks to Dr. W. C. Elrod my thesis advisor and mentor for this research. Also, thanks to the other members of my thesis committee, Drs. Franke and King, for their scrutiny of my project.

Quite a few people have been added to my will since this experimental investigation began. Probably the most deserving of my worldly goods are the technicians in the AFIT/ENY laboratories. Andy Pitts, Mark Derriso, and Jay Anderson made this blind man see many things and lugged a lot of helium to and fro. My thanks also to the leader of their pack, Nick Yardich, who made it possible to use the new Nicolet 500 Data Acquisition System (just in the Nick of time).

Probably my strongest supporters were my family. My phenomenal wife Nancy and our three beautiful children (see Vita for names) kept me sane when I thought the nut was about to crack and kept the whole knowledge gainin' thing in perspective.

Last, but not least, my thanks to Jean-Michel Jarre, Ollie Roberts, Four Who Dared, Bach, and Tchaikovsky whose music inspired words when the words wouldn't surface.

Curt D. Botts

List of Figures

Figure	Page
1.1. Source Flow Chemical Laser Concept (3.1)	1-2
3.1 Flow System Layout	3-3
3.2 Helium Flow Control Nozzle	3-4
3.3 Air/Helium Mixer Design	3-6
3.4 Supersonic Diffuser, Top View	3-8
3.5 Nozzle Segment	3-10
3.6 Test Section Nozzle Configuration	3-11
3.7 Data Acquisition System	3-13
3.8 Test Section Transducer Tap Locations	3-16
3.9 Schlieren Optical System	3-18
4.1 Data Acquisition Procedures	4-3
5.1 Schematic of Cavity Flow at Approximately 2 Seconds	5-4
5.2 Cavity Flow Dynamics from High Speed Film	5-6
5.3 Specific Heat Ratios vs Time for Various P_{He} Values	5-9
5.4 Nozzle Exit Mach Numbers for Various P_{He} Values	5-10
5.5 Experimental and Theoretical Nozzle Exit Mach Number Comparison	5-11
5.6 Horizontal Stilling Chamber Pressure vs Time for Various P_{He} Settings	5-13
5.7 Cavity Pressures vs Time for Run 029 ($P_{He}=350$ psig, $\gamma \approx 1.58$)	5-14
5.8 Cavity Pressures vs Time for Run 020 ($P_{He}=0$, Air Only, $\gamma \approx 1.4$)	5-15

Figure	Page
5.9 Cavity Pressures vs Time for Run 034 ($P_{He}=0$, Air Only, $\gamma \approx 1.4$, No Mixer)	5-16
5.10 Cavity Pressures vs Time for Run 023 ($P_{He}=175$ psig, $\gamma \approx 1.48$)	5-17
5.11 Cavity Pressures vs Time for Run 024 ($P_{He}=200$ psig, $\gamma \approx 1.51$)	5-18
5.12 Cavity Pressures vs Time for Run 025 ($P_{He}=225$ psig, $\gamma \approx 1.54$)	5-19
5.13 Cavity Pressures vs Time for Run 027 ($P_{He}=275$ psig, $\gamma \approx 1.56$)	5-20
5.14 Cavity Pressures vs Time for Run 035 ($P_{He}=225$ psig, No Mixer)	5-20
5.15 Specific Heat Ratio Comparison	5-22
5.16 Air and Helium Mass Flow Rates	5-23
5.17 Helium Venturi Meter Differential Pressures	5-24
5.18 Position 1 Pressure History for Various P_{He} Values	5-27
5.19 Position 2 Pressure History for Various P_{He} Values	5-27
5.20 Position 3 Pressure History for Various P_{He} Values	5-28
5.21 Position 17 Pressure History for Various P_{He} Values	5-28
5.22 Position 18 Pressure History for Various P_{He} Values	5-29
5.23 Position 14 Pressure History for Various P_{He} Values	5-30
5.24 Position 15 Pressure History for Various P_{He} Values	5-30
5.25 Position 16 Pressure History for Various P_{He} Values	5-31

Figure	Page
5.26 Position 11 Pressure History for Various P_{He} Values	5-33
5.27 Position 12 Pressure History for Various P_{He} Values	5-33
5.28 Position 13 Pressure History for Various P_{He} Values	5-34
5.29 Position 9 Pressure History for Various P_{He} Values	5-34
5.30 Position 10 Pressure History for Various P_{He} Values	5-35
5.31 Cavity Mach Number Comparison with Mixer Installed	5-36
5.32 Cavity Mach Number Comparison sans Mixer	5-36
A.1 Calibration Curve for Pressure Transducer Serial Number PP81	A-1
A.2 Calibration Curve for Pressure Transducer Serial Number 78HB	A-2
A.3 Calibration Curve for Pressure Transducer Serial Number 79HB	A-2
A.4 Calibration Curve for Pressure Transducer Serial Number 89TA	A-3
A.5 Calibration Curve for Pressure Transducer Serial Number 23LG	A-3
A.6 Calibration Curve for Pressure Transducer Serial Number 74BF	A-4
A.7 Calibration Curve for Pressure Transducer Serial Number PP67	A-4
A.8 Calibration Curve for Pressure Transducer Serial Number 83BF	A-5
A.9 Calibration Curve for Pressure Transducer Serial Number HE99	A-5

Figure	Page
A.10 Calibration Curve for Pressure Transducer Serial Number 75BF	A-6
A.11 Calibration Curve for Pressure Transducer Serial Number 92BF	A-6
A.12 Calibration Curve for Pressure Transducer Serial Number KL52	A-7
A.13 Calibration Curve for Pressure Transducer Serial Number 97BF	A-7
A.14 Calibration Curve for Pressure Transducer Serial Number 79BF	A-8
A.15 Calibration Curve for Pressure Transducer Serial Number MO38	A-8
A.16 Calibration Curve for Pressure Transducer Serial Number TCPT69-25	A-9
A.17 Calibration Curve for Pressure Transducer Serial Number 1472	A-9
A.18 Calibration Curve for Pressure Transducer Serial Number 63DL	A-10
A.19 Calibration Curve for Pressure Transducer Serial Number 43YB	A-10

List of Tables

Table	Page
2.1 Specific Heat Values	2-1
3.1 Nozzle Contour Coordinates	3-10
3.2 Nozzle Design Parameters	3-11
3.3 Transducer/Thermocouple Locations	3-14
5.1 Run Numbers and Operating Conditions	5-7

List Of Symbols

<u>Symbol</u>	<u>Definition</u>
AFWL	Air Force Weapons Laboratory
c_p	specific heat at constant pressure
c_v	specific heat at constant volume
DAS	Data Acquisition System
DAU	Data Acquisition Unit
GPIB	General Purpose Interface Bus
h	characteristic height
\dot{m}_{air}	air mass flow rate
\dot{m}_{He}	helium mass flow rate
\dot{m}_{mix}	mass flow rate of air-helium mixture
M	Mach number
P, p	pressure
psia	pounds per square inch, absolute
psid	pounds per square inch, differential
psig	pounds per square inch, guage
P_{He}	injection pressure of helium supply
Re	Reynolds number
SCFM	standard cubic feet per minute
SCU	signal conditioning unit
T	temperature
t	time

SymbolDefinition

V	velocity
δ	boundary layer thickness
ϵ	area ratio (A_e/A_t)
γ	ratio of specific heats
ν	kinematic viscosity

Subscripts

0	stagnation value
1,2,3,4,...	conditions at a position
e	exit conditions

Abstract

Mixing of primary cold flow air and secondary helium to control the ratio of specific heats for the medium flowing through a simulated chemical laser nozzle/lasing cavity was accomplished. The effects of a range of mixture specific heat ratios on flowfield behavior were examined using static pressure ports in the test cavity. Schlieren photography and high speed filming aided description of the flow dynamics. Results indicated that boundary layer effects became evident in the nozzles as specific heat ratios increased. Large pressure fluctuations were observed in the cavity when helium was introduced into the flow to raise the specific heat ratio. This unstable behavior was attributed to the helium mass flow into the mixer and the mixer design itself. Use of the air/helium mixer brought about the pressure fluctuations earlier in a test run than with the mixer removed under the same conditions. Favorable pressure conditions for lasing were achieved for at least two seconds for the supersonic nozzles' design specific heat ratio of 1.51. Adverse pressure behavior was also attributed to three dimensional viscous effects along the cavity walls.

EFFECTS OF SPECIFIC HEAT RATIO ON A SIMULATED CHEMICAL LASER CAVITY FLOW

I. Introduction

Background

Interest in chemical laser research has increased due to the possible application of this type of laser to the Strategic Defense Initiative (SDI). The Alpha chemical laser, a key component of the SDI Zenith Star program, is now in development and testing (1:23). The decision on whether or not the chemical laser will be utilized is related to the performance of the laser which depends directly on the flow structure in the lasing cavity (2:1-1).

Patterson, Batten, and Howie introduce their source flow chemical laser with the following:

Figure 1 shows a typical source flow laser configuration. These lasers are characterized by supersonic oxidizer streams which enter the laser cavity from an array of source flow nozzles. A secondary fuel stream is injected either sonically or supersonically into the oxidizer stream through wedges placed at the exit of the source flow nozzle. The mixing of the two streams and the subsequent reaction generates vibrationally excited molecules which are the source of the laser radiation. As indicated by the figure, the plane in which mixing occurs is orthogonal to the expansion plane and lasing [cavity] axis. The purpose of the source flow is to reduce the amount of diluent required by using area expansion to help control the temperature and pressure rise in the laser cavity. (3:1)

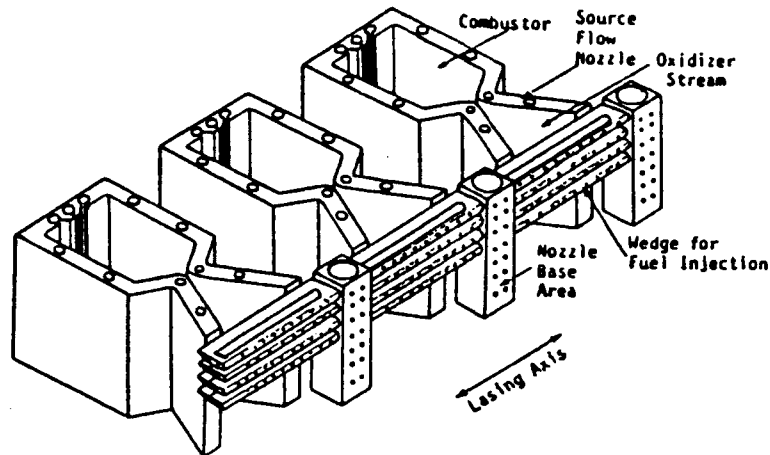


Figure 1.1 Source Flow Chemical Laser Concept (3:1)

Laser performance is strongly connected to the fluid mechanics processes of the flow crossed by the beam.

Rapagnani and Lankford from the Air Force Weapons Laboratory (AFWL) state

Computer modelling of the flow through cavities is not a trivial task. Analysis of the flows are complicated by the existence of strong cross stream pressure gradients and subsonic recirculation zones that are embedded in the supersonic cavity. This analysis of a high base relief cavity has indicated the existence of large property variations and significant regions of subsonic flow. These subsonic recirculating regions are essentially dead spaces in the cavity since mass is neither convected in or out of an area surrounded by a closed streamline. These regions are local hot spots since the temperature is approaching its stagnation value. Large pressure variations occurred in this cavity. (3:344)

The previous discussion illustrates the great need for experimental investigation of chemical laser cavity flow-fields. Research is needed not only to better "map out" the quantitative and qualitative structure of the flow in the lasing cavity; but, also to make available data which can be used for comparison of results obtained through computer simulation.

Scope

The thesis research completed by Stiglich (4) is the basis of this investigation. A major portion of his work involved the design and construction of a test facility capable of investigating flow conditions in a simulated laser nozzle assembly and lasing cavity. The nozzle assembly was modelled after the Alpha laser which was designed for use with a gas specific heat ratio, γ , of 1.51. Stiglich's study used only air as the medium which has a γ value of about 1.4. Using a cold flow mixture of compressed air and bottled helium, a method of controlling the gas γ value was devised for this investigation. The addition of hypersonic wedges (see Figure 1.1) for secondary flow injection was not accomplished in this research. Based on time histories of pressures in the cavity, schlieren photographs of the cavity flowfield, and high speed film of the flow dynamics, the operating characteristics of the nozzle/cavity system of this simulated section of a chemical

laser were investigated. The data was scrutinized for patterns and effects caused by use of different γ values.

Additionally, the Data Acquisition System (DAS) used for this research was substantially upgraded to include 20 channel simultaneous recording of pressure transducer voltage output throughout a single test run. Previous equipment allowed only 6 pressure readings to be evaluated per run. Data reduction software was developed to convert transducer voltage output to pressure values, calculate mass flow rates of the primary and secondary gases, determine mixture γ values, and compute nozzle exit Mach numbers.

II. Theory

Analysis of the pressure data obtained during experimentation included determination of the mixture specific heat ratio for the combination of air and helium, and nozzle fluid dynamics.

Mixture Specific Heat Ratio

Several assumptions were made to calculate the ratio of specific heats, γ , for the gas after the air and helium supply mixed. Since cold flow was used, the inherent complexity of high temperature reaction chemistry common in actual chemical laser operation was greatly simplified. The gases, air and helium at room temperature, were assumed to behave as perfect gases and applicable relations were employed. The specific heats of the individual supply gases were considered constant in the temperature range of testing. Wark (5:844) states that the values of specific heats for monatomic gases over a wide range of temperatures are constant. Table 2.1 lists the specific heat values used for air and helium.

Table 2.1 Specific Heat Values

Gas (Molecular Wt.)	C_p (Btu/lb _m ·°F)	C_v (Btu/lb _m ·°F)
Air (28.97)	0.240	0.17155
Helium (4.003)	1.24906	0.74944

The ratio of specific heats is defined as

$$\gamma = \frac{C_p}{C_v} \quad (1)$$

To determine γ for the mixture of gases the conservation of mass yields

$$\dot{m}_{mix} = \dot{m}_{air} + \dot{m}_{He} \quad (2)$$

For the mixture specific heats

$$C_{p_{mix}} = \frac{\dot{m}_{air} C_{p_{air}} + \dot{m}_{He} C_{p_{He}}}{\dot{m}_{mix}} \quad (3)$$

and

$$C_{v_{mix}} = \frac{\dot{m}_{air} C_{v_{air}} + \dot{m}_{He} C_{v_{He}}}{\dot{m}_{mix}} \quad (4)$$

Combining the above equations yields

$$\gamma_{mix} = \frac{C_{p_{mix}}}{C_{v_{mix}}} = \frac{\dot{m}_{air} C_{p_{air}} + \dot{m}_{He} C_{p_{He}}}{\dot{m}_{air} C_{v_{air}} + \dot{m}_{He} C_{v_{He}}} \quad (5)$$

So, given the mass flow rate of each gas, the mixture γ can be determined. The mass flow rate for the air line was determined using a square-edge orifice meter and for the helium line via a venturi flow meter. The calculation methods for these meters are described in reference 6.

Nozzle Flow

Since the converging-diverging laser nozzles were contoured, transverse velocities inside were considered to be small and the flow was treated as one-dimensional. From Shapiro (7:83), the following relation is given for isentropic flow of a perfect gas:

$$\frac{p_0}{p} = \left(1 + \frac{\gamma-1}{2} M^2\right)^{\frac{\gamma}{\gamma-1}} \quad (6)$$

Solving for Mach number and applying to the nozzle exit conditions gives an equation for the nozzle exit Mach number based on experimental data

$$M_e = \left[\frac{2}{\gamma-1} \left(\left(\frac{p_0}{p_e} \right)^{\frac{\gamma-1}{\gamma}} - 1 \right) \right]^{\frac{1}{2}} \quad (7)$$

where p_0 is the stagnation pressure upstream of the nozzles, p_e the static pressure at the nozzle exit and γ the value obtained from equation 5. Equations 5 and 7 were incorporated into the data reduction computer program

POSTRUN.BAS listed in Appendix B.

A theoretical counterpart for the exit Mach number of the nozzles was derived from the isentropic equation given in Shapiro (7:86) for area ratio as a function of γ and Mach number applied to the exit

$$\frac{A_e}{A_t} = e = \frac{1}{M_e} \left[\left(\frac{2}{\gamma+1} \right) \left(1 + \left(\frac{\gamma-1}{2} \right) M_e^2 \right) \right]^{\frac{\gamma+1}{2(\gamma-1)}} \quad (8)$$

Solving for M_e gives a theoretical equation for Mach number as a function of γ and the constant area ratio for the laser nozzle of 32.6

$$M_e = \left[\frac{(\gamma+1) \left(M_e e \right)^{\frac{2(\gamma-1)}{\gamma+1}} - 2}{\gamma-1} \right]^{\frac{1}{2}} \quad (9)$$

Solving M_e iteratively, theoretical and experimental exit Mach numbers for a range of γ values were then plotted for comparison.

III. Experimental Apparatus

Four major systems make up the experimental apparatus: the flow system, the test section nozzle/cavity system, the data acquisition system, and the schlieren optical system.

Flow System

Figure 3.1 diagrams the flow system for the blowdown wind tunnel. Description of each of the system components follows:

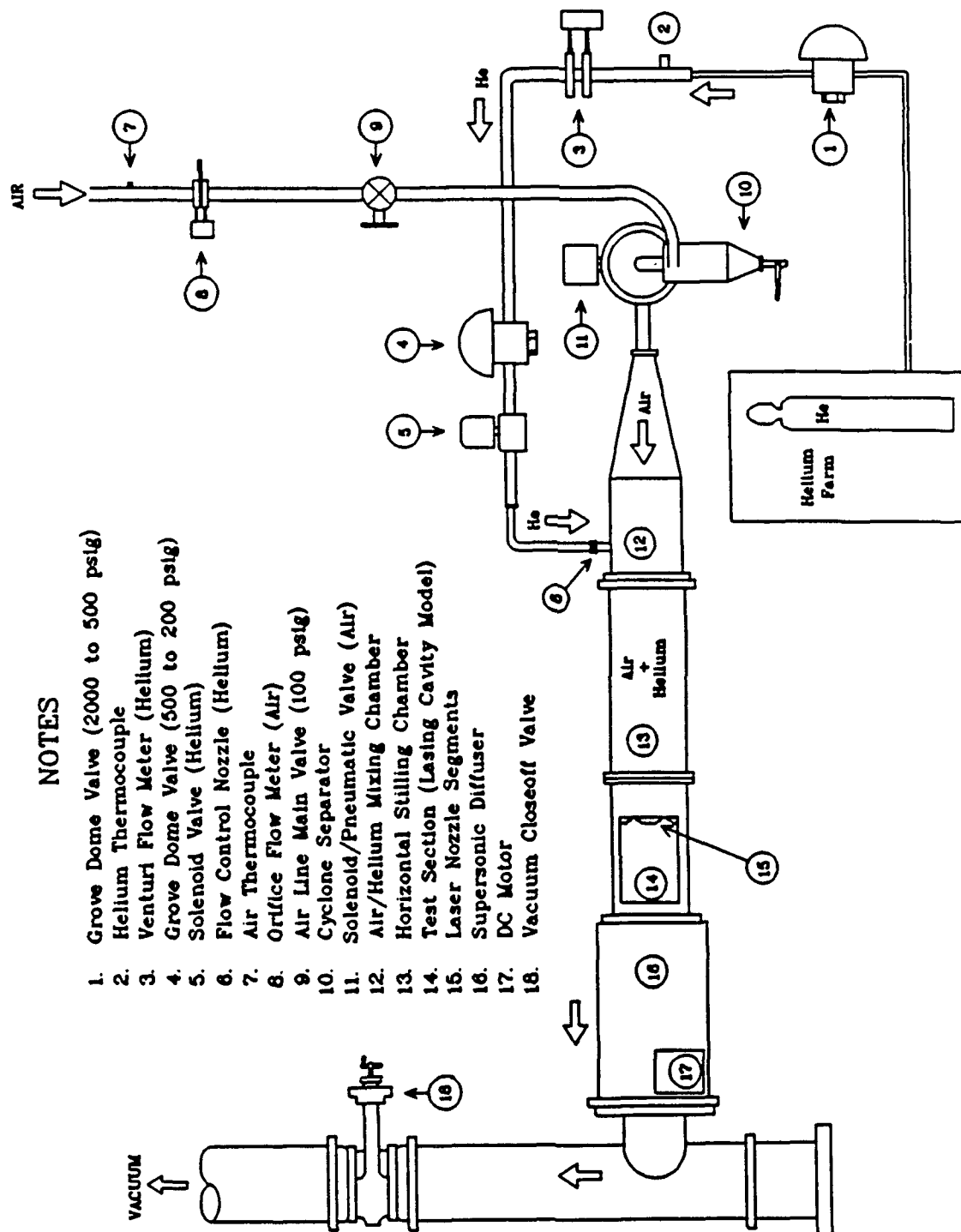
Compressed Air System. The compressed air system consists of two ATLAS COPCO Air Compressors, Model GAU-807; two DELTECH Filters, Model 819; two Pioneer Refrigerant Air Dryers, Model R550A; and two Arrow Compressed Air Dryers. Each of the air cooled compressors is capable of providing 520 standard cubic feet per minute (SCFM) at 102 pounds per square inch gauge (psig). The DELTECH filters are used to eliminate any pollutants, such as oil, from the air flow. The Pioneer refrigerant air dryers eliminate moisture from the air flow and support a mass flow rate up to 500 SCFM. The calculated pressure loss across the refrigerant air dryers is approximately 3.6 psig. A second drying stage is available through the Arrow Chemical Air Dryers. Normally, the chemical air dryers are by-passed due to their large pressure loss, approximately 10 psig. Once the air flow is

through the final stages of drying, it is piped to the laboratories. In the laboratory the air goes through a globe valve and into a cyclone separator. The cyclone separator is the final station used to eliminate particulate matter from the air flow. Next, the air is routed through an electrically controlled 3 inch ball valve. The Starlite model 666-F Ball Valve provides quick opening via pneumatic actuation and the 3 inch diameter provides the maximum air flow to fill the horizontal stilling chamber and start the nozzles (4:3-1).

Orifice Meter. Mass flow measurement of the compressed air was calculated using a square edge orifice meter with a 0.8 inch throat. Calculation of the mass flow rate was accomplished using the method of reference 6.

Horizontal Stilling Chamber. The six foot horizontal stilling chamber houses a steel honeycomb mesh to help straighten and distribute the air evenly prior to entering the mixer.

Helium Supply System. The supply of secondary helium was provided from a farm of five helium tanks at 2000 psig pressure. Pressure reduction was provided by two Grove Powreactor Dome Controllers. The first dome valve was a Model WBX-304-K3 and reduced the storage pressure of 2000 psig to 500 psig. The helium then passed through a venturi flow meter followed by the second dome valve, a Model



NOTES

1. Grove Dome Valve (2000 to 500 psig)
2. Helium Thermocouple
3. Venturi Flow Meter (Helium)
4. Grove Dome Valve (500 to 200 psig)
5. Solenoid Valve (Helium)
6. Flow Control Nozzle (Helium)
7. Air Thermocouple
8. Orifice Flow Meter (Air)
9. Air Line Main Valve (100 psig)
10. Cyclone Separator
11. Solenoid/Pneumatic Valve (Air)
12. Air/Helium Mixing Chamber
13. Horizontal Stilling Chamber
14. Test Section (Lasing Cavity Model)
15. Laser Nozzle Segments
16. Supersonic Diffuser
17. DC Motor
18. Vacuum Closeoff Valve

Figure 3.1 Flow System Layout

11010-PO55B, which further reduced the flow pressure to the desired pressure. Exiting this dome valve, the flow encountered a solenoid valve which was controlled from the operator control panel. With this valve open, the helium flow is choked via a control nozzle which was designed for the purpose of preventing pressure fluctuations downstream of the nozzle from varying the helium mass flow rate. Figure 3.2 depicts the design of this nozzle which consisted of a brass insert silver soldered into a 19/32 inch inner diameter stainless steel pipe connector. The brass was then drilled to the desired throat diameter and the nozzle shaped. Once through this flow controller, the helium entered the horizontal stilling chamber and the mixer.

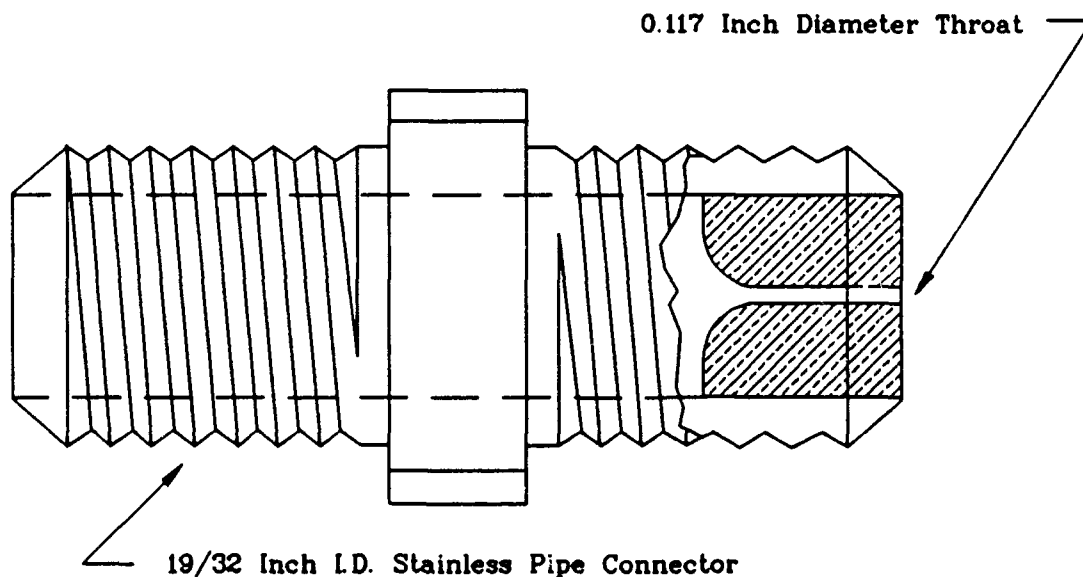


Figure 3.2 Helium Flow Control Nozzle

Venturi Flow Meter. Mass flow measurement of the helium supply was accomplished using a venturi flow meter with a 0.5 inch diameter throat. The mass flow rate was calculated using the method of reference 6.

Mixer. The mixer design was based on the Vassilatos parallel multitube ejector design described by Zakanycz (8). The dimensions of the discharge end of the Vassilatos multitube ejector were enlarged so that a large scale version could be placed inside the horizontal stilling chamber. The mixer was made of stainless steel tubing, plywood, plexiglas, 8 inch PVC, and aluminum plate. The mixer design is shown in Figure 3.3. The mixer slipped into the forward section of the horizontal stilling chamber and was held in place by sandwiching the flange end of the mixer plate between the flange ends of the forward and rearward portions of the horizontal stilling chamber. Entering the mixer, the air was forced to flow around a chamber full of glass beads (marbles). The glass beads caused an even distribution of air to flow into the air tubes. A fine wire mesh was placed between the glass beads and the entrance to the tubes to filter out any debris. Once in the tubes, the air was directed through the remaining part of the mixer and out the end plate. The secondary flow of helium entered the sidewall of the horizontal stilling chamber and was deflected by the sidewall of the mixer to flow into holes

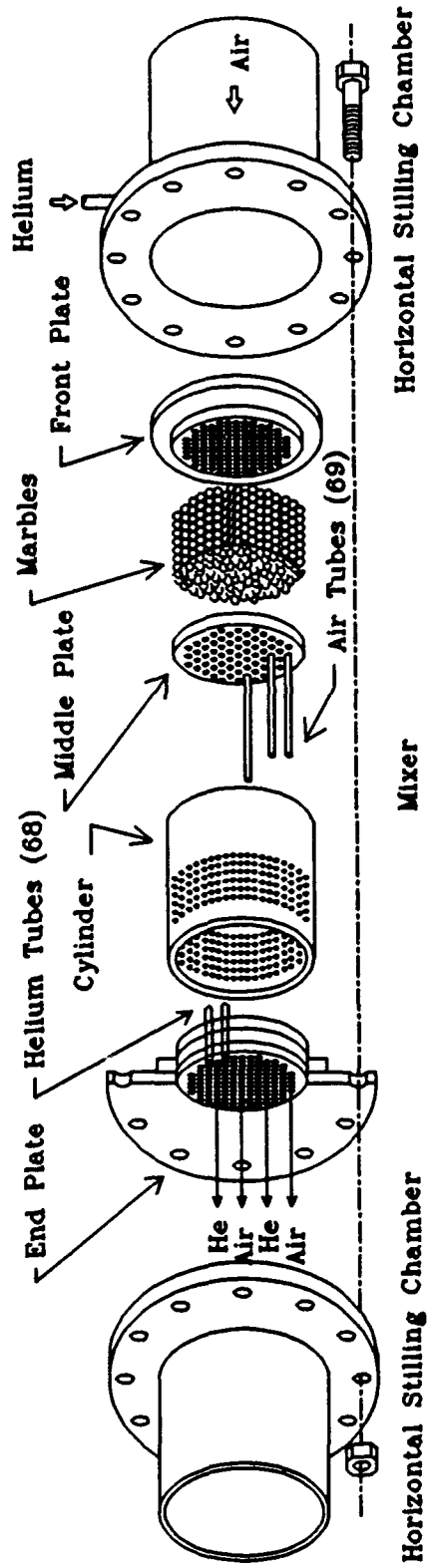


Figure 3.3 Air/Helium Mixer Design

drilled in the side of the PVC cylinder. Once inside this cavity in the mixer, the helium flow was forced to move around the air tubes traversing the cavity, into a second set of tubes, and then directed out the end plate. The alternating of the primary/secondary tubes exiting the end plate induced a thorough mixing in the downstream end of the horizontal stilling chamber (4:3-4).

Variable Supersonic Diffuser. A supersonic diffuser was built to maintain the low pressures in the cavity portion of the test section. The diffuser was made out of aluminum and plexiglas and actuated by a 24 v dc Delco motor. Power for the motor was provided by the laboratory dc power supply, a Rapid Electric Co. Model S-528. The motor was electrically controlled from the operator control panel. Figure 3.4 shows the motor mounted on the outside of the diffuser box. This motor drove a shaft that penetrates the diffuser side wall through a pressure tight seal. The shaft drives a gearing mechanism that turns a threaded shaft. The threaded shaft moves back and forth either pushing or pulling the diffuser slide bracket which in turn closes or opens the diffuser blades (diminishing or enlarging its throat). To protect the apparatus from damage, contacts positioned on the threaded shaft deactivate the motor as contact bars close micro-switches mounted on the adjustment bracket behind the gear box (4:3-6).

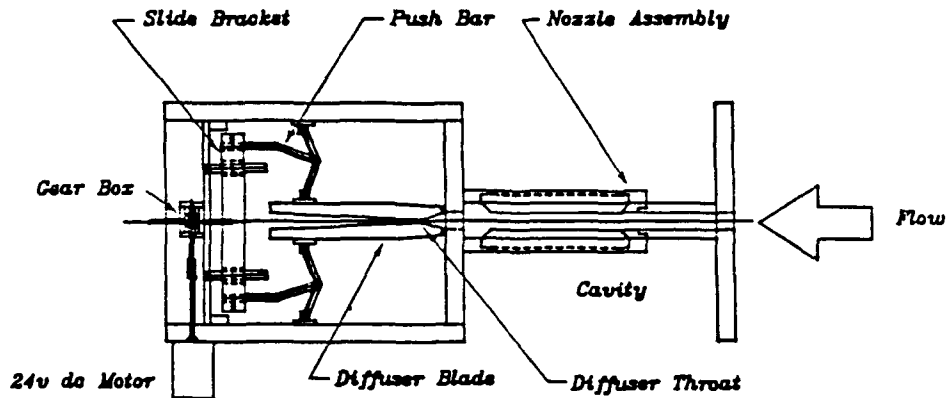


Figure 3.4 Supersonic Diffuser, Top View

Vacuum System. To establish the desired test section operating conditions it was necessary to have high pressure on one end of the wind tunnel and a vacuum on the other end. The vacuum system consists of 16 large tanks suspended from the laboratory ceiling and three vacuum pumps located in the pump room. Two of the three vacuum pumps are Leiman, no model number, radiator cooled pumps, and the third pump is a Stokes, Model 212-H. The Stokes pump has the capacity to pump 140 SCFM. The 16 vacuum tanks, along with the piping, provide approximately 650 ft³ of vacuum space. A network of 8 inch PVC pipe connected the test section to the vacuum

system. The interface between the PVC pipe and the test section was a Consolidated Vacuum Corporation, Model VCS-41, high vacuum valve. The high vacuum valve allowed the operator to isolate the wind tunnel from the vacuum system. A Meriam U-tube mercury manometer, Model 20DA40, was incorporated to provide the operator with the vacuum pressure reading while the tunnel was being evacuated (4:3-7).

Nozzle/Cavity Test Section. The nozzle/cavity design selected and its general operating conditions were established from information provided by the Air Force Weapons Laboratory (AFWL), Kirtland AFB, NM. Figure 3.5 shows the design of one nozzle segment and Table 3.1 (9) lists the coordinates from the throat (0.0000,0.0000) to the exit (0.5560,1.1530) of the nozzle contour. The nozzle design parameters are listed in Table 3.2. Three pressure ports were drilled into each of the nozzle segments to allow static pressure measurements in the region of the base and the nozzle exit plane. Figure 3.6 displays the three nozzle segments as they are mounted in the test section. The current design allows enough material to machine the base region to accommodate future modifications for attachment of the secondary flow wedges which were not included in this investigation (4:3-9). The test section was constructed out of aluminum and the windows were cut from 1 inch thick optical plexiglas.

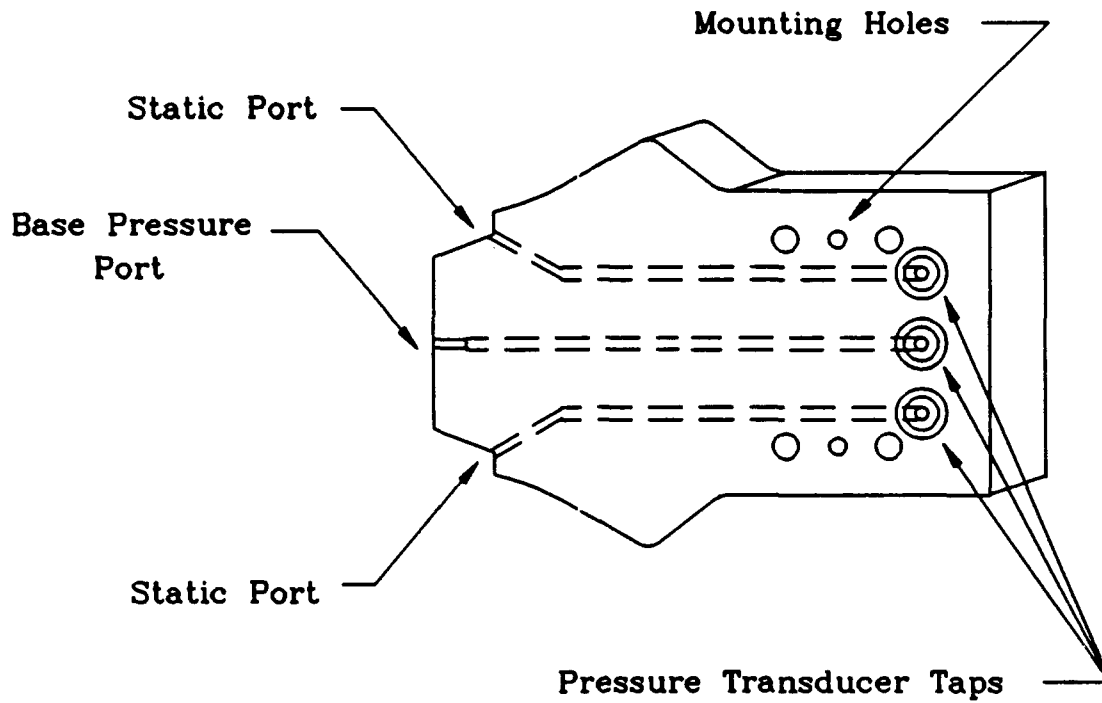


Figure 3.5 Nozzle Segment

Table 3.1 Nozzle Contour Coordinates

	X Position (inches)	Y Position (inches)
1	0.0000	0.0000
2	0.0013	0.0240
3	0.0055	0.0480
4	0.0204	0.0960
5	0.1429	0.2880
6	0.2604	0.5040
7	0.3657	0.7200
8	0.4742	0.9600
9	0.5560	1.1530

Table 3.2 Nozzle Design Parameters

Parameter	Quantity
Specific heat ratio, γ	1.51
Upstream stagnation pressure, P_0	100 psia
Upstream stagnation temperature, T_0	73°F
Isentropic exit Mach number, M_e	6.21
Isentropic exit pressure, P_e	0.0886 psia
Nozzle area ratio, A_e/A^*	32.589

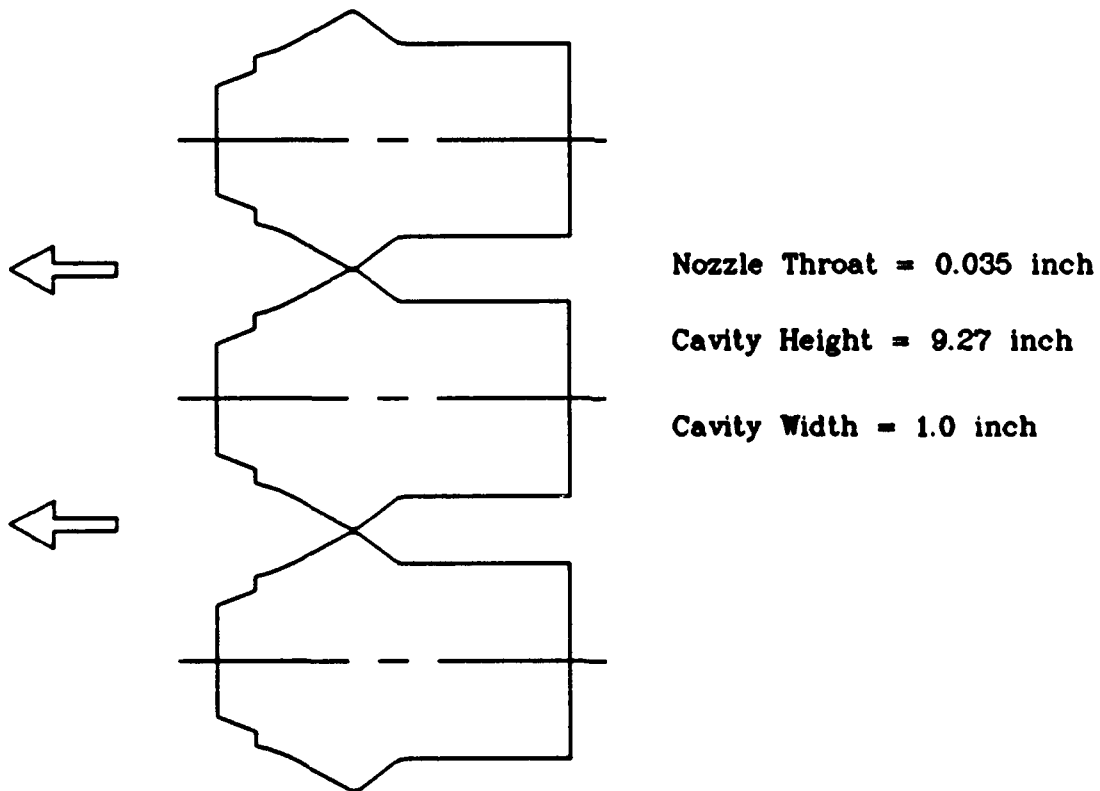


Figure 3.6 Test Section Nozzle Configuration

Data Acquisition System

Figure 3.7 depicts the Data Acquisition System (DAS) hardware. Analog signals from piezoresistive pressure transducers are passed to Signal Conditioning Units (SCUs) for amplification. From the SCU each analog signal is transferred via a BNC cable to the Nicolet System 500 Data Acquisition System which consists of the Data Acquisition Unit (DAU), the Controller, and the Video Display.

Piezoresistive Pressure Transducers. Nineteen piezoresistive pressure transducers were used to monitor the flow. Table 3.3 shows the position number, appointed Nicolet channel, location, serial number (ENDEVCO unless otherwise stated), linear operating range, and signal conditioner assigned to each transducer. Figure 3.8 displays the available transducer tap locations in the test section. ENDEVCO Models 8506-2, 8506B-5, and 8510B-5 were used in the test section. Their low range of linear operation (the dash numbers indicate the psig range) was needed for the very low pressure of the flow beyond the nozzle exit. An ENDEVCO Model 8510B-15 was utilized in the vertical stilling chamber to monitor the evacuation of the system prior to a test run. An ENDEVCO Model 8510B-100 was placed in the horizontal stilling chamber to measure the stagnation pressure just upstream of the test section entrance. Pressure measurements were also needed for air

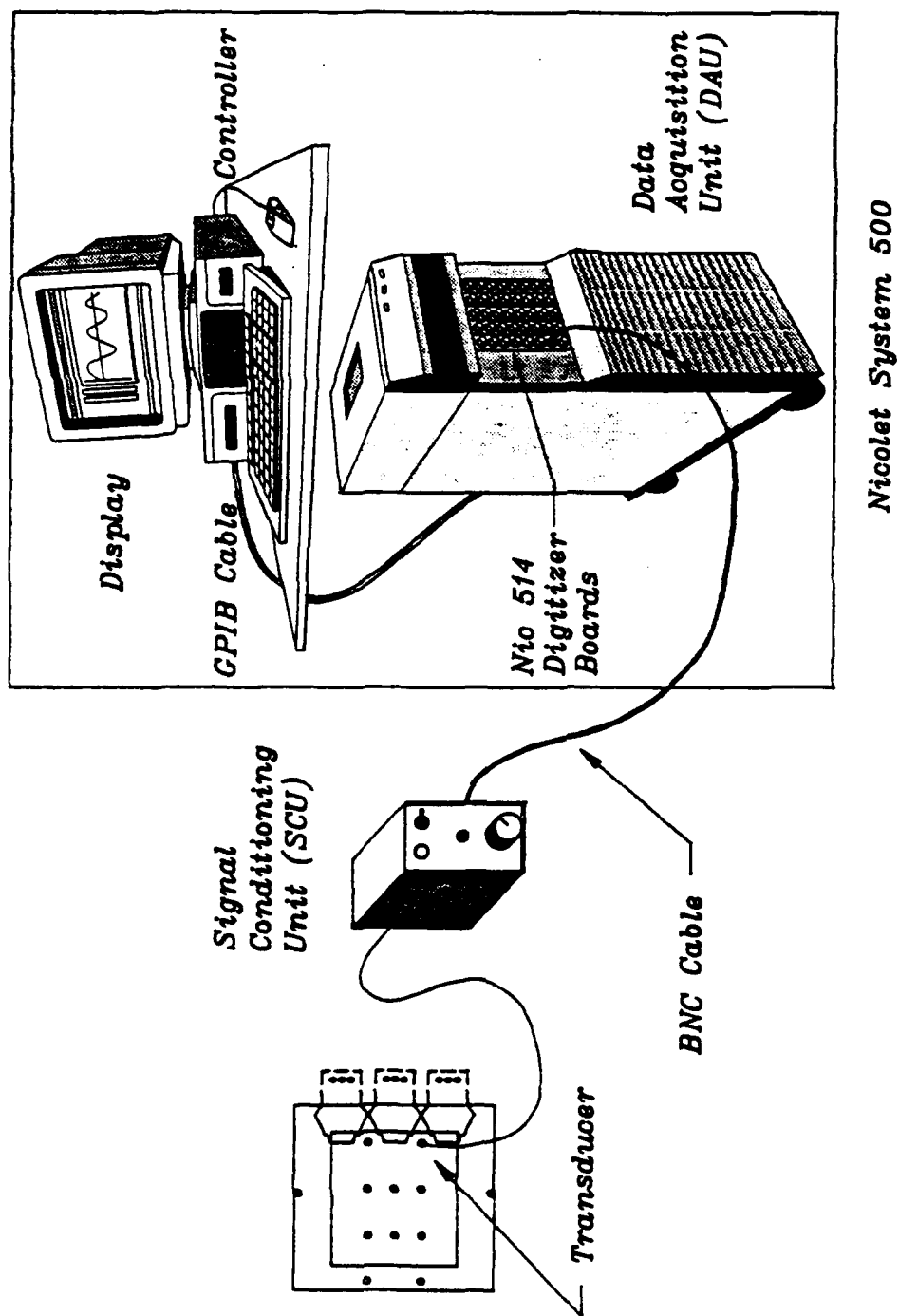


Figure 3.7 Data Acquisition System

Table 3.3 Transducer/Thermocouple Locations

Position Number	Nicolet Channel	Location	S/N (Model)	Range (psig)	SCU No. (S/N)
1	1A	Nozzle Segment B, Top	PP81 (8510B-5)	5	4 (BA64)
2	1B	Nozzle Segment B, Center	78HB (8510B-5)	5	5 (BA68)
3	1C	Nozzle Segment B, Bottom	79HB (8510B-5)	5	6 (BA82)
4		Room Air	Barometer		
5	1D	Vertical Stilling Chamber	89TA (8510B-15)	15	8 (BA84)
6	2A	Horizontal Stilling Chamber	23LG (8510B-100)	100	9 (BA83)
7		Test Section, Top			
8		Test Section, Bottom			
9	2B	Test Section, Row 1, Col 1	748F (8506B-5)	5	10 (AE82)
10	2C	Test Section, Row 3, Col 1	PP67 (8510B-5)	5	16 (BA57)
11	2D	Test Section, Row 1, Col 2	838F (8506B-5)	5	3 (AF03)
12	3A	Test Section, Row 2, Col 2	HE99 (8506-5)	5	11 (AM03)
13	3B	Test Section, Row 3, Col 2	758F (8506B-5)	5	15 (BA56)
14	3C	Test Section, Row 1, Col 3	928F (8506B-5)	5	2 (AE77)
15	3D	Test Section, Row 2, Col 3	KL52 (8506-2)	2	12 (AE80)
16	4A	Test Section, Row 3, Col 3	978F (8506-5)	5	14 (AF84)
17	4B	Test Section, Row 1, Col 4	798F (8506B-5)	5	7 (BA85)
18	4C	Test Section, Row 3, Col 4	M038 (8506A-5)	5	17 (BA55)
19		Nozzle Segment A, Top			
20		Nozzle Segment A, Center			
21		Nozzle Segment A, Bottom			
22		Nozzle Segment C, Top			
23		Nozzle Segment C, Center			
24		Nozzle Segment C, Bottom			
25	4D	He Venturi Meter, Dwnstrm	Dynisco Differential	0-25psid	20 (2310)
26		He Venturi Meter, Upstream	TCPT69-25	6 v	Vishay
27	5A	Air Orifice Meter, Upstream	Statham Differential	± 1 psid	0 (BA63)
28		Air Orifice Meter, Dwnstrm	1472 P96-1D-350	10 v max	
29		Air Thermocouple	Microstar (Left)		
30		He Thermocouple	Microstar (Right)		
31	5B	Air Orifice Meter, Upstream	WL44 (8530A-100)	100 psia	1 (BA67)
32	5C	He Venturi Meter, Upstream	43YB (8510B-500)	500	18 (BA96)

mass flow and helium mass flow rate calculations through a square edge orifice meter and venturi meter. The pressure of the air flow at the upstream tap of the orifice plate was measured using an ENDEVCO Model 8530A-100. The differential pressure across the orifice plate was monitored by a Statham Model 1472 P96-1D-350 differential pressure transducer with a ± 1 psid range. Upstream of the venturi meter throat the helium pressure was measured by an ENDEVCO Model 8510B-500 transducer. The differential pressure across the venturi was measured using a Dynisco differential pressure transducer, Model TCPT69-25, with a 0 to 25 psid range.

Signal Conditioning Units/Power Supplies. Five ENDEVCO Model 4225 ac-operated power supplies were used to provide ± 18 volts to the 18 ENDEVCO Model 4423 Signal Conditioning Units (SCUs). These SCUs provide 10 volts excitation to the 17 ENDEVCO pressure transducers and the Statham differential pressure transducer (position 27-28). The SCUs also amplify output voltage from each transducer. A gain of 20 was selected for these transducers. The Dynisco differential transducer (position 25-26) required 6 volts excitation voltage and high gain in order to resolve the low pressure differential. A Vishay Measurements Group Signal Conditioner Amplifier, Model 2310, was utilized with a gain setting of 500. Table 3.3 lists the serial numbers of each SCU and which transducer it was assigned to.

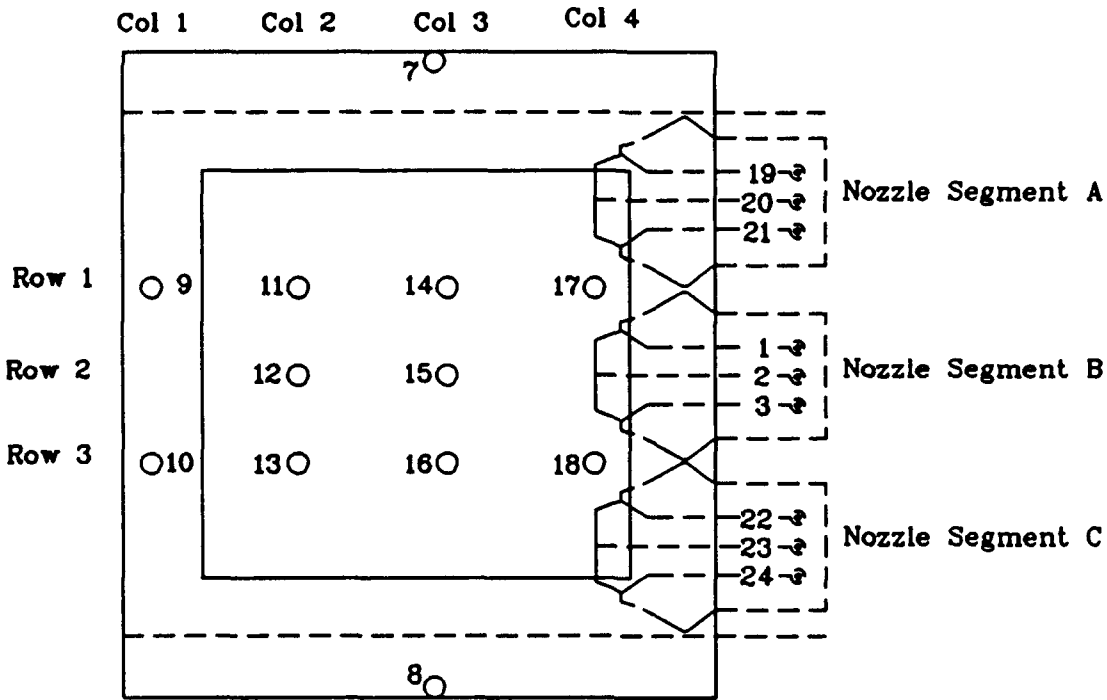


Figure 3.8 Test Section Transducer Tap Locations

Nicolet System 500. The Nicolet System 500 is a complete Data Acquisition System. A pedestal style Data Acquisition Unit (part no. 886-501) houses one 540 CPU board and five digitizer boards. Each of these Nic 514 digitizer boards has a four channel capability making a total of 20 channels available for simultaneous sampling of analog signals. Once digitized, signals are transferred through a General Purpose Interface Bus (GPIB) to the system controller. The controller is an IBM compatible 386 computer with 2 Megabytes of RAM, a 150 Megabyte hard drive,

one 1.2 Megabyte 5.25 inch floppy disk drive, one 3.5 inch disk drive, and a VGA video display terminal. Nicolet system software, version 5.10, runs in a Microsoft Windows/386 format to provide control of all aspects of the acquisition and display of data. For air-only runs triggering of the Nicolet System 500 occurred when voltage output of the transducer placed in the horizontal stilling chamber (position 6) began to rise from its initial steady-state condition indicating opening of the 3-inch ball valve in the air supply. The triggering criteria for air-helium runs was the voltage level output from the helium venturi meter differential pressure transducer (position 25-26). A step increase in voltage from this transducer indicated onset of helium flow and started data collection.

Two computer programs, written in GW-Basic, control the pre-run inputs and the post-run data reduction. Appendix B contains the program listings.

Schlieren Optical System

Schlieren photography and filming of the test section flow dynamics were accomplished using the setup shown in Figure 3.9. A Cordin spark lamp, Model 5401, provided lighting for still photographs using Polaroid 3000 ASA film. A Cordin Power Supply, Model 5205, powered the spark lamp. The two mirrors were 7.5 inch diameter concave with 40 inch focal lengths. A second set of 10 inch diameter, concave,

30 inch focal length mirrors was also used. A steady 300 watt arc-lamp point source illuminated the test section for filming. A Redlake 16mm intermittent high speed motion picture camera, Model 51-0003, Serial Number 647, was placed just behind the knife-edge and the image focused on the film plane. Film speeds ranged from 100 to 500 frames per second.

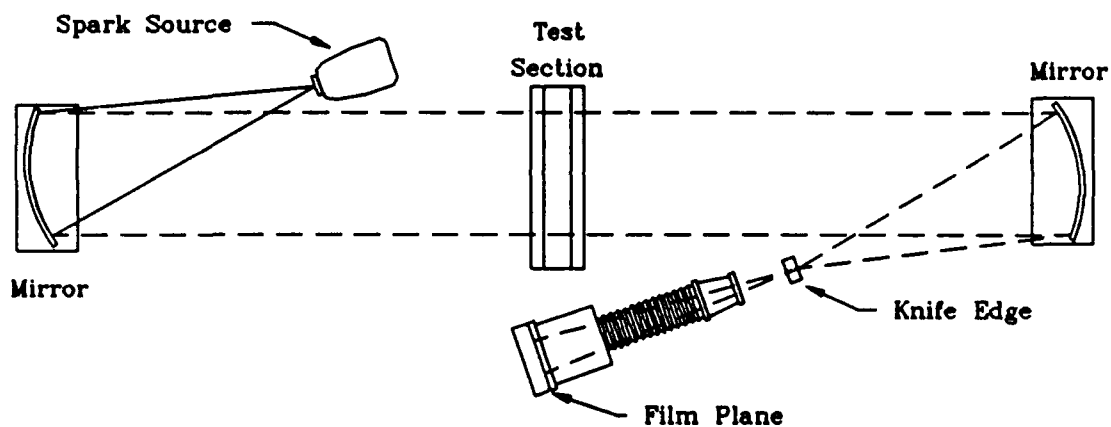


Figure 3.9 Schlieren Optical System

IV. Experimental Procedures

The experimental procedures followed during this research included calibration of pressure transducers, schlieren photography techniques, and data acquisition and reduction steps.

Pressure Transducer Calibration

AMETEK Pneumatic Dead Weight Testers, Model PK-2 (low pressure, 300 inches of water) and Model HK-500 (high pressure, 500 psig), were used to calibrate all transducers. The manufacturer of these pneumatic dead weight testers cautions that the use of any gas other than clean compressed air or nitrogen could cause discrepancies in the calibration data (10). The pressure transducers were calibrated with their respective SCUs in line. Since the SCU does not have a unity gain setting, it will always multiply the pressure transducer output voltage by some factor depending on which gain setting has been selected. The ENDEVCO SCUs have four gain settings (5, 10, 20, 50) and a bridge balance adjustment screw. The Vishay 2310 Signal Conditioner Amplifier has a variable gain adjustment and was set at 500. The gain factors were not exactly as indicated on the front panel; therefore, the pressure transducers were calibrated with the SCU in line so that the exact gain factor is included in the slope of the calibration curve (4:4-1). The

calibration curves of the pressure transducers used in this research are presented in Appendix A.

Schlieren Photographic Techniques

The setup of the schlieren equipment shown in Figure 3.9 was accomplished using the guidelines of AGARDograph No. 23 (11:13-15). Obtaining quality photographs involved much trial and error due to the extremely low density and small optical depth in the test section. For high speed filming, it was discovered that placing the camera directly behind the knife-edge's focal point provided the best focus and lighting capabilities. An attempt to film directly off the image projected on the still camera's ground glass captured some flow dynamics; however, the lighting was severely diminished. Various film speeds were examined to determine if an optimum existed. Results were very similar for film speeds in the range of 100 to 500 frames per second.

Data Acquisition and Reduction

Figure 4.1 shows the steps used in acquiring and reducing data. Details concerning the use of Nicolet's System 500 are contained in the user's operation manual (12). The Nicolet software runs in a Windows 3.0 environment. For further information on Windows procedures refer to the manual (13).

1. Zero Run

With the system open to atmosphere and the reference vacuum off, acquire one minute's data on all channels. This records the voltage output from each transducer when there is a zero pressure differential.

2. Reference Vacuum

Start the reference pressure vacuum pump and monitor via the 20 mm mercury range vacuum pressure gauge. This vacuum pump can achieve a reference pressure of 1.0 mm mercury (0.01933 psia).

3. Cavity Vacuum

Evacuate the test cavity by starting the three vacuum pumps located in the pump room. Make certain that the vacuum valve in the vertical stilling chamber is open prior to doing a run. Pressurizing the system with 100 psia can damage the plexiglas windows of the test section. Monitor the evacuation of the cavity via the 20 mm mercury vacuum gauge. These pumps can bring the system down to approximately 7 mm of mercury (0.1353 psia).

4. Helium Supply

Open the helium supply at the tank farm. Open the rear farm supply and set the first dome regulator pressure gauge at 400 psia. Set the second dome regulator pressure to the desired level. This variable controls the helium mass flow rate. Open the front farm supply and set the regulator pressure for the pneumatically actuated 3 inch air valve to 100 psia.

5. Pre-run Inputs

Run the program PRERUN.BAS by pointing to the Prerun icon in the Windows Program Manager. This program prompts the user for information utilized during post run data processing and calculation.

6. Nicolet System 500 Data Acquisition

Begin the Nicolet System 500 software by clicking on the Nicolet icon in the Windows Program Manager. Acquire 20 channel simultaneous data for a 10 second run and save the waveform data for post-run reduction.

7. Data Reduction

Begin the post-run data reduction by clicking on the POSTRUN icon in the Windows Program Manager. This program can reduce a single run's data or a range of runs' data. POSTRUN.BAS converts voltage data to pressures, and calculates helium and air mass flow rates, gamma values, and nozzle exit mach numbers. Output files are compatible with Grapher for plotting of data.

Figure 4.1 Data Acquisition Procedures

V. Results and Discussion

Results of the research accomplished include evaluation of the simulated laser cavity test equipment, examination of the schlieren still and high speed photography, and analysis of pressure data obtained during runs made under various flow conditions.

Test Equipment Performance

Monitoring of pressure data over a one hour period revealed the stable characteristics of the pressure-vacuum flow system. The 100 psig air pressure supply exhibited a cyclic fluctuation of approximately 5 minutes period and 2.5 psi amplitude. This cycle appeared to correspond to the on/off cycling of the air dryers connected to the air supply line. The period was not considered detrimental as test runs were only of 10 seconds duration and the air supply pressure during operation was observed to remain steady. The vacuum pumps were capable of achieving a minimum pressure inside the cavity of approximately 6 mm Hg (0.116 psia) in roughly 25 minutes of evacuation. Cavity pressure was monitored via a calibrated vacuum gauge prior to each run to determine a steady condition and maximum vacuum.

The reference vacuum applied to each psig pressure transducer was monitored by a calibrated portable vacuum standard. The minimum reference pressure achieved was

stable at 1.0 mm Hg (0.0193 psia) in approximately 30 minutes of pumping. The selection of transducers with reference ports that did not leak was essential to maintain the lowest possible reference vacuum. ENDEVCO transducer reference ports were tested for leakage using a hand pumped vacuum gauge prior to selection for use.

Early testing of the helium supply line disclosed a tendency for fluctuations from the air supply to travel upstream to the helium venturi flow meter which caused erroneous mass flow rate calculations. To overcome this, a helium flow control nozzle was designed to choke the stream prior to entering the horizontal stilling chamber. Mass flow of the helium was controlled by the second dome valve pressure on the helium supply line. This pressure (P_{He}), set at the helium farm regulator board, was varied from zero for air-only test runs to 100 to 350 psig for runs with helium injected into the mixer. Data runs made with the P_{He} supply pressure set below approximately 175 psig failed to prevent the fluctuations from travelling upstream as this was the pressure where choking of the flow control nozzle occurred. Data for these runs was examined; but, was not considered reliable enough for use.

Schlieren Photography Observations

Flow dynamics inside the simulated laser cavity were viewed at single time points using still schlieren photography. High speed schlieren filming also captured the flowfield for the duration of ten second runs. The quality of these photographic endeavors was marginal. It is believed that the very low pressures, and consequently the low density gradients, in the test cavity as well as the poor quality plexiglas walls contributed to the inferior pictures. Dark zones were abundant in many of the photographs and obtaining a uniform field was not possible. Despite this, much information was gleaned from the many photographs and film runs made. Because the reproducibility of the photographs was limited, presentation of these observations will be made schematically.

Figure 5.1 illustrates the steady state flowfield in the cavity which occurred for all visualized runs during at least the first 2 seconds of operation. Jet boundaries develop at the exit of the nozzles forming triangular base zones in which recirculation of the flow can take place. At the apex of each triangle a base wake region appears followed by oblique shocks. Varying the P_{H_2} value changed the conditions beyond the 2 second range. These effects will be discussed in the next section concerning pressure data results.

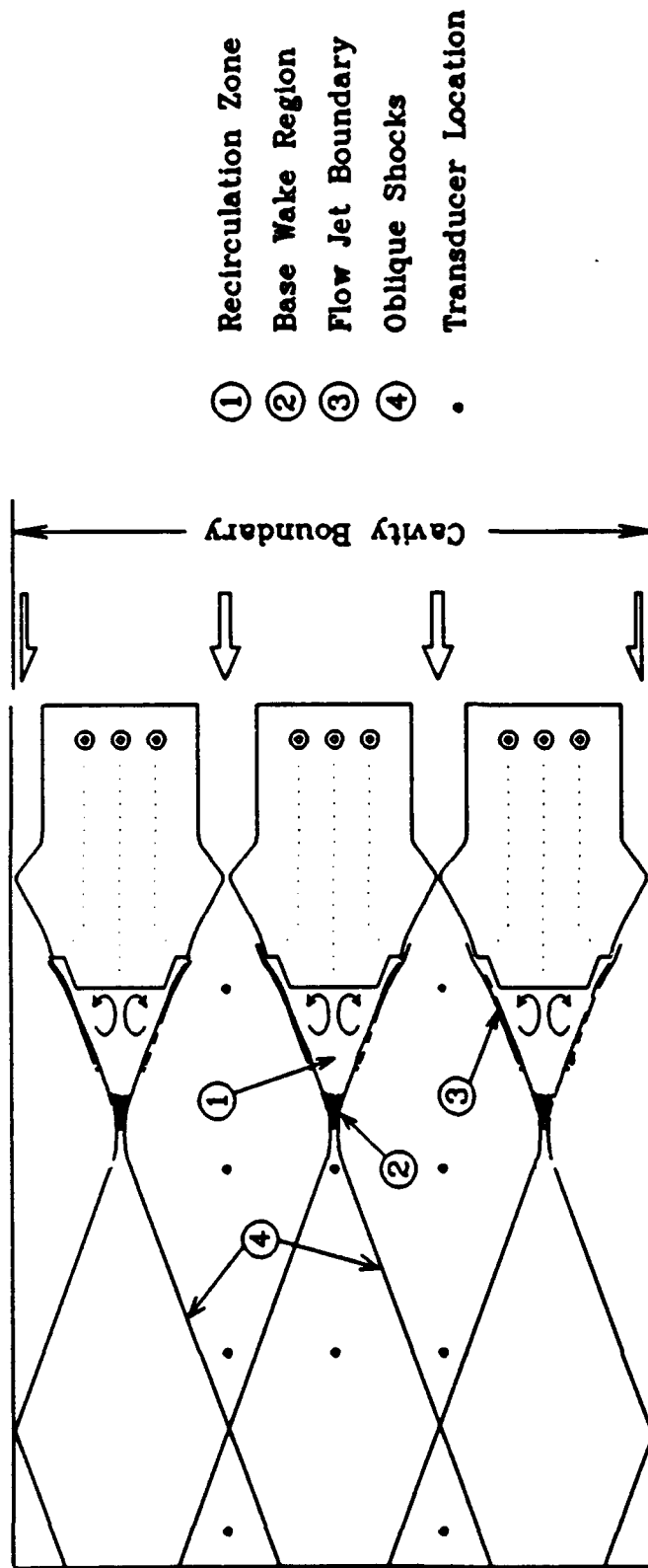
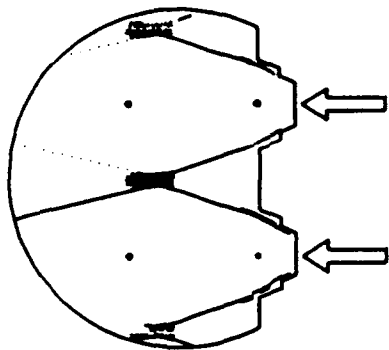
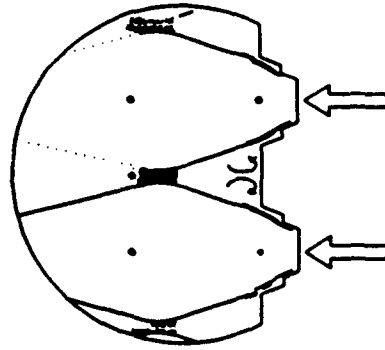


Figure 5.1 Schematic of Cavity Flow at Approximately 2 Seconds

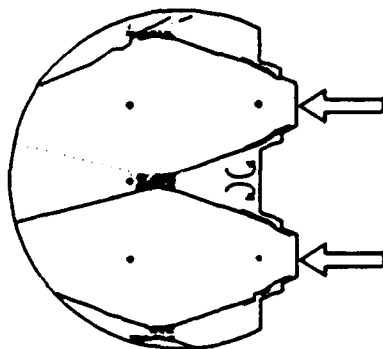
The area observed in filming included a circular portion of the cavity from the two whole nozzle exits downstream to approximately half the test section length. Figure 5.2 depicts the flow dynamics from a typical 10 second high speed film run. The flow rapidly established the pattern of Figure 5.1 within the first second of operation and maintained this wave formation for approximately 2 seconds. As the cavity pressure increased during a test run density gradients became larger improving the visibility of the jet boundaries and oblique shocks. These jets and shocks were also observed in still schlieren photographs. Following the 2 seconds of apparent steady flow, transient wave pulses were observed exiting the nozzles causing disturbance of the previously stable oblique shocks. From approximately 3 seconds to 6 seconds these transients continued while the uppermost oblique shock began rotating into the cavity. The shock could be seen beginning to nearly impinge on the transducer at position 14 at approximately 5.0 seconds after flow initiation. It is possible that boundary layer growth along the cavity ceiling builds up as the pressure in the cavity begins to rise forcing the oblique shock downward at a sharper angle. As the vacuum system begins to fill, the back pressure rises and the base wake begins to open ($t \approx 7.0$ seconds). The wake becomes fully open at approximately 10 seconds.



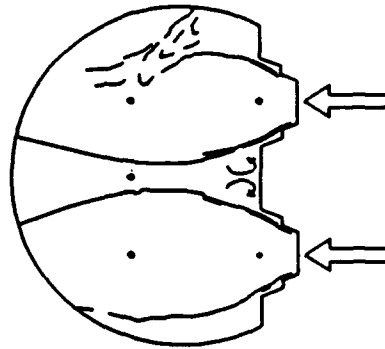
t approx. 0.1 seconds



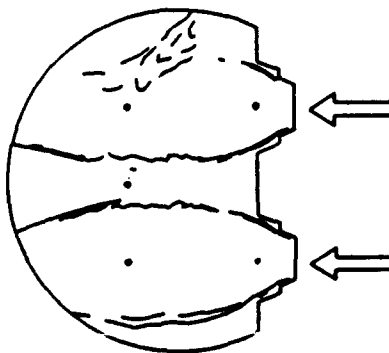
t approx. 2.0 seconds



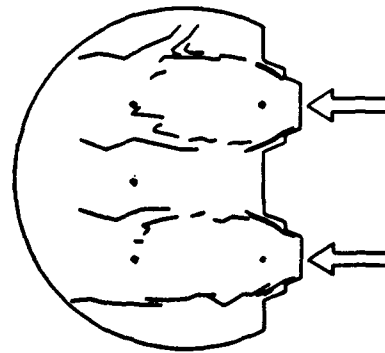
t approx. 3.0 seconds



t approx. 5.0 seconds



t approx. 7.0 seconds



t approx. 10 seconds

Figure 5.2 Cavity Flow Dynamics from High Speed Film

Pressure Data Analysis

Voltage readings from piezoresistive pressure transducers placed in the test apparatus were converted to pressure values by the computer program POSTRUN.BAS listed in Appendix B. This program also calculated mass flow rates of the air and helium supplies, nozzle exit Mach numbers and mixture specific heat ratios during a run.

Table 5.1 lists the run numbers and operating conditions for the most significant runs made. These runs were selected as most illustrative of effects of changes in specific heat ratio (γ), and effects of the presence or absence of the air/helium mixer.

Table 5.1 Run Numbers and Operating Conditions

Run Number	P _{He} (psig)	Mixer
020	0 Air Only	Yes
023	175	Yes
024	200	Yes
025	225	Yes
026	250	Yes
027	275	Yes
028	300	Yes
029	350	Yes
034	0 Air Only	No
035	225	No

To control the mixture γ value in the cavity the mass flow rate of helium was varied by increasing the helium injection pressure, P_{He} . Figure 5.3 shows the effect of increasing P_{He} on the mixture γ value. Trends are illustrated using a seventh degree polynomial best fit curve through all data points for a given P_{He} . The design γ value of 1.51 is approximately achieved by using a P_{He} pressure of 200 psig. Increasing the helium injection pressure increases the helium mass flow which consequently raises the γ value.

Figure 5.4 shows calculated (experimental) nozzle exit Mach numbers for various helium injection pressures. Trends again are depicted using a seventh degree polynomial best fit curve through all data points; however, to retain clarity only one third of the data points are displayed. The flow readily established velocities in the hypersonic range. Higher nozzle exit Mach numbers are achieved for increased P_{He} values. This is attributed to the increased gas γ values.

When results of experimental and theoretical exit Mach numbers are compared (equations 7 and 9, chapter 2) a Reynolds number effect is discovered. Figure 5.5 plots experimental and theoretical nozzle exit Mach numbers for a range of γ from 1.4 (air only) to 1.58 ($P_{He}=350$ psig). The boundary layer thickness, δ , is proportional to the inverse

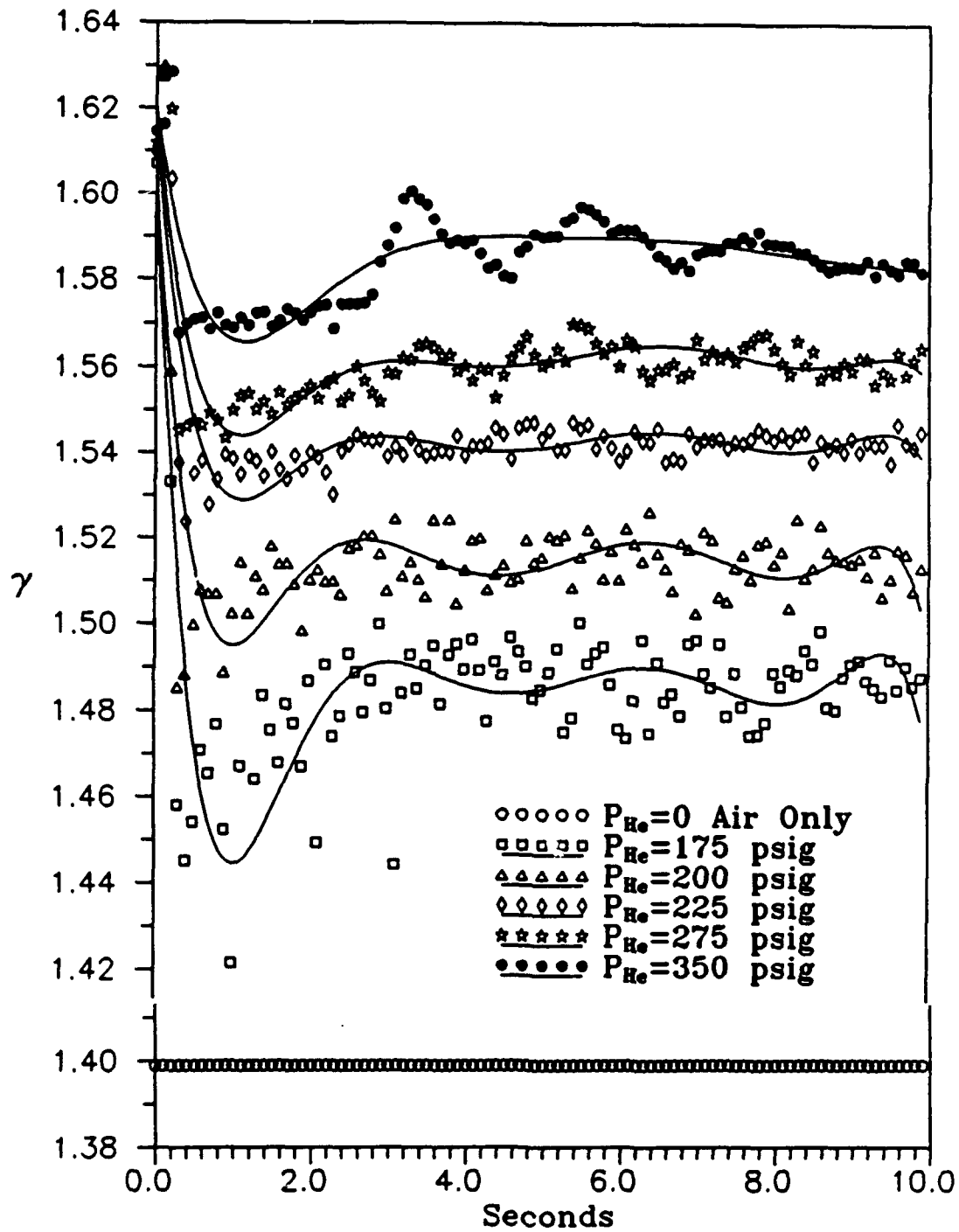


Figure 5.3 Specific Heat Ratios vs Time for Various P_{He} Values

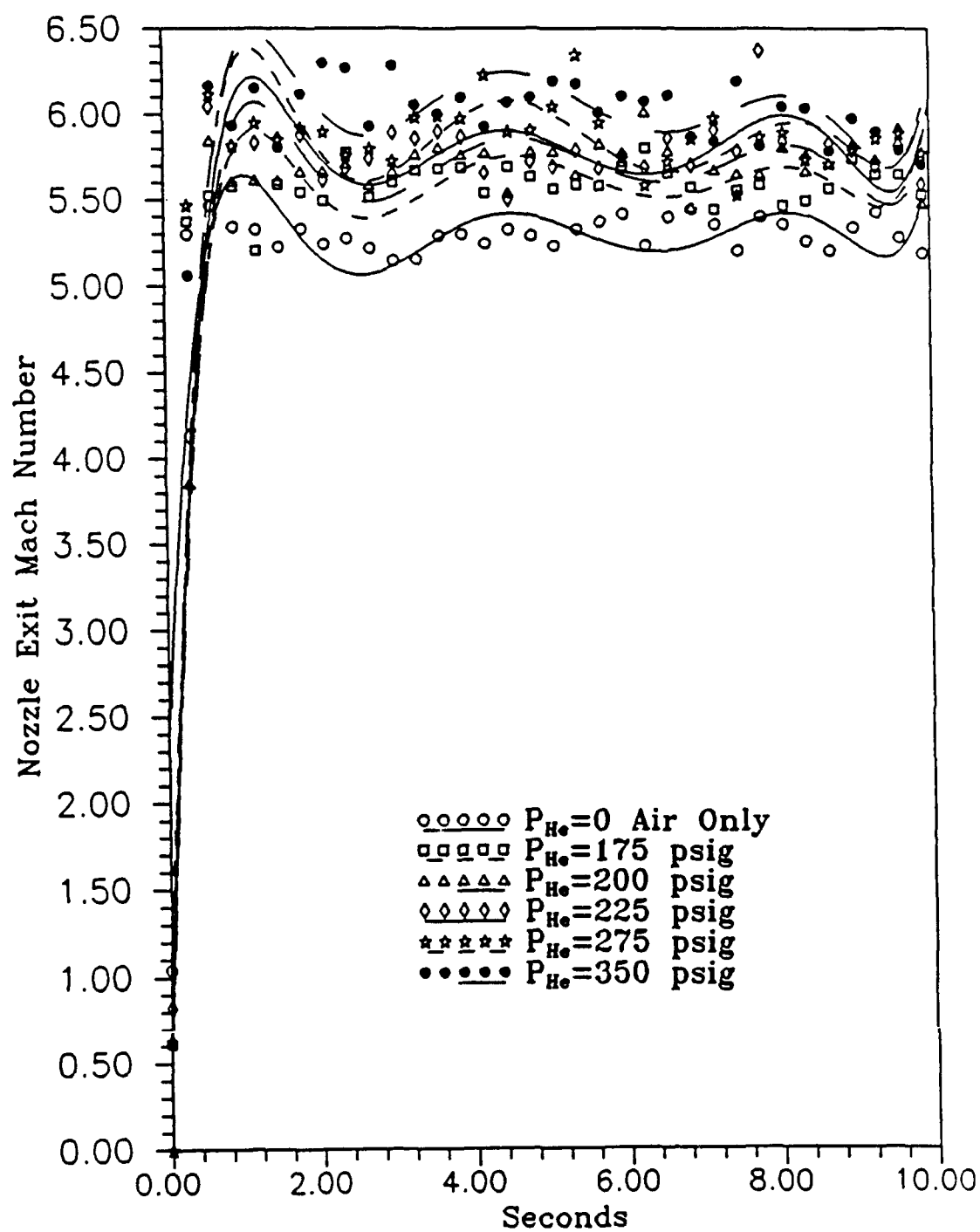


Figure 5.4 Nozzle Exit Mach Numbers for Various P_{He} Values

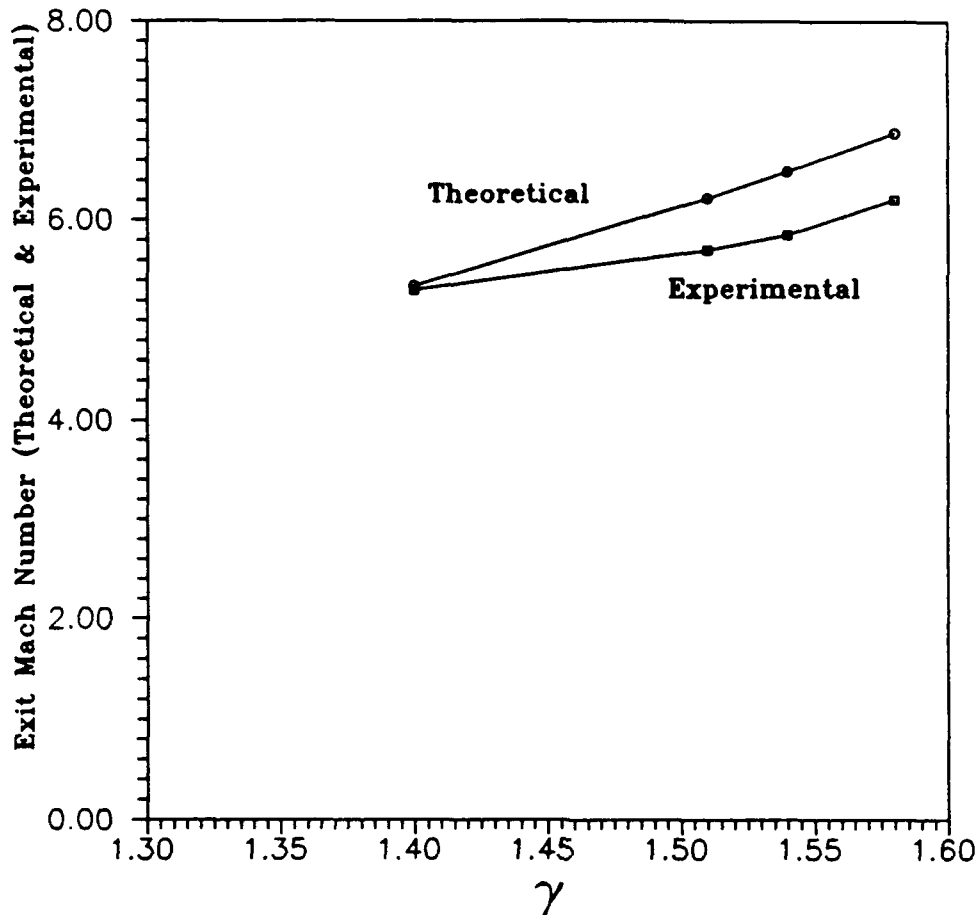


Figure 5.5 Experimental and Theoretical Nozzle Exit Mach Number Comparison

of the Reynolds number usually by a power law. Reynolds numbers at the nozzle throat were approximately 1.4×10^5 for flow with air only ($Re = Vh/\nu$) which relates to thin boundary layers and the isentropic assumption is valid (14). However, as helium is introduced into the flow γ increases as well as the acoustic velocity and kinematic viscosity of the flow medium. Also, the density and Reynolds numbers decrease which relates to an increase in δ along the nozzle

wall. This consequently decreases the effective area ratio (ϵ) of the nozzle and the exit Mach number diverges from the isentropic case as seen in Figure 5.5.

Figure 5.6 plots the horizontal stilling chamber pressure during the first 3 seconds of operation for various P_{He} values. Pressures remain at their 3 second value for the remainder of the 10 second run. Three runs in which helium was not injected into the system ($P_{He}=0$) demonstrate the repeatability of operating the test apparatus. Repeat runs were made for each condition examined with similar results; however, these were not plotted to retain clarity in the graphs. The air-helium runs indicated a slightly increased chamber pressure for increasing P_{He} settings. As helium is introduced into the mixer there is an increased lag before the initial pressure rise in the horizontal stilling chamber. This is probably due to the different methods used in triggering the data acquisition sequence for air-only or air-helium runs (refer to page 3-17).

To compare cavity pressure conditions under various P_{He} levels graphs of pressure versus time for several of the runs listed in Table 5.1 are presented in Figures 5.7 through 5.15. Each graph contains recorded pressure values in the lasing cavity over a ten second run viewed as a population. Stable pressure conditions in the cavity are characterized as low level (below approximately 0.25 psia)

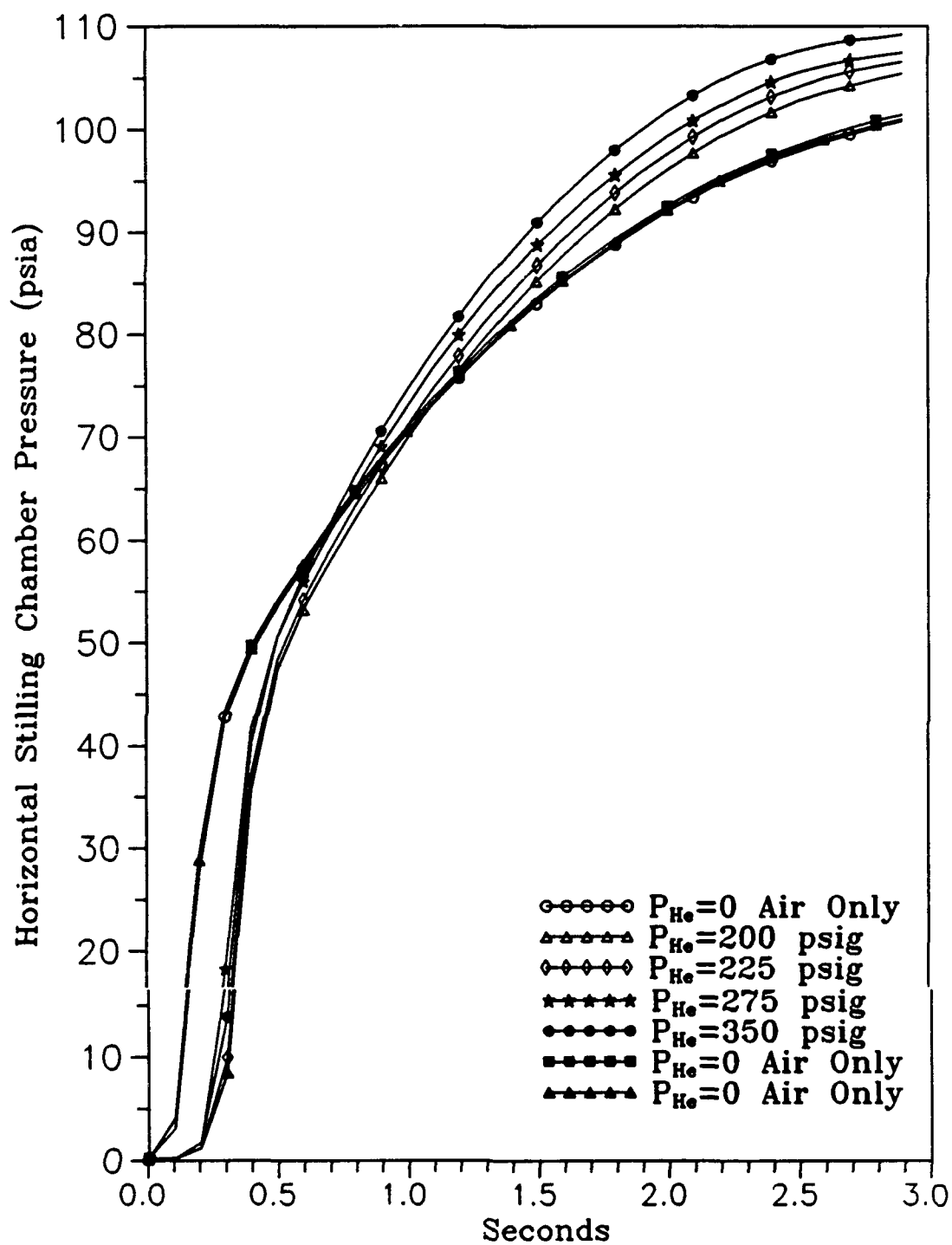


Figure 5.5 Horizontal Stilling Chamber Pressure vs Time for Various P_{He} Settings

maintained for as long a possible.

Figure 5.7 represents data obtained during run 029 which used a helium inlet pressure of 350 psig achieving an approximate γ of 1.58. This condition was considered the upper operating limit of the test apparatus as unstable pressures prevailed and no stable performance time was observed. This condition was compared to other operating conditions but will not be presented in any further data correlations as no beneficial information was found.

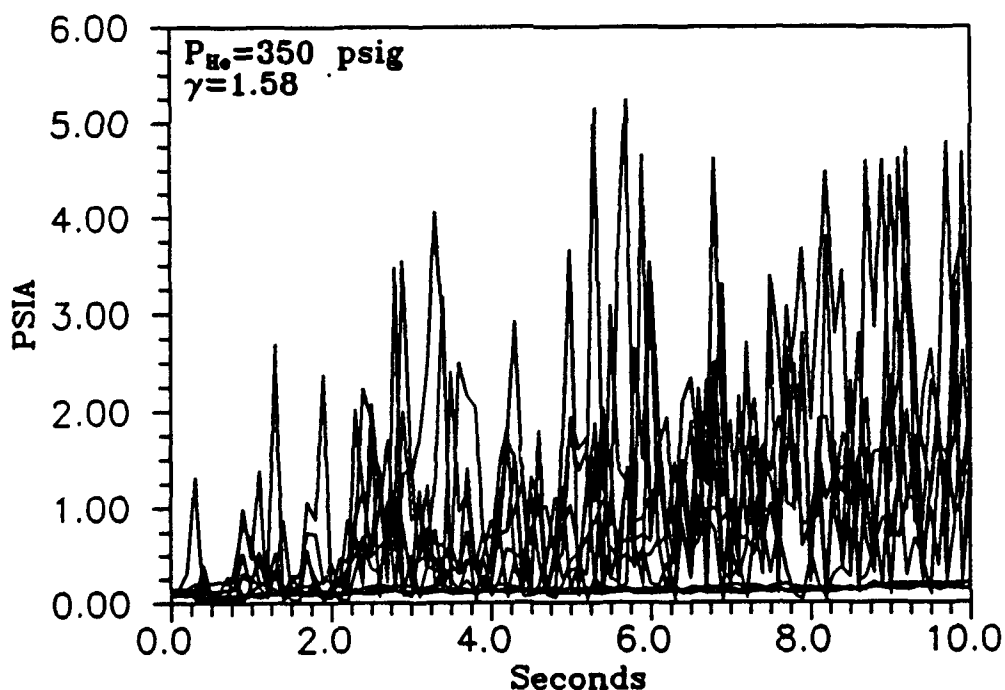


Figure 5.7 Cavity Pressures vs Time for Run 029
($P_{He} = 350 \text{ psig}$, $\gamma \approx 1.58$)

To examine the opposite end of the helium injection pressure range, a run was done with air only. Figure 5.8 plots pressures in the cavity during run 020, a typical ten second air-only run. Approximately 5 seconds of stable pressure performance occurs before the pressure fluctuations seen in Figure 5.8 appear. A pressure peak of approximately 1.0 psia at 0.1 second could indicate a shock passing through the system at start-up. Another around 4.0 seconds could be a precursor to the unstable behavior at 5.0 seconds. This would seem to indicate that the process of injecting helium into the mixer was at least partly

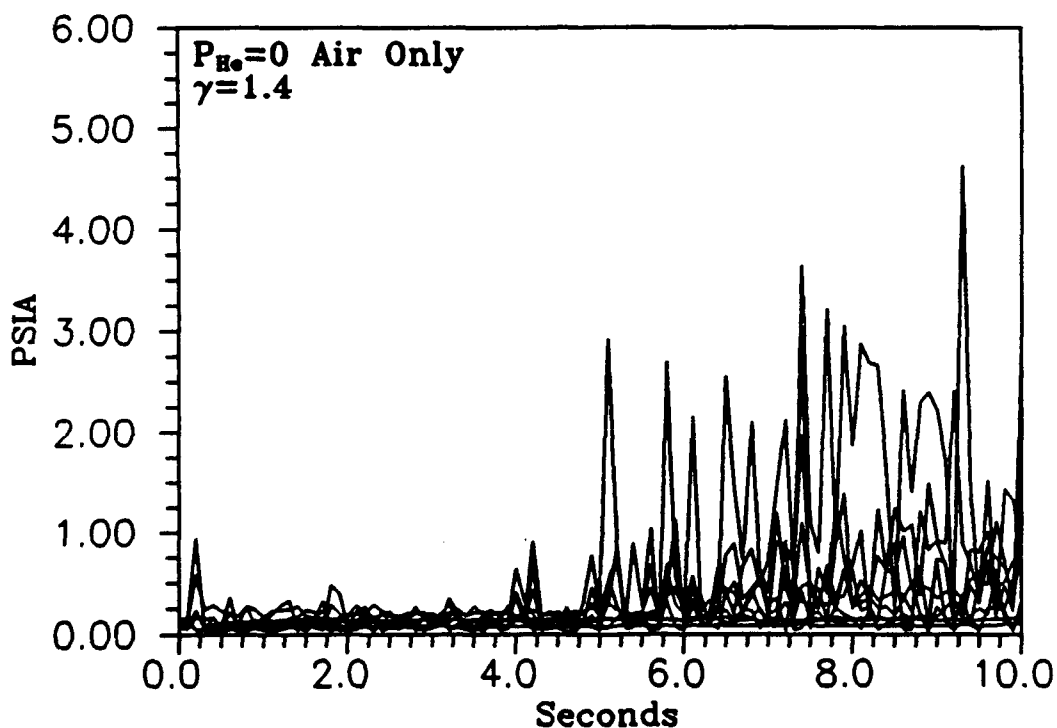


Figure 5.8 Cavity Pressures vs Time for Run 020
($P_{He}=0$, Air Only, $\gamma \approx 1.4$)

responsible for the onset of the unfavorable pressure behavior.

To discover another possible factor which may have caused the pressure fluctuations to occur, the mixer was removed and a ten second run was accomplished using the same air-only condition. Run 034 cavity pressure measurements are displayed in Figure 5.9. Stable performance occurred for the duration of the run which means that the mixer was also contributing to the onset of fluctuations as seen in Figure 5.8.

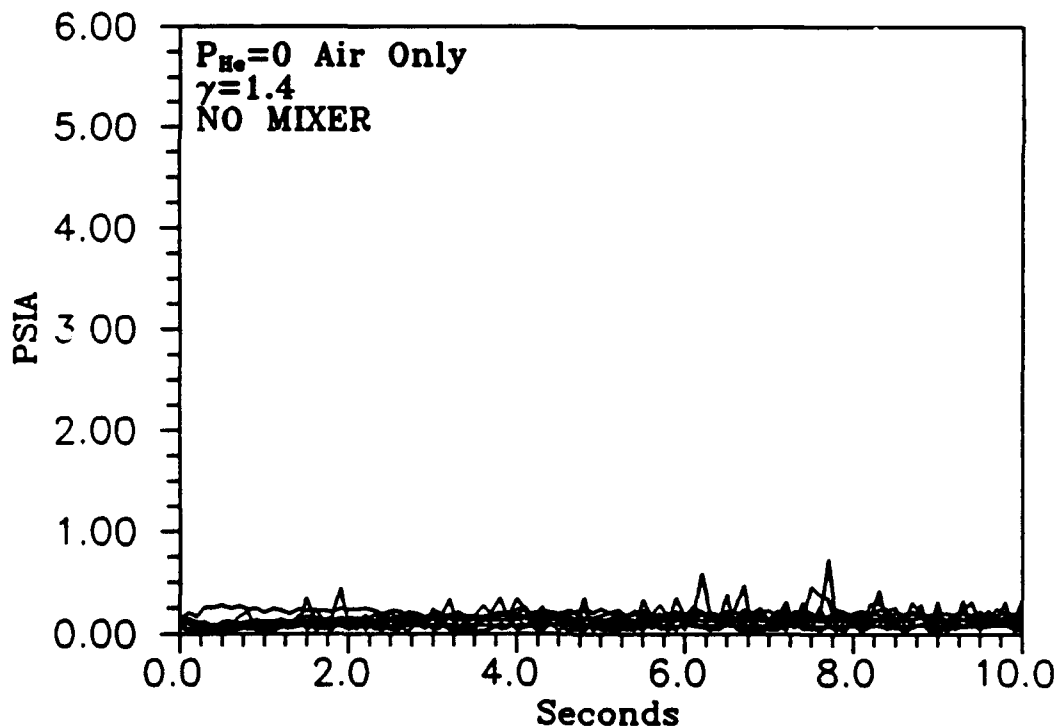


Figure 5.9 Cavity Pressures vs Time for Run 034
($P_{He}=0$, Air Only, $\gamma \approx 1.4$, No Mixer)

So stable run time is affected by the helium injection pressure and by the use of the mixer. Stable performance should be seen for runs made with P_{He} settings between the extremes of 0 and 350 psia. Figures 5.10 through 5.13 verify this trend for runs made with the mixer installed.

Figure 5.10 shows pressure data in the cavity during run 023 which used a P_{He} value of 175 psig corresponding to an approximate γ value of 1.48 (see Figure 5.3). There was approximately 2.5 seconds of stable performance for this run.

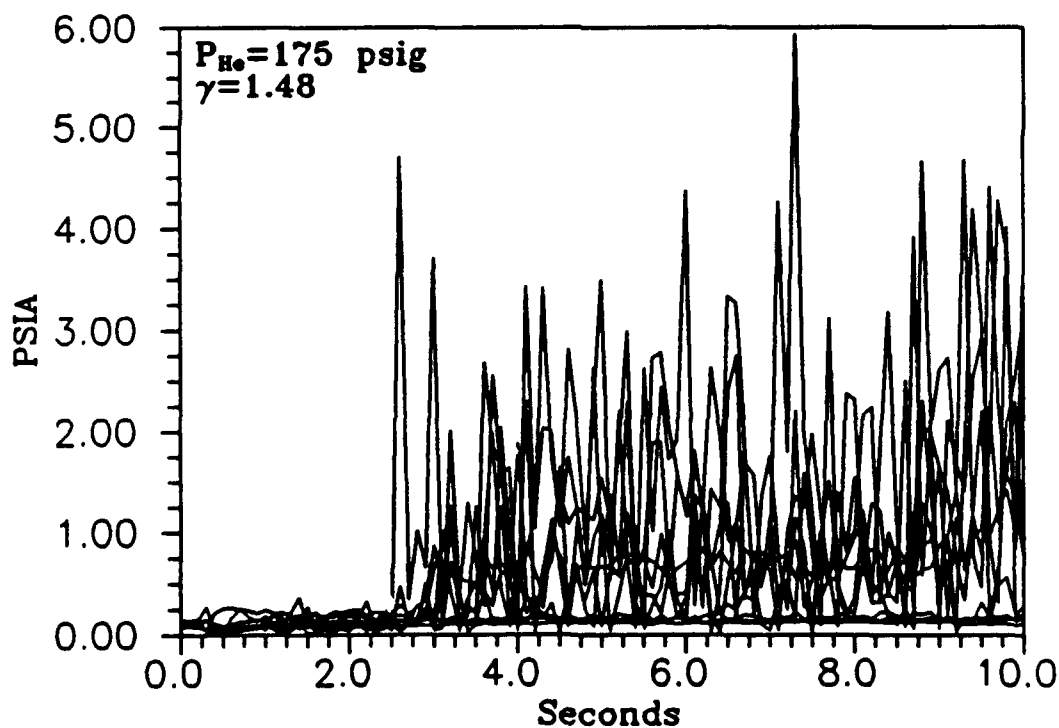


Figure 5.10 Cavity Pressures vs Time for Run 023
(P_{He} = 175 psig, $\gamma \approx 1.48$)

Run 024 pressure data (Figure 5.11) for a P_{He} setting of 200 psig reveals approximately the same stable time as run 023, 2.5 seconds. The 25 psig delta from 175 to 200 psig did not influence the stability time. It should be noted that this case provided the γ value most near the nozzle design γ of 1.51.

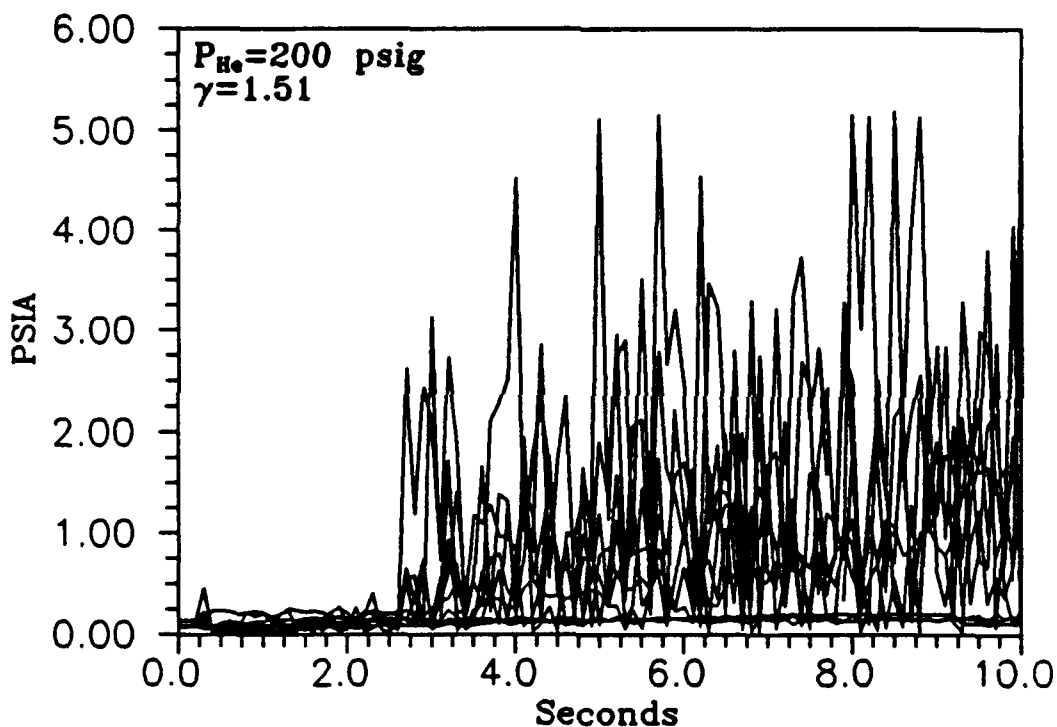


Figure 5.11 Cavity Pressures vs Time for Run 024
($P_{He}=200$ psig, $\gamma \approx 1.51$)

Increasing the helium injection pressure to 225 psig ($\gamma \approx 1.54$) decreased the stable run time to approximately 2.25 seconds as seen in Figure 5.12.

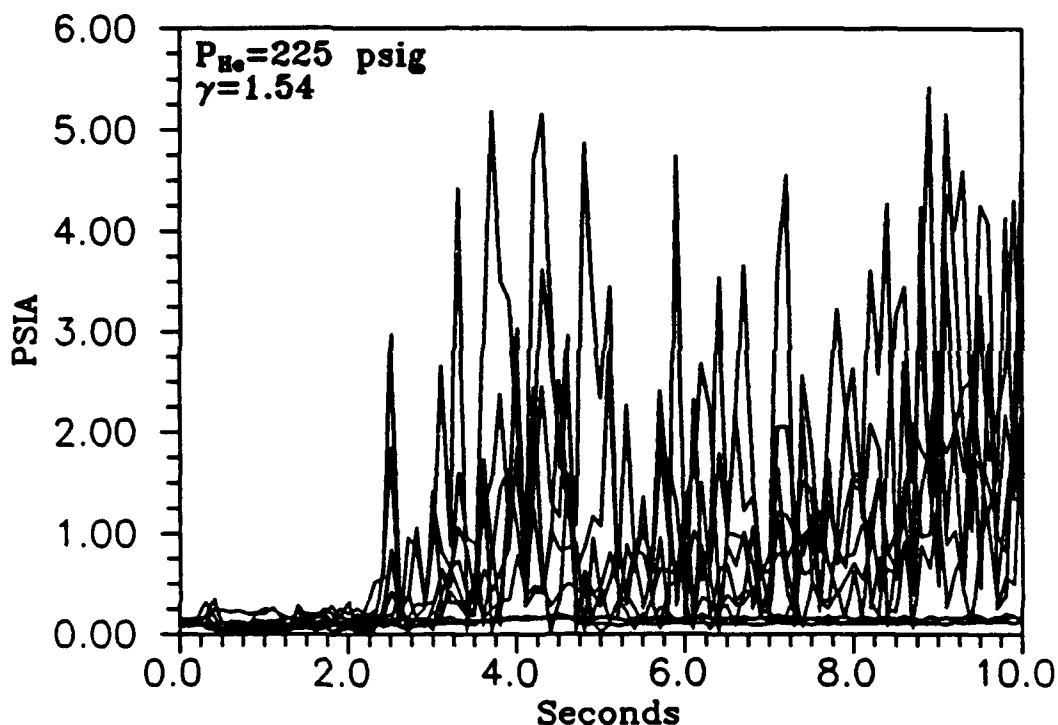


Figure 5.12 Cavity Pressures vs Time for Run 025
($P_{\text{He}}=225$ psig, $\gamma \approx 1.54$)

Figure 5.13 displays the decrease in stable run time to 1.8 seconds as P_{He} was increased to 275 psig in run 027 ($\gamma \approx 1.56$).

A final configuration was examined in which the mixer was removed and helium was injected directly into the air stream. Mixing of the air and helium was then by turbulent and molecular diffusion. Figure 5.14 shows the pressure data for this case, run 035, which used a P_{He} of 225 psig. When compared to run 025 (Figure 5.12) the influence of the mixer on the onset of the pressure fluctuations becomes evident. An increase in stable run time to approximately

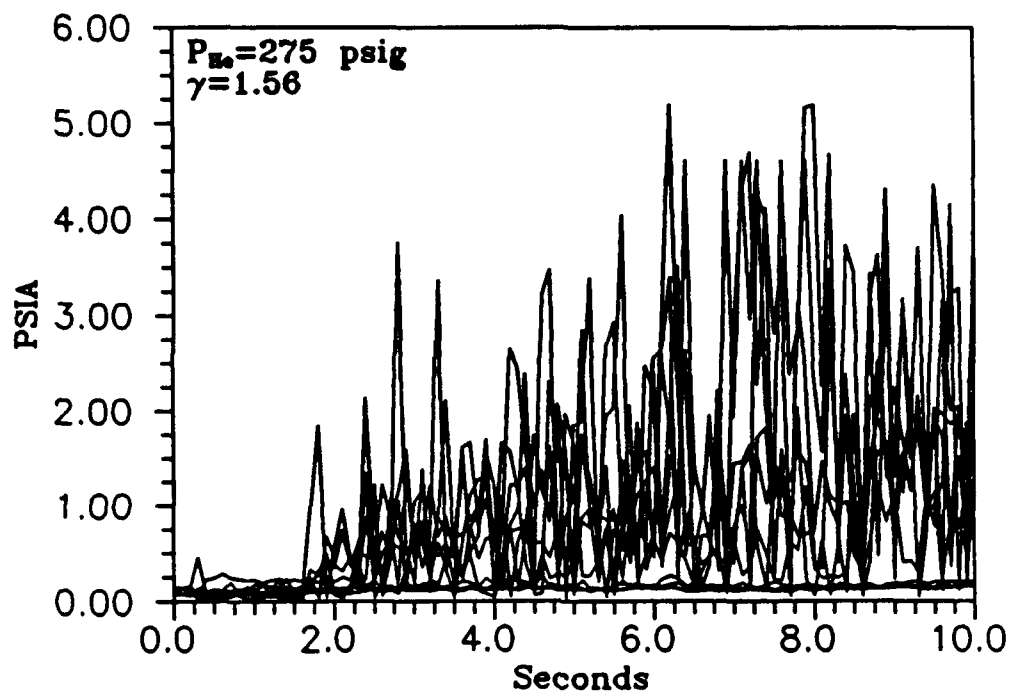


Figure 5.13 Cavity Pressures vs Time for Run 027
($P_{He}=275$ psig, $\gamma \approx 1.56$)

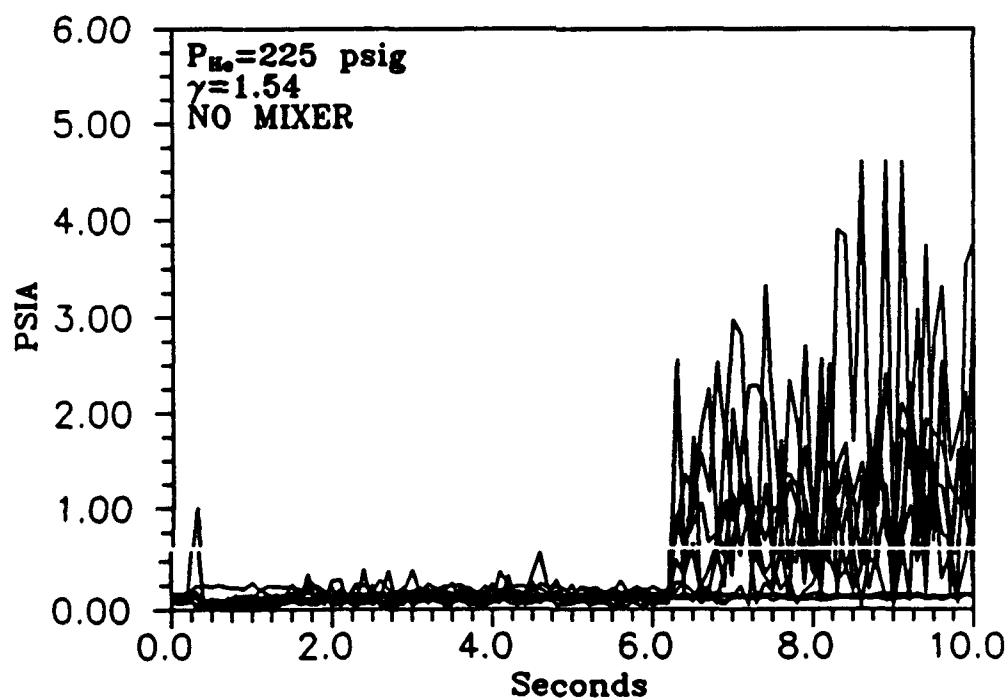


Figure 5.14 Cavity Pressures vs Time for Run 035
($P_{He}=225$ psig, Nc Mixer)

6.0 seconds occurred.

This would indicate that a different form of mixing the air and helium supplies is warranted if test times with longer stability are desired. However, it should be understood that a stable run time of approximately 2 seconds is long compared to the short duration of most chemical lasers. Reference 15 gives pulse durations in the microsecond range.

A closer examination of the γ values plotted in Figure 5.3 may reveal a relation between the oscillating trends of those γ s and the pressure fluctuations in the cavity.

Figure 5.15 graphs γ during a 3 second duration for 3 cases, $P_{He}=200$ psig, $P_{He}=225$ psig, and $P_{He}=225$ psig sans mixer. Note that the case in which the mixer was removed does not provide a stable γ as it begins lower than its counterpart with the mixer installed and slowly increases to approximately 1.53. Also notice the oscillating pattern of the trends represented using a seventh degree polynomial best fit curve. Since the values for γ are calculated from experimental data, in particular the mass flow rates of air and helium for a given run, an examination of those variables is warranted.

Mass flow rates for runs 025 and 035 which used a P_{He} setting of 225 psig with and without the mixer installed are plotted in Figure 5.16. The mass flow rate for air in both

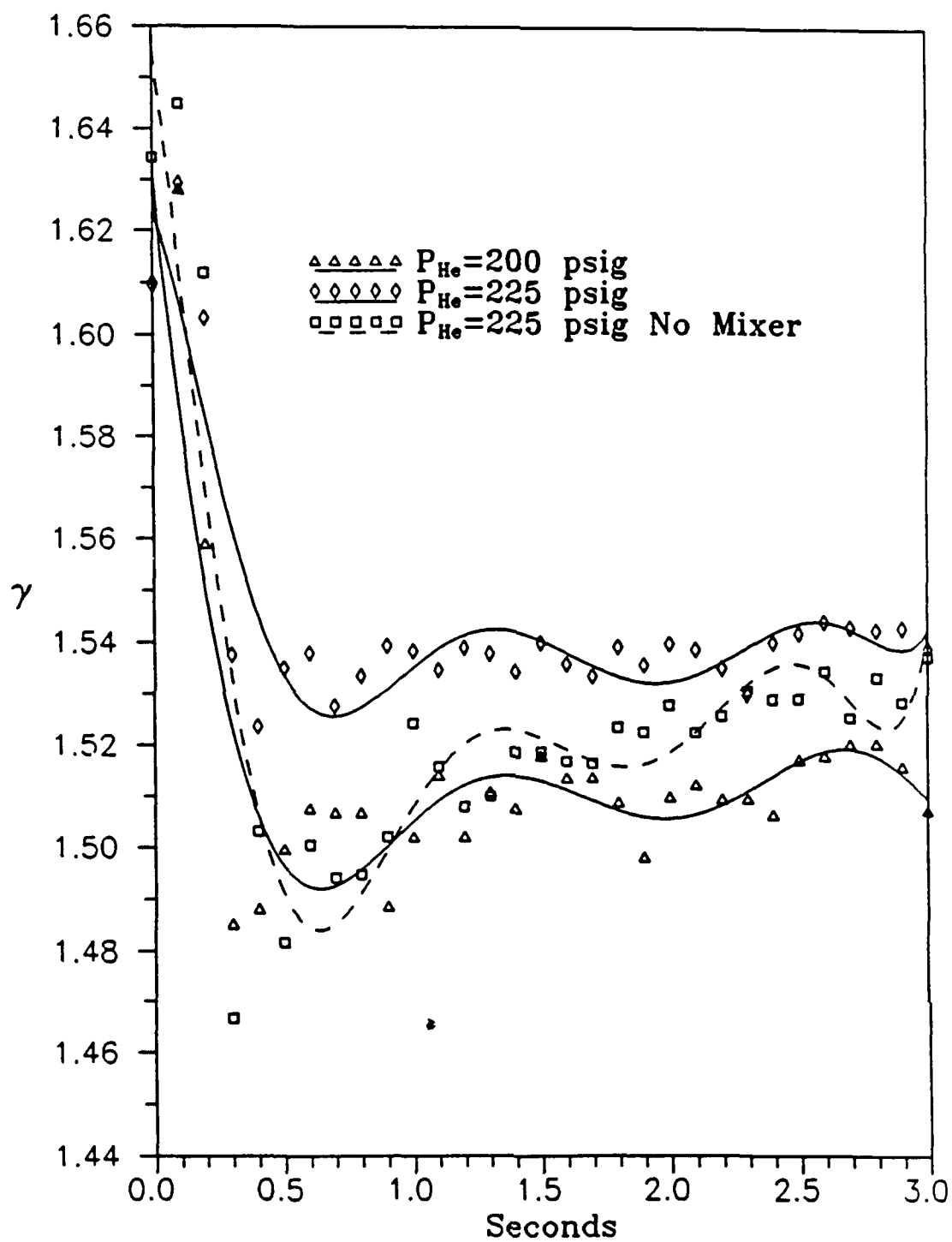


Figure 5.15 Specific Heat Ratio Comparison

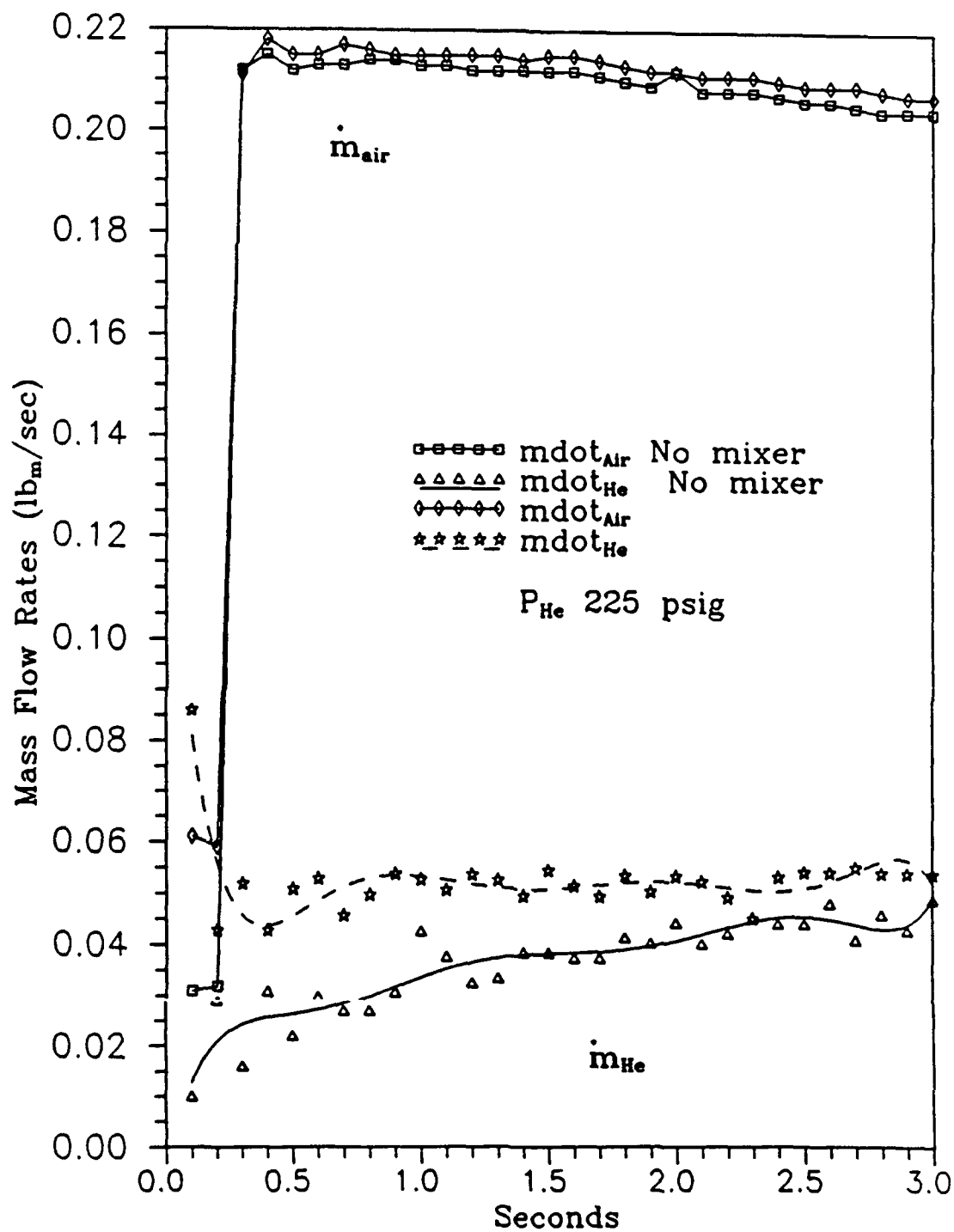


Figure 5.16 Air and Helium Mass Flow Rates

cases remains fairly stable with a slightly negative slope. The helium mass flow rates however exhibit trends similar to those of γ in Figure 5.15. Note the same increasing trend in the helium mass flow for the non-mixer case as seen in the γ value.

The mass flow calculation for helium is a function of the helium supply pressure upstream of the venturi meter and the differential pressure across the venturi throat. Examination of the helium supply pressure (position 32) revealed stable pressure at approximately 500 psia. When the differential pressure across the venturi (positions 25-26) was plotted (Figure 5.17) the trends were nearly identical to that of the γ values (Figure 5.15). Further investigation of the helium supply pressure and differential pressure is needed to determine whether a direct relation exists between the oscillations seen in γ trends and the pressure fluctuations seen in the cavity.

Focussing attention on the initial pressure responses in the cavity during the first two seconds of operation, the following graphs of pressure versus time at each transducer location were generated. Figures 5.18 through 5.30 display the pressure history at each position for air-helium runs 023, 024, 025, and 027 made with the mixer installed to determine possible effects of varying γ . Refer to Figure 3.8 for position number locations.

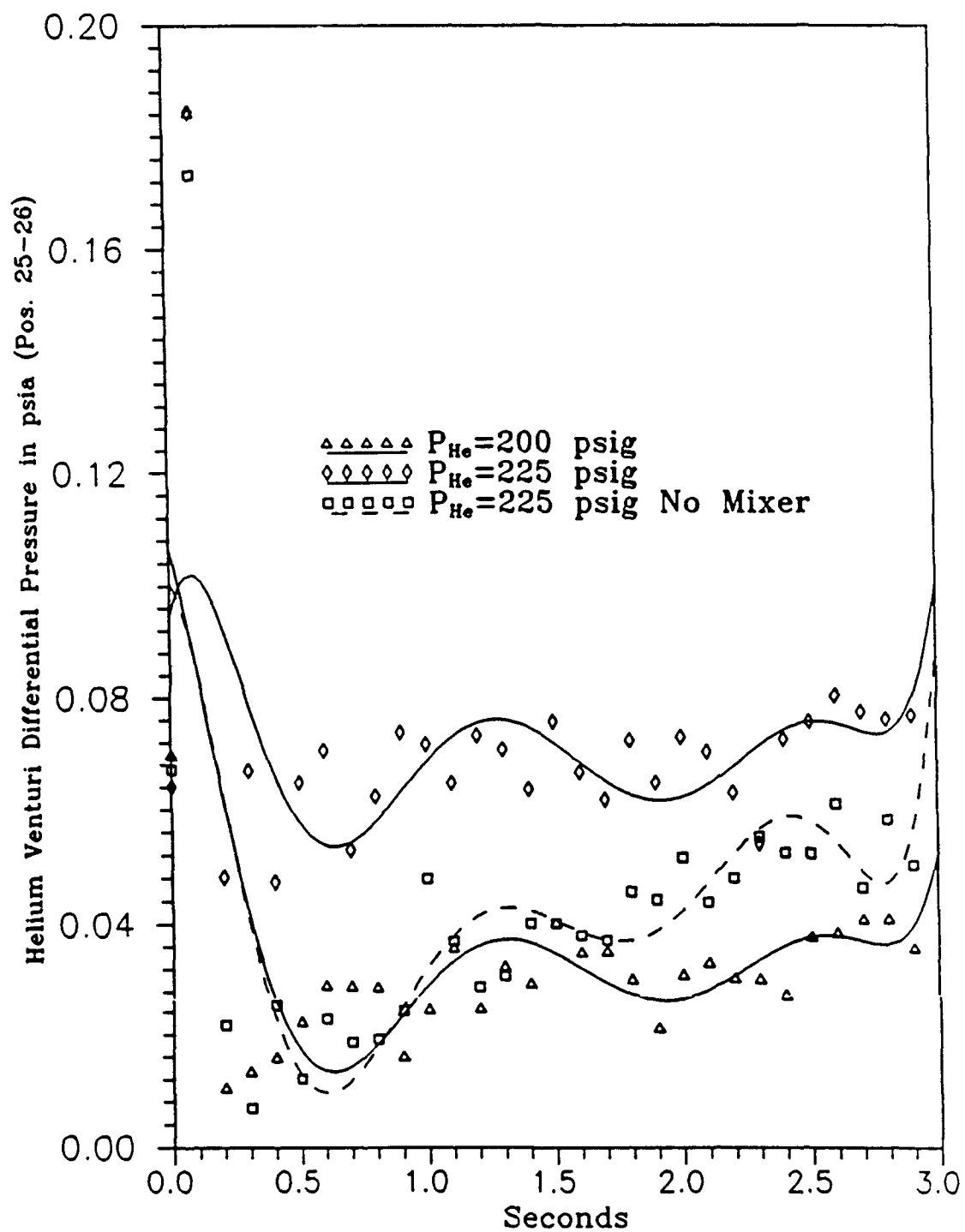


Figure 5.17 Helium Venturi Meter Differential Pressures

Figure 5.18 displays static pressure histories for position 1. Behavior for each run is similar and no effect of increasing γ can be discerned. An initial pressure drop to approximately 0.04 psia indicates the starting of the system followed by a gradual increase in pressure to a stable level at approximately 0.1 psia. This trend of gradually increasing pressure is a reflection of the upstream horizontal stilling chamber pressure which is in transition to its maximum as previously seen in Figure 5.6.

The base pressure at position 2 (Figure 5.19) also drops initially and increases gradually. The pressure in this base region fluctuates more than at position 1 which could be attributed to the recirculation characteristic of the flow at the base.

Position 3 pressures shown in Figure 5.20 resemble those recorded at position 1 with no apparent γ effect observed.

Nozzle exit pressures at positions 17 and 18 are plotted in Figures 5.21 and 5.22 respectively. Behavior reflects that seen from the base transducers (positions 1 through 3) and γ seems to have no effect on the amount of initial pressure drop.

Moving downstream, into the cavity, 2 second pressure histories for column 3 of the test cavity are presented in Figures 5.23 through 5.25.

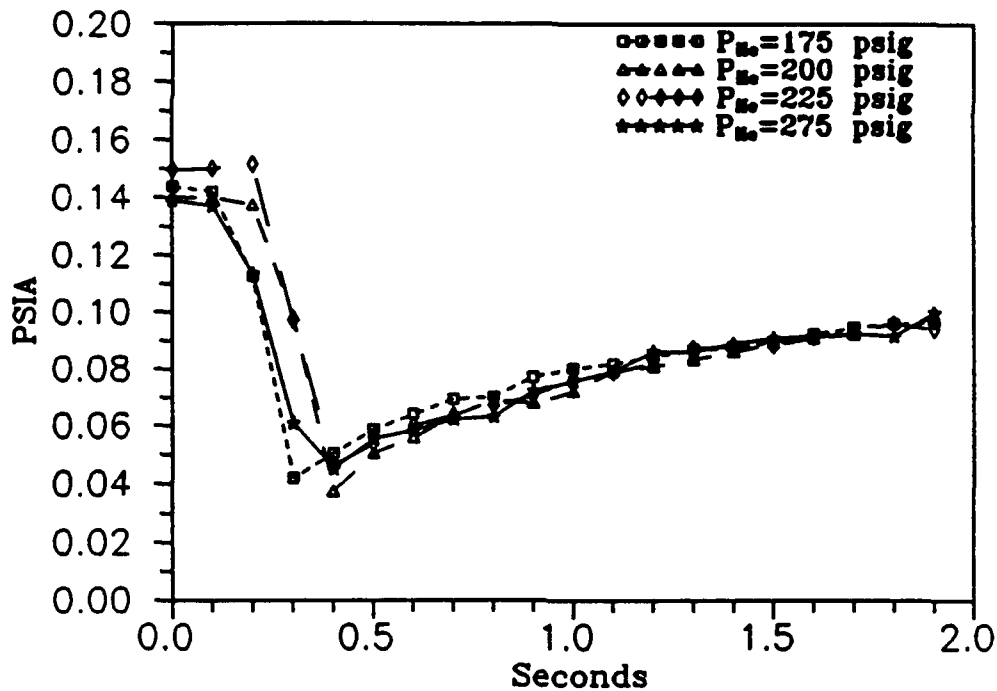


Figure 5.18 Position 1 Pressure History for Various P_{He} Values

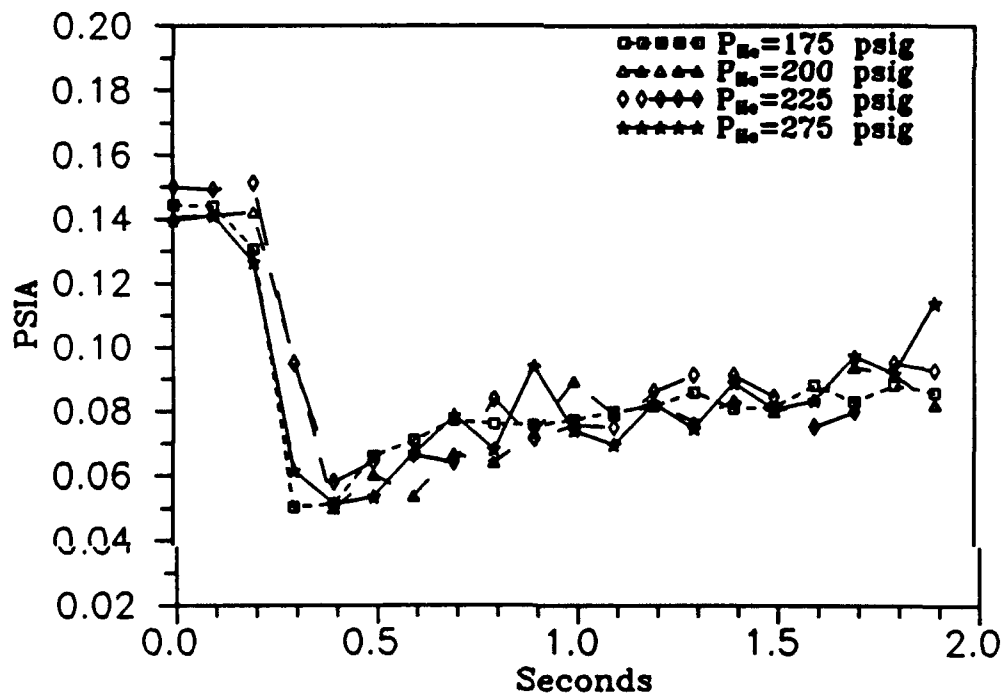


Figure 5.19 Position 2 Pressure History for Various P_{He} Values

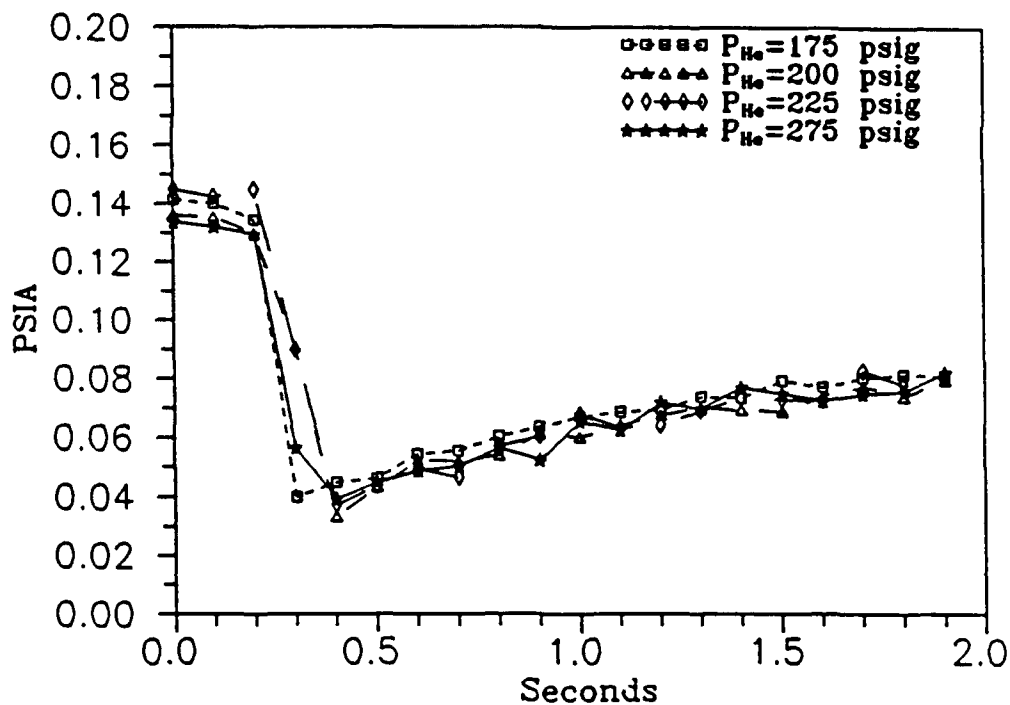


Figure 5.20 Position 3 Pressure History for Various P_{He} Values

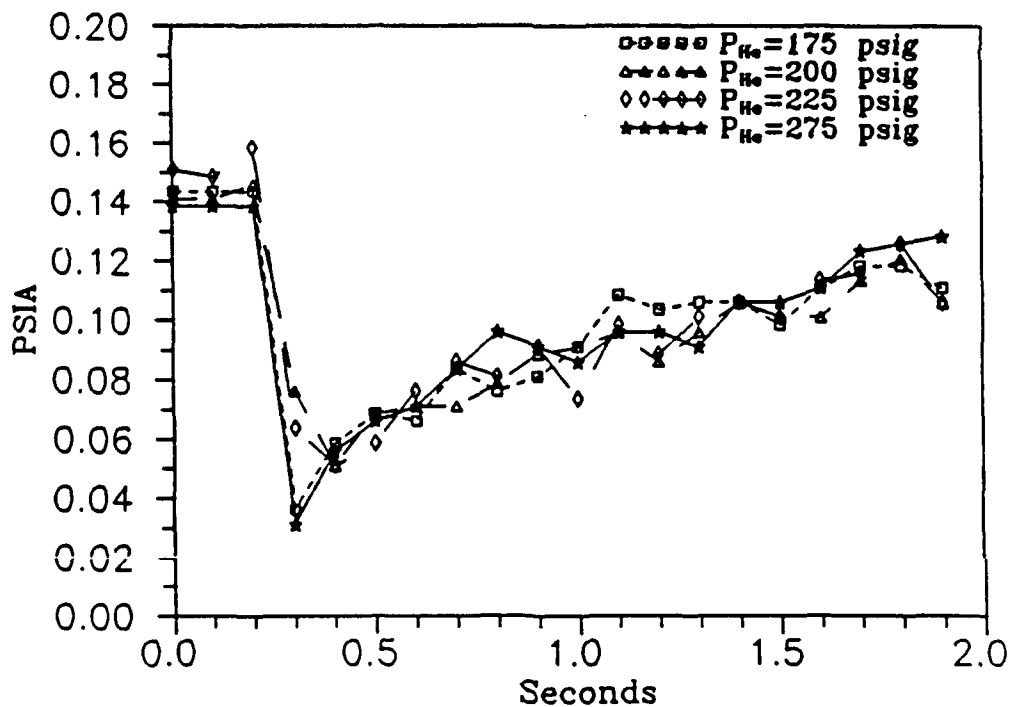


Figure 5.21 Position 17 Pressure History for Various P_{He} Values

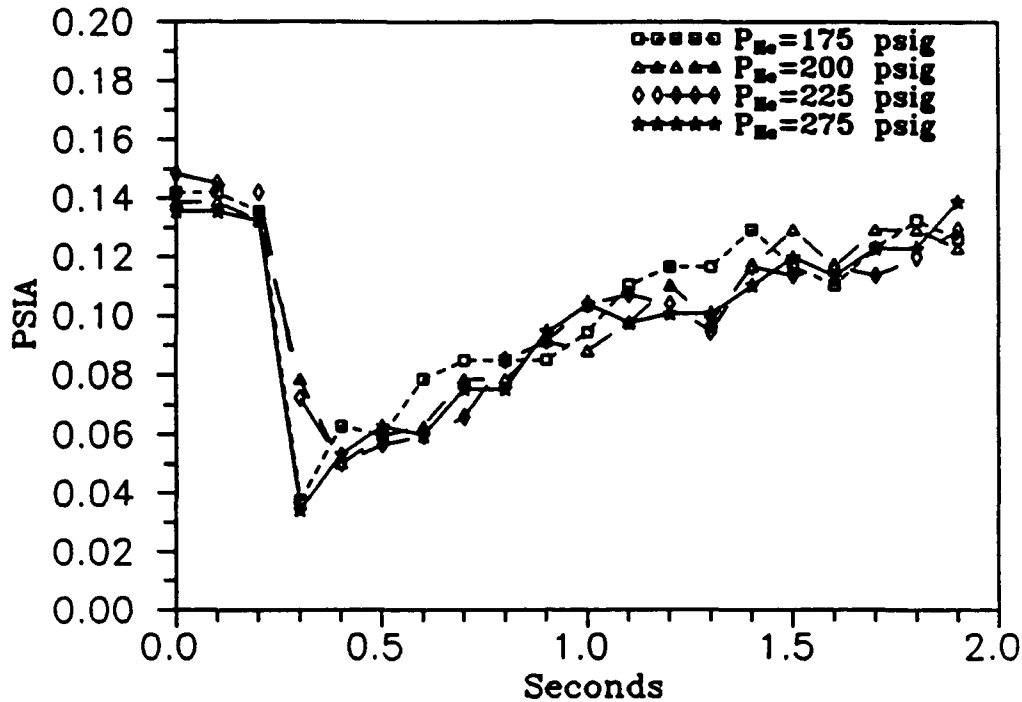


Figure 5.22 Position 18 Pressure History for Various P_{He} Values

Position 14 (Figure 5.23) pressures are similar to those observed upstream. This is contrary to what is expected from theory. If the flow is expanding from the nozzle exit into the cavity, pressure should decrease downstream relating to higher velocity. This phenomenon will be addressed further in a later discussion about Mach number. The onset of the pressure fluctuations is seen at approximately 1.6 seconds for run 027 when P_{He} is set at 275 psig.

Figure 5.24 displays the pressures for position 15. After the initial drop, pressures rapidly increase as the

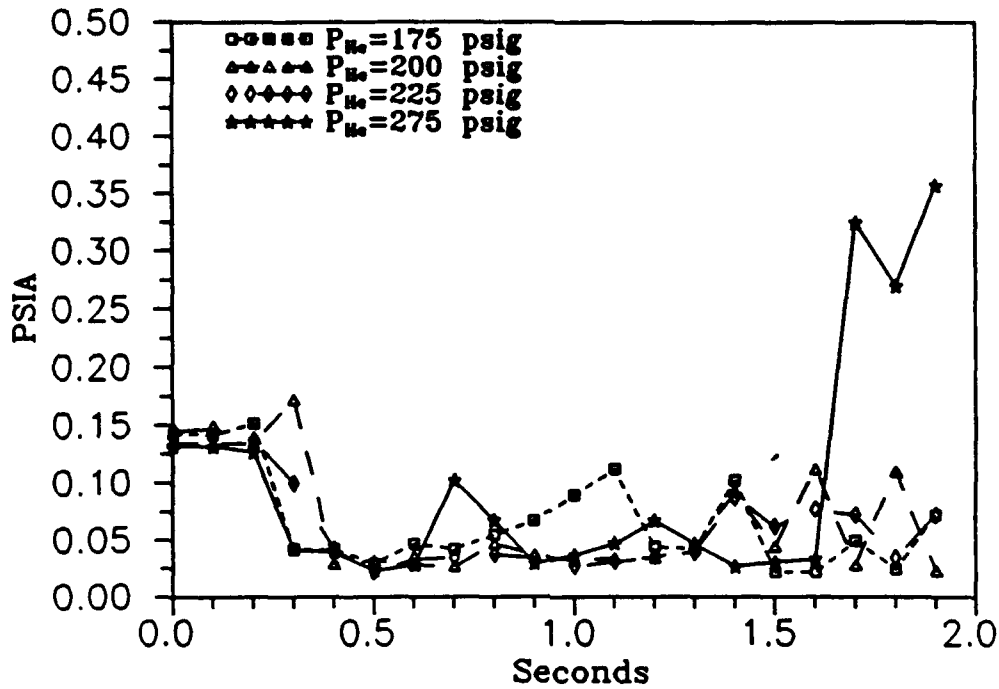


Figure 5.23 Position 14 Pressure History for Various P_{He} Values

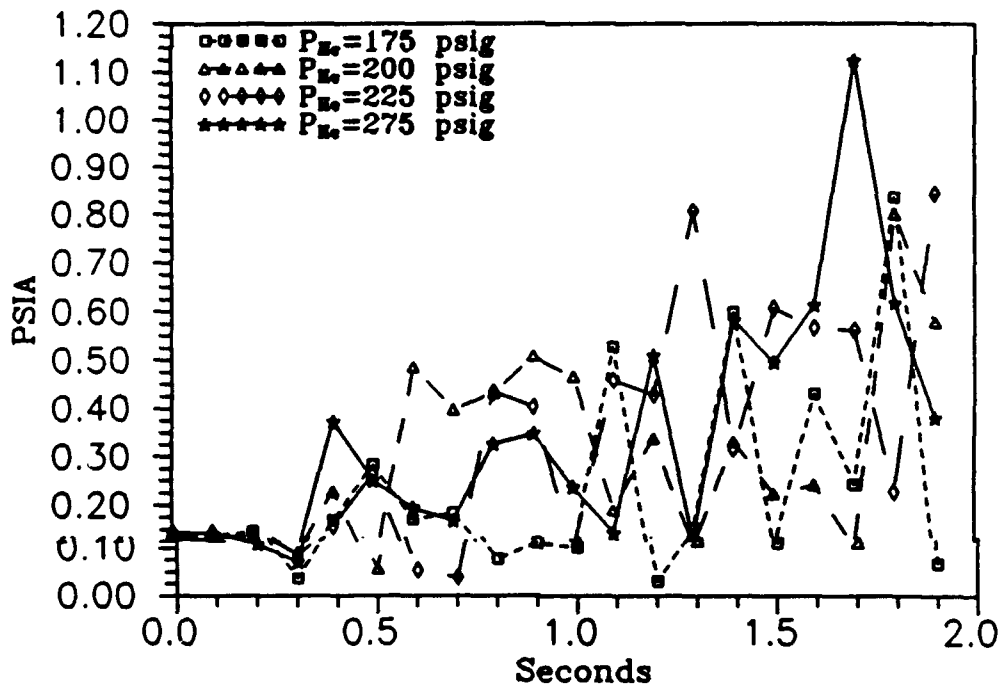


Figure 5.24 Position 15 Pressure History for Various P_{He} Values

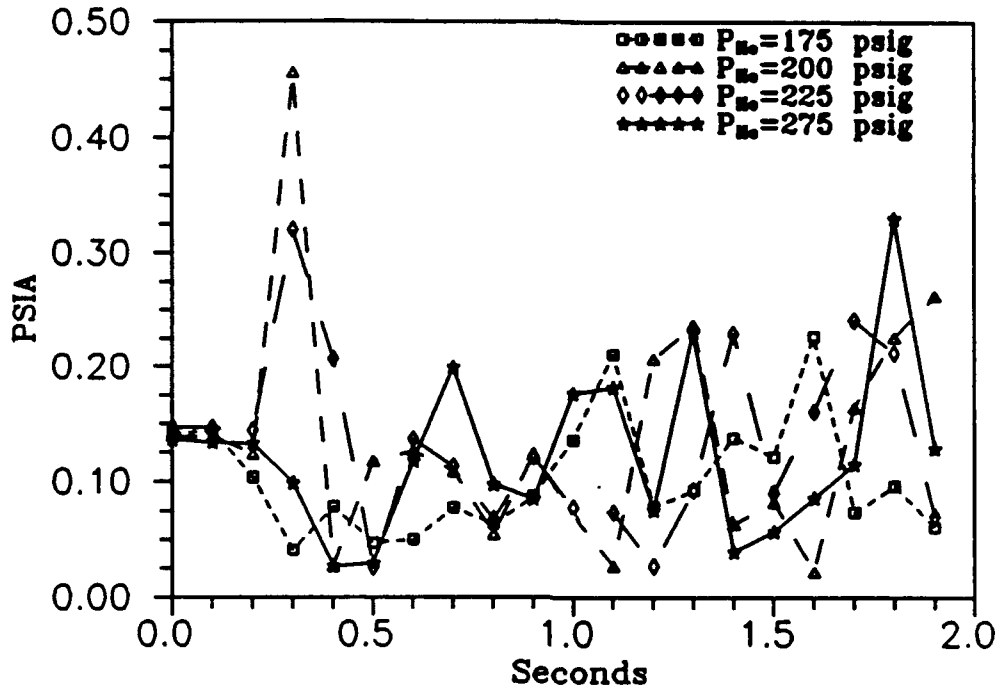


Figure 5.25 Position 16 Pressure History for Various P_{He} Values

base wake is established and the oblique compression shocks form. The onset of the unstable pressure fluctuations is again seen at approximately 1.6 seconds for the 275 psig case.

An interesting event is observed in the lower row of the cavity as seen in the pressure trends of position 16 (Figure 5.25). The runs with P_{He} set at 200, and 225 psig have a pressure spike at 0.3 seconds. Since the magnitude of the spike does not correspond to an increase in γ the effect is probably not attributable to that variable. Instead, the presence of a weak shock passing through the cavity during start-up is a more probable cause. This

start-up shock may not be captured during data acquisition due to its short duration and therefore does not appear in other run's pressure results.

Figures 5.26 through 5.28 show pressures for various P_{He} settings downstream along column 2 in the cavity.

Increased pressure trends in Figure 5.26 would indicate that the oblique shocks shown in Figure 5.1 may actually be crossing near position 11.

Position 12 pressures depicted in Figure 5.27 reflect reasonably stable performance with a dip in pressure of approximately 0.05 psia followed by a gradual increase. Boundary layer buildup along the cavity walls could be acting to diffuse the flow; lowering the velocity and raising the pressure.

Pressure data at position 13 in row 3 of the cavity (Figure 5.28) would also indicate oblique compression shocks crossing at that point.

Position 9 and 10 pressures are shown in Figures 5.29 and 5.30 respectively. The onset of unstable pressure behavior at both of these positions is again observed for the 275 psig case at approximately 1.6 seconds. Position 10 pressures shown in Figure 5.30 show the initial pressure peak previously seen which could be caused by a shock passing through the cavity.

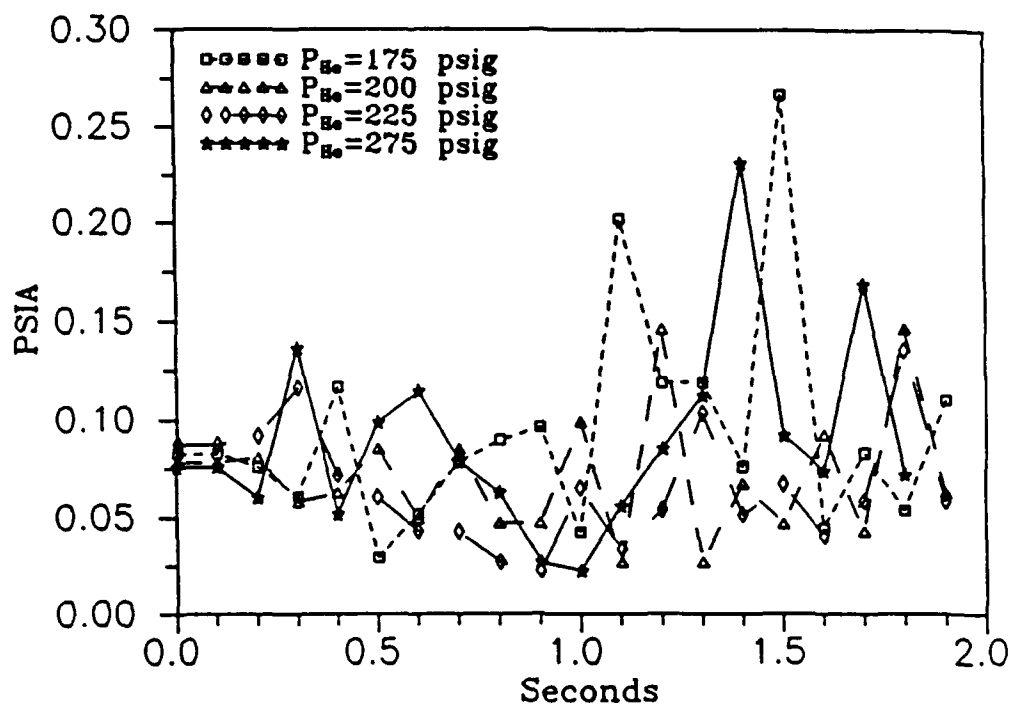


Figure 5.26 Position 11 Pressure History for Various P_{He} Values

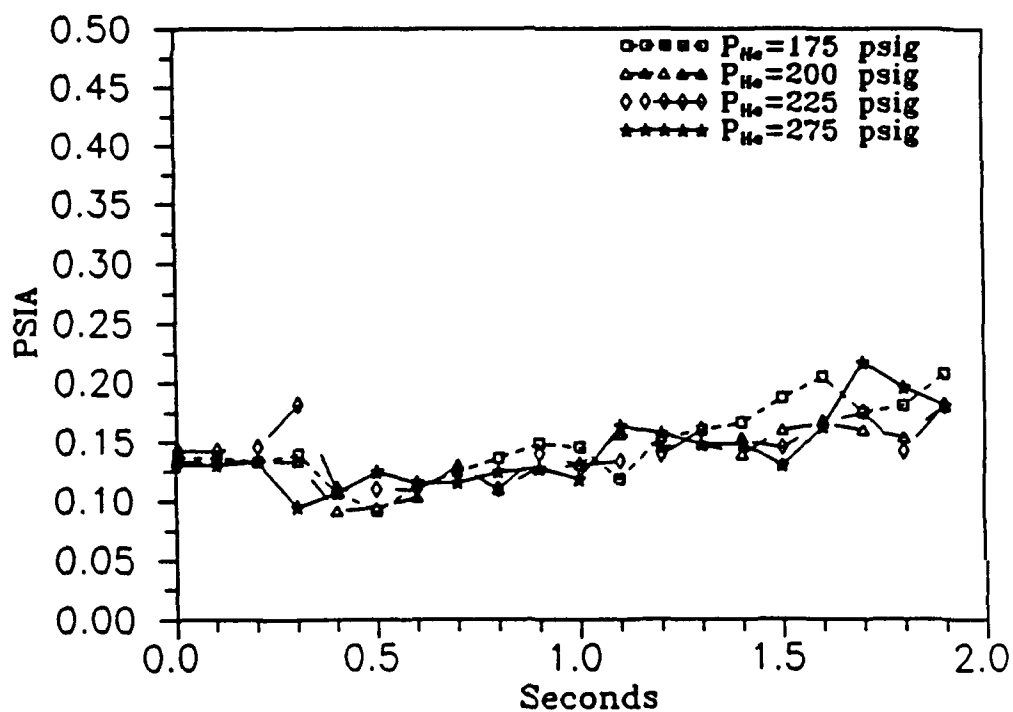


Figure 5.27 Position 12 Pressure History for Various P_{He} Values

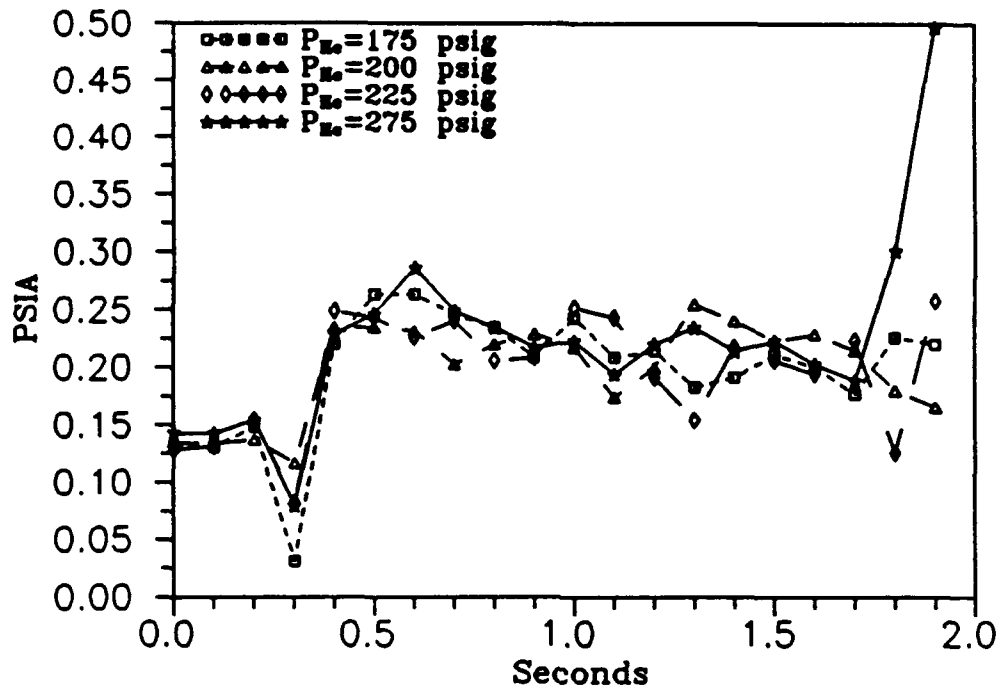


Figure 5.28 Position 13 Pressure History for Various P_{He} Values

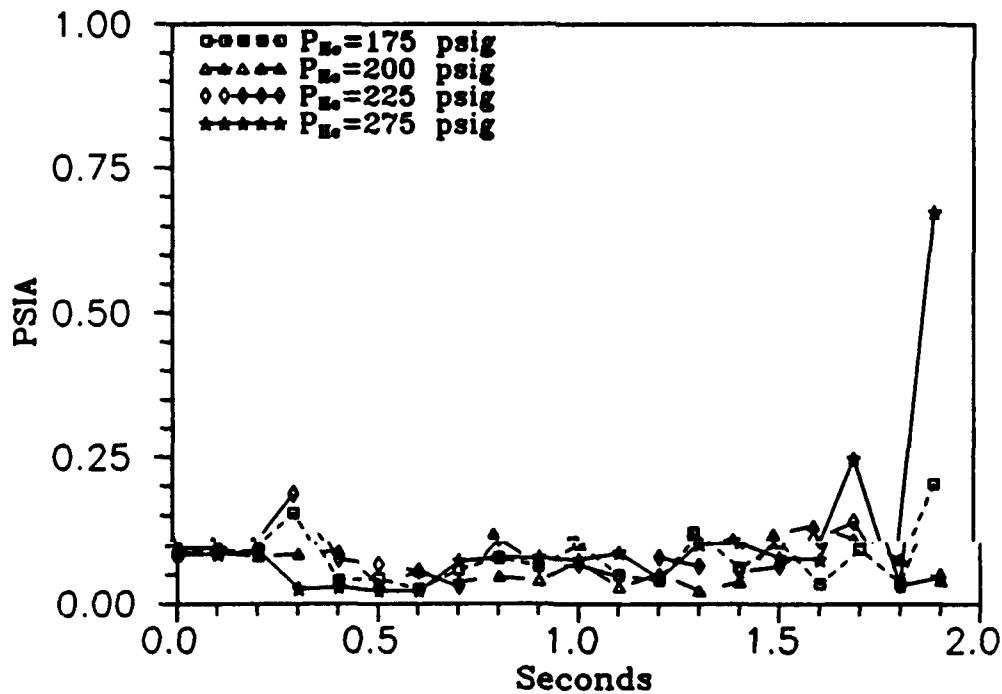


Figure 5.29 Position 9 Pressure History for Various P_{He} Values

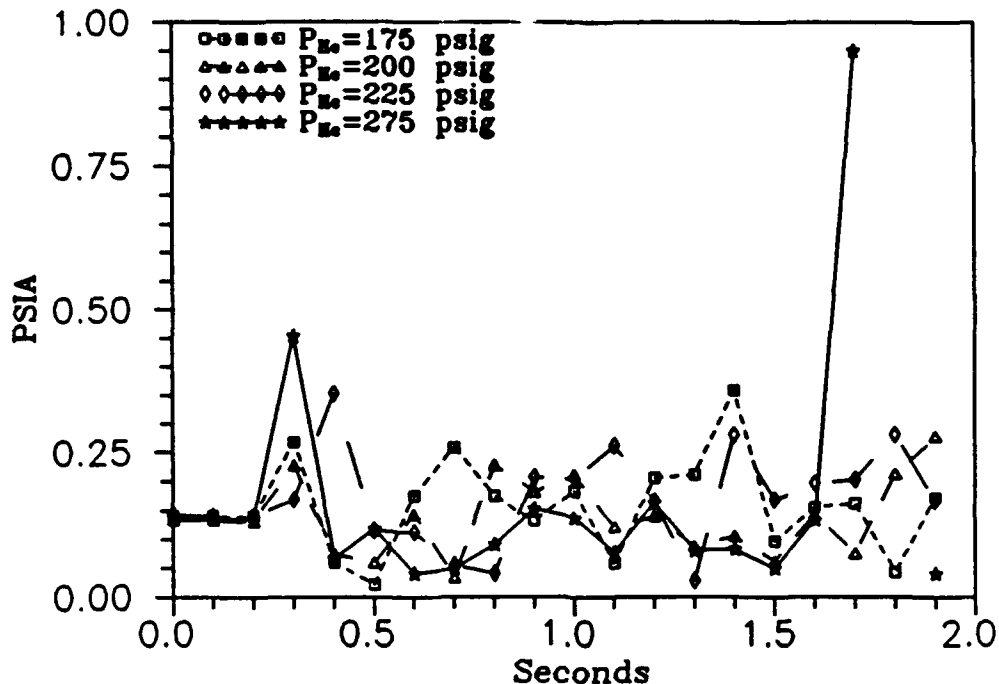


Figure 5.30 Position 10 Pressure History for Various P_{He} Values

To further examine the expected expansion of the flow into the cavity, Mach numbers at position 14 and 16 were calculated assuming isentropic flow to those locations. These Mach numbers are compared to Mach numbers calculated at the nozzle exits in Figures 5.31 and 5.32 for the cases of P_{He} at 225 psig with and without the mixer installed.

With the mixer present (Figure 5.31), unsymmetrical behavior in the cavity was observed as the row 1 Mach number at position 14 was greater than the Mach number at position 17 indicating expansion as the flow moved downstream. In the lower portion of the cavity, row 3 Mach numbers remained fairly constant.

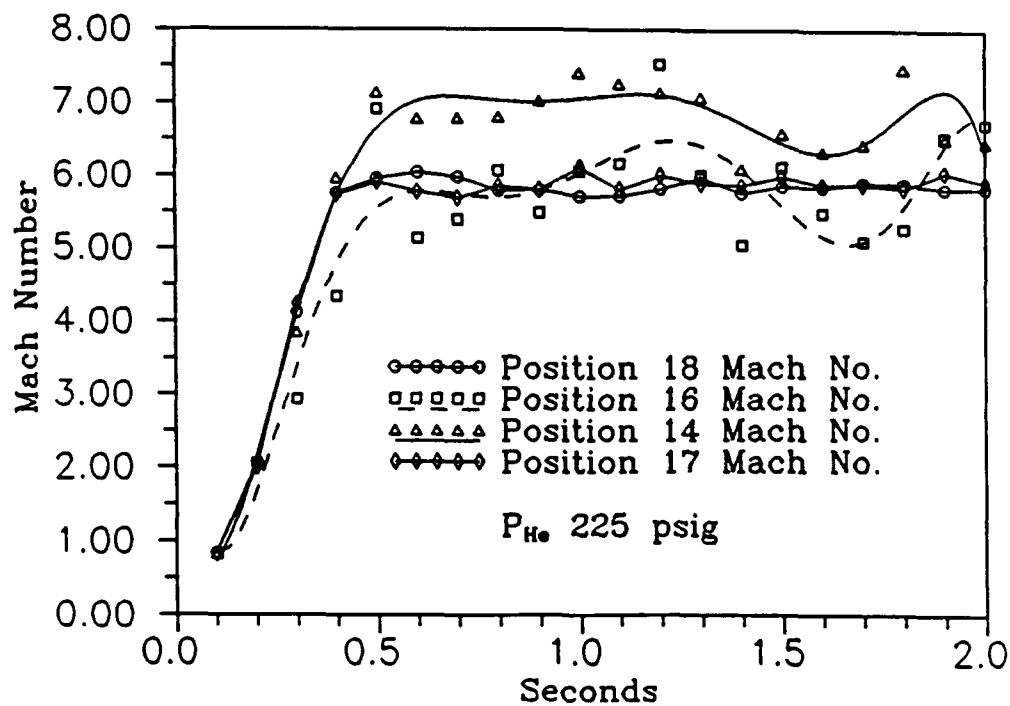


Figure 5.31 Cavity Mach Number Comparison with Mixer Installed

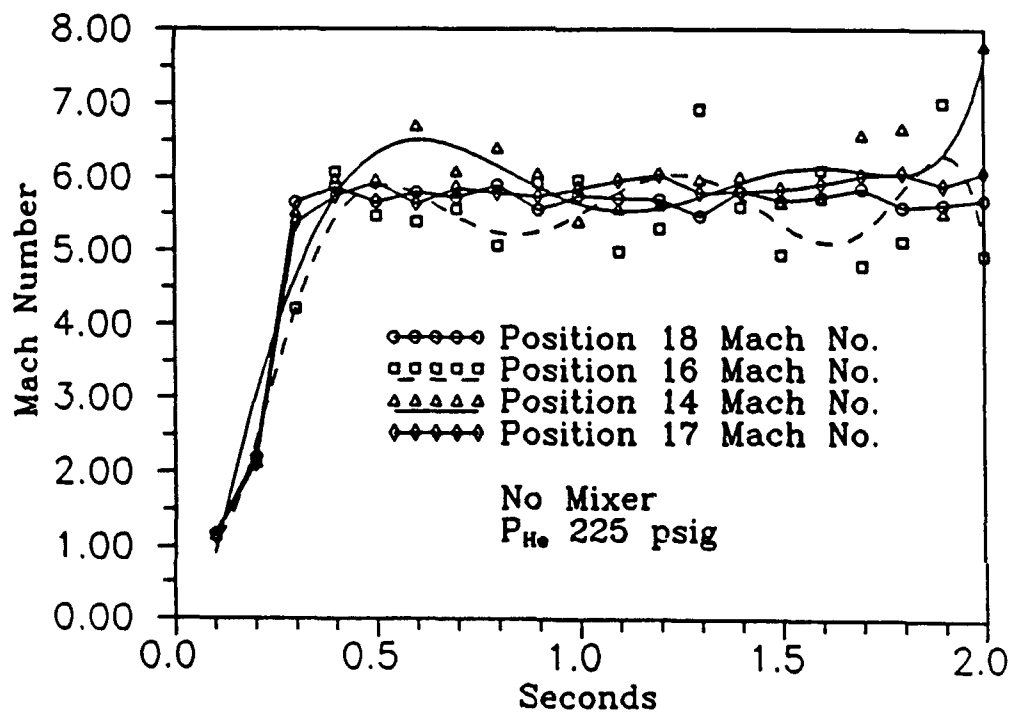


Figure 5.32 Cavity Mach Number Comparison sans Mixer

Mach numbers at position 14 and 16 with the mixer removed reflected their upstream levels as no distinct indication of expansion is seen in Figure 5.32.

Flow dynamics in the test cavity are very complex. Boundary layer growth along the upper and lower walls of the cavity as well as along the vertical sidewalls can contribute to increasing 3 dimensional effects as the flow moves downstream. This can cause a diffusing effect which cancels out the expected expansion into the cavity.

VI. Conclusions

An experimental investigation of the effect of varying the specific heat ratio for the flow through a simulated chemical laser cavity was accomplished. A survey of static pressures in the cavity, still schlieren photographs, and high speed schlieren film of the flowfield determined the behavior of the flow. The following conclusions were reached:

- (a) The equipment designed to supply helium to the system functioned to provide control of the mixture specific heat ratio of the air-helium flow. However, it was not determined if the injection of helium into the system was the direct cause of unstable pressure behavior.
- (b) For specific heat ratios ranging from approximately 1.40 to 1.56 the experimental apparatus provided similar cavity flow conditions. The length of stable run time (before pressure instabilities began) decreased as specific heat ratio was increased. The upper limit on specific heat ratio for this system was approximately 1.58 corresponding to a helium injection pressure of 350 psig which gave no favorable pressure behavior. At the nozzle design specific heat ratio of 1.51 the stable run time was approximately 2.5 seconds.

- (c) Increased specific heat ratio related to decrease Reynolds number and consequently increased boundary layer thickness. This caused a decrease in effective area ratio of the nozzles, thus exit Mach numbers were lower than the isentropic assumption predicted as specific heat ratio was raised from the level of approximately 1.4.
- (d) Boundary layer effects along the sidewalls of the test section tended to cancel out pressure expansion in the cavity. However, unsymmetrical pressure behavior indicated some expansion in the upper half of the cavity when the mixer was installed.
- (e) Use of the mixer decreased stable run time by introducing unstable pressure fluctuations earlier.

VII. Recommendations

Further investigation of the cavity flow dynamics in the simulated laser is recommended. To continue this research the following suggestions are presented:

- (a) Since it is desired to have the cavity operate at the nozzle design specific heat ratio of 1.51, a longer stable testing time would be beneficial. To achieve this, a new method of mixing the secondary helium supply with the primary air should be explored. A ring manifold mounted inside the 10 inch diameter air supply pipe with small helium supply perforations around its circumference could provide sufficient mass flow without adverse pressure effects. Or direct injection of the secondary helium at circumferential stations through the pipe itself could serve as a delivery system without positioning a body directly in the flow of primary air. Also, the addition of a concentration probe could be used to verify the mixture specific heat ratio.
- (b) The initial seconds of flow through the cavity is important. More rapid filling of the horizontal stilling chamber upstream of the supersonic nozzles would bring the system to operating condition more

readily. By decreasing the volume of the system prior to the test cavity the existing mass flow of air would facilitate a more rapid pressure response. Shortening of the horizontal stilling chamber downstream of the mixer location would benefit.

- (c) Addition of hypersonic wedges to more closely model the actual chemical laser nozzle system. Milling of the existing nozzle segments to attach several rows of hypersonic wedges would be a logical step in furthering this research.
- (d) To improve flow visualization, the plexiglas walls of the test cavity should be replaced with optical glass. The superior quality should greatly improve schlieren photography and high speed film of the cavity flow dynamics. Also, increasing the width of the lasing cavity from its present value would provide greater bending of the light as a result of the density gradient and consequently improve the flow features captured by the cameras.

Appendix A: Pressure Transducer Calibration Curves

The calibration curves of the nineteen pressure transducers used in this investigation are presented in the following figures:

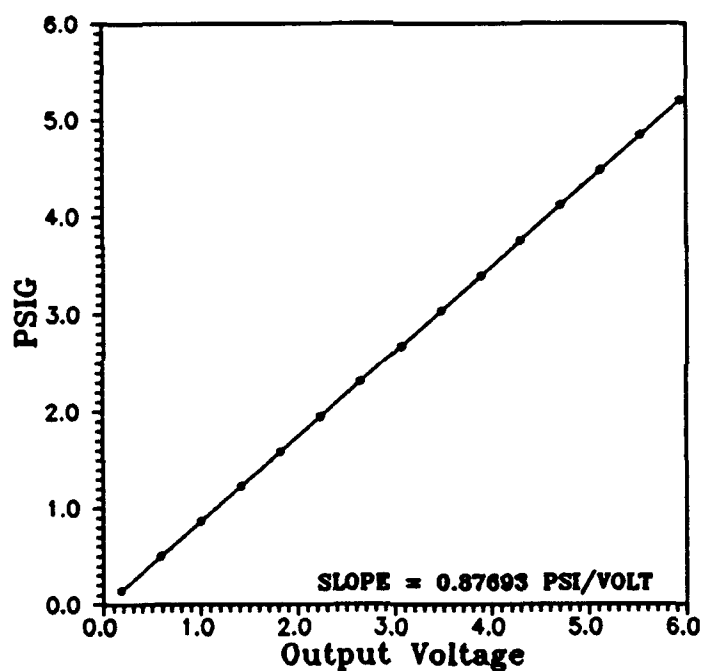


Figure A.1 Calibration Curve for Pressure Transducer Serial Number PP81

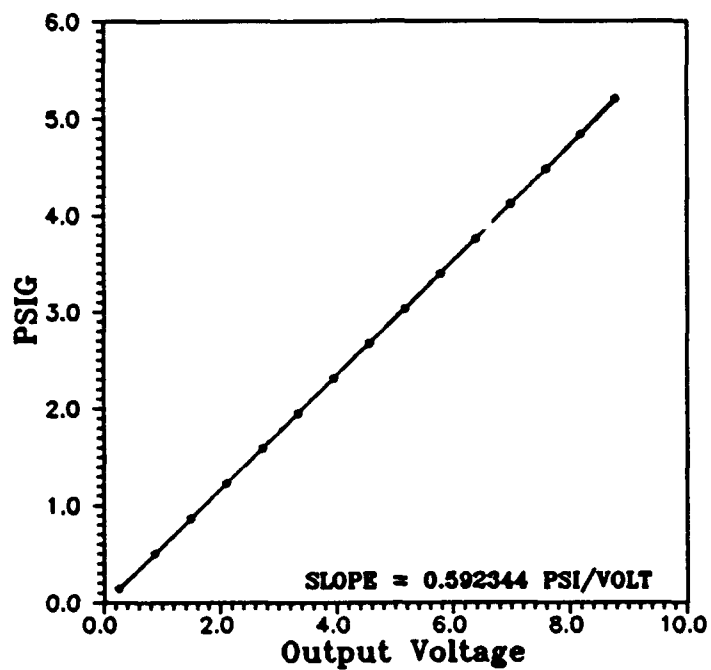


Figure A.2 Calibration Curve for Pressure Transducer Serial Number 78HB

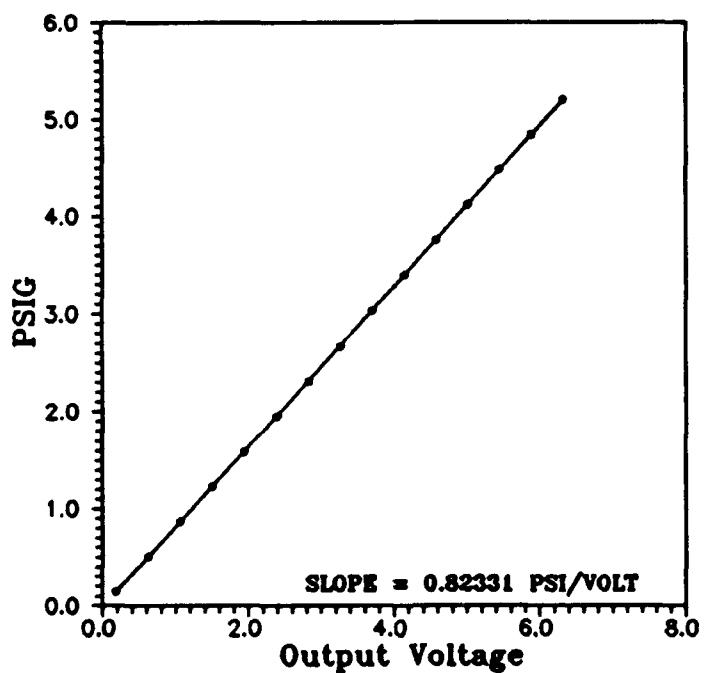


Figure A.3 Calibration Curve for Pressure Transducer Serial Number 79HB

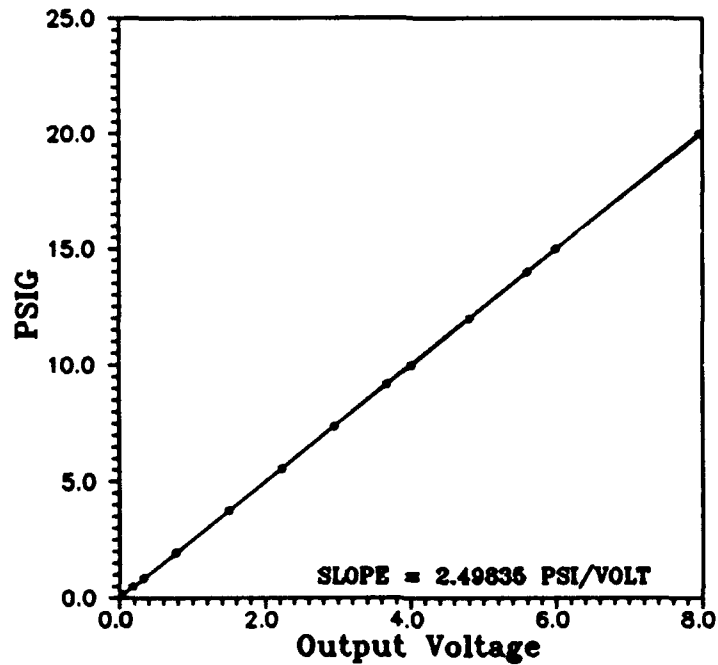


Figure A.4 Calibration Curve for Pressure Transducer Serial Number 89TA

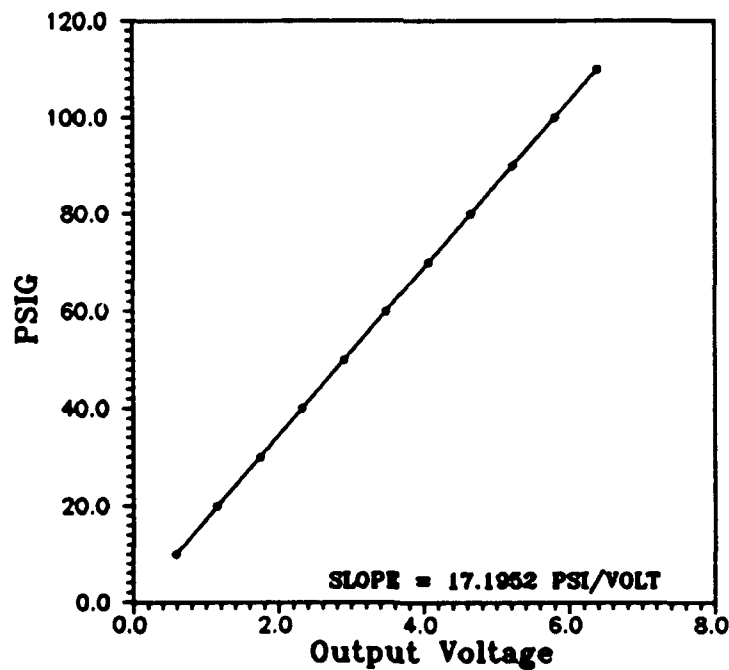


Figure A.5 Calibration Curve for Pressure Transducer Serial Number 23LG

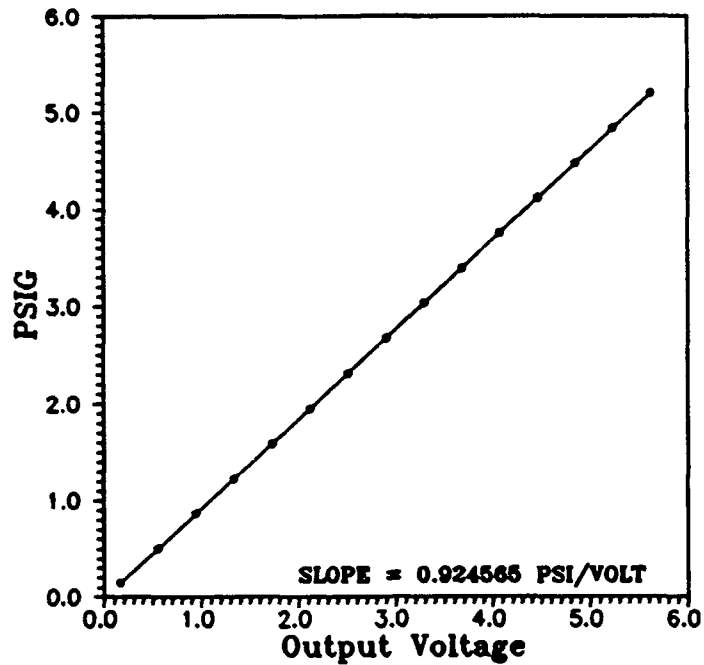


Figure A.6 Calibration Curve for Pressure Transducer Serial Number 74BF

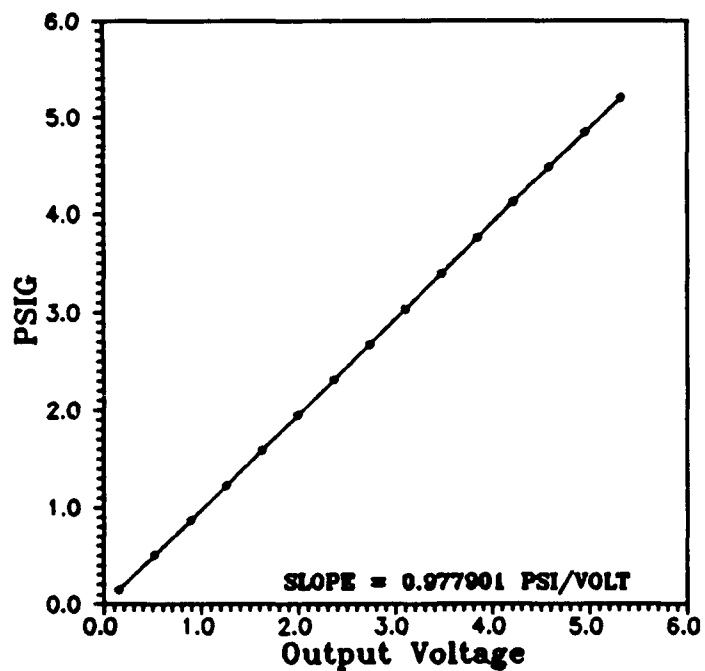


Figure A.7 Calibration Curve for Pressure Transducer Serial Number PP67

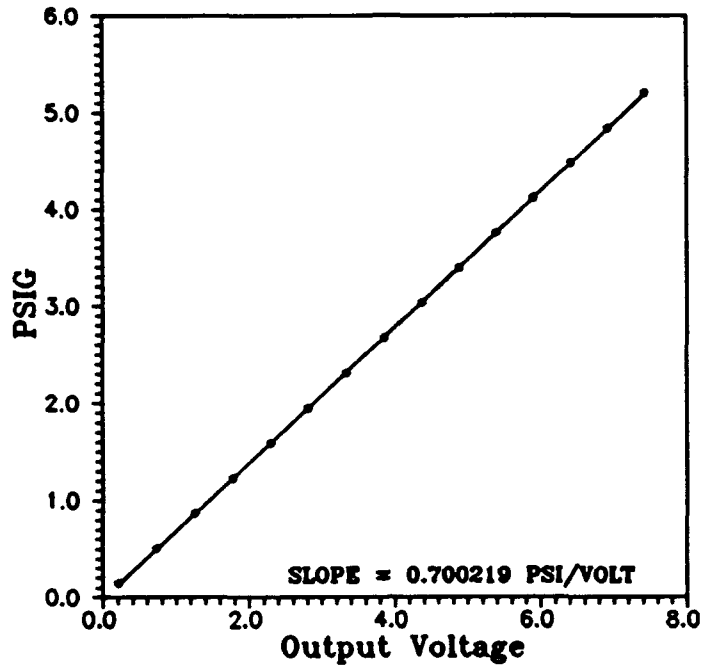


Figure A.8 Calibration Curve for Pressure Transducer Serial Number 83BF

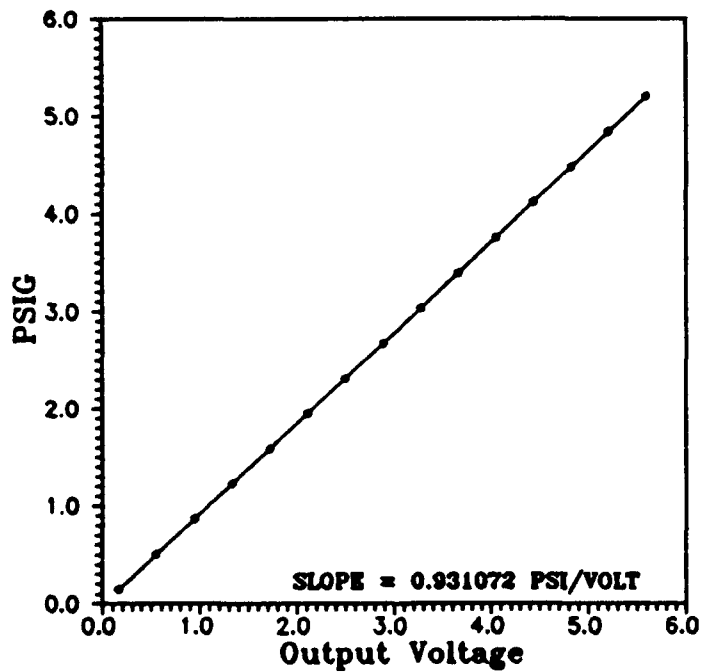


Figure A.9 Calibration Curve for Pressure Transducer Serial Number HE99

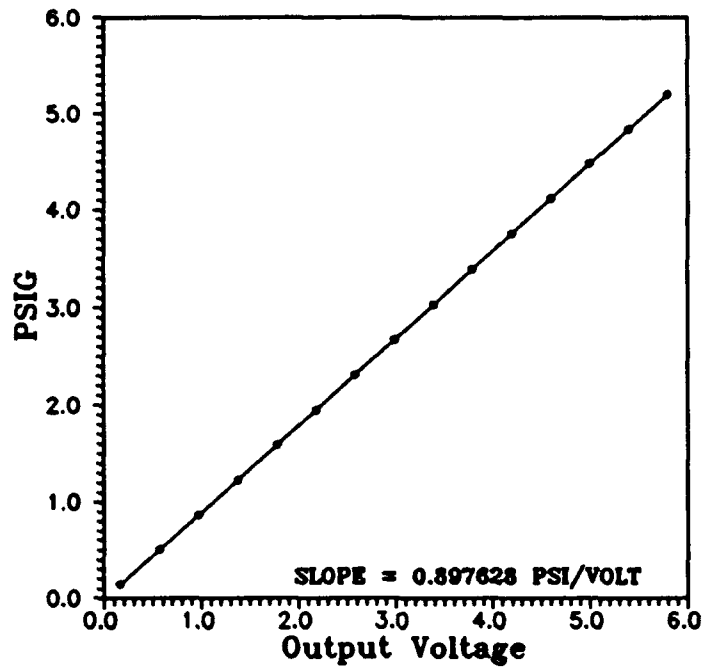


Figure A.10 Calibration Curve for Pressure Transducer Serial Number 75BF

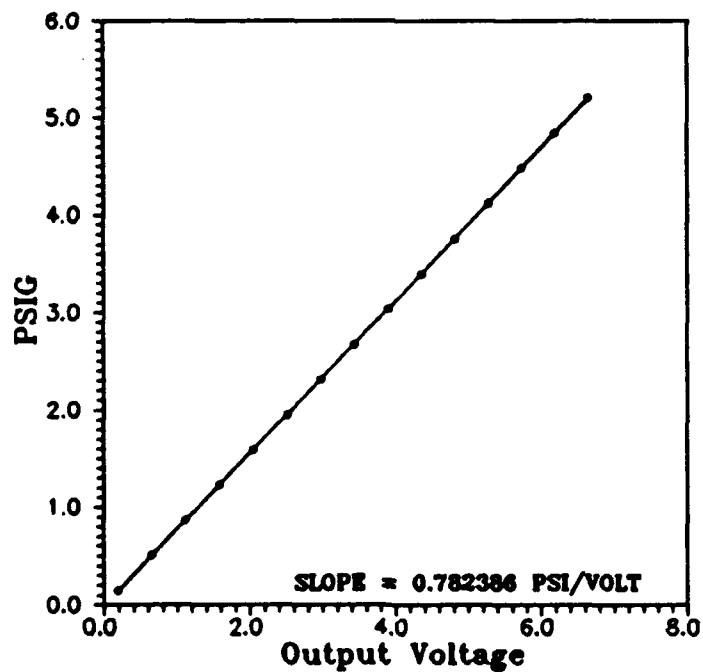


Figure A.11 Calibration Curve for Pressure Transducer Serial Number 92BF

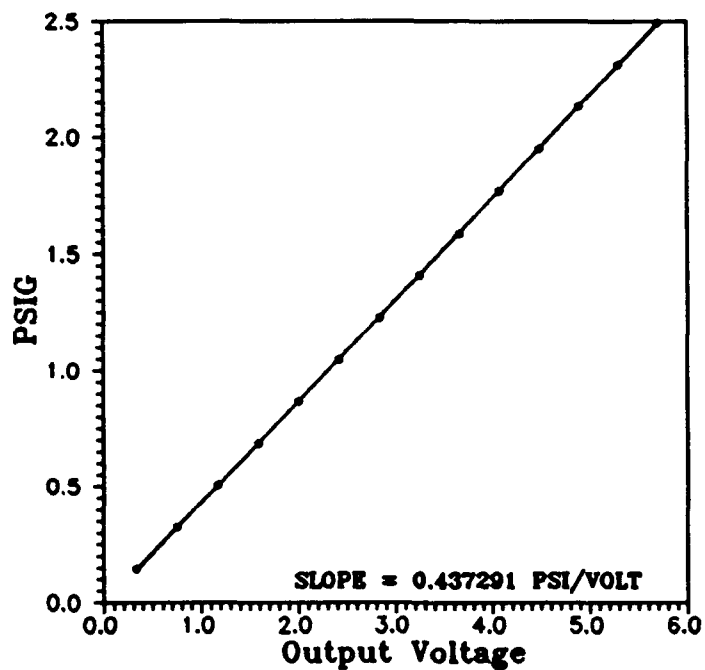


Figure A.12 Calibration Curve for Pressure Transducer Serial Number KL52

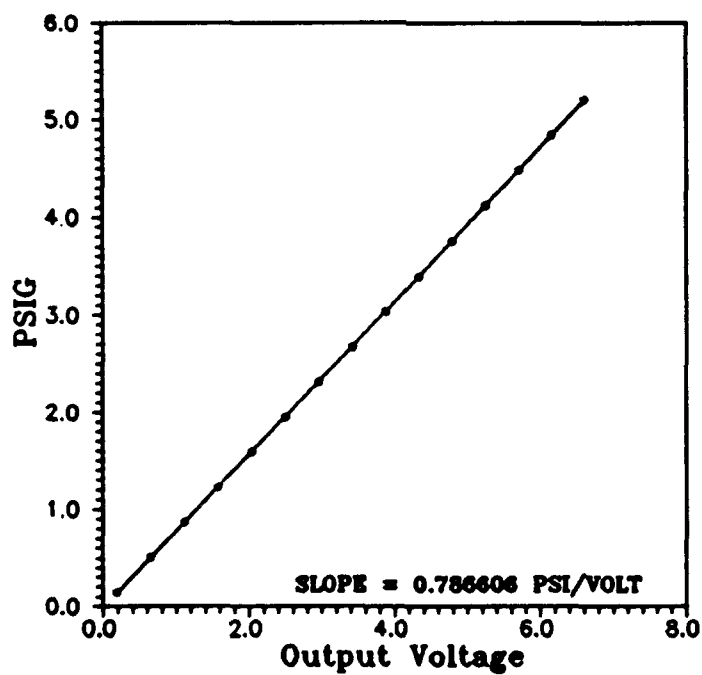


Figure A.13 Calibration Curve for Pressure Transducer Serial Number 97BF

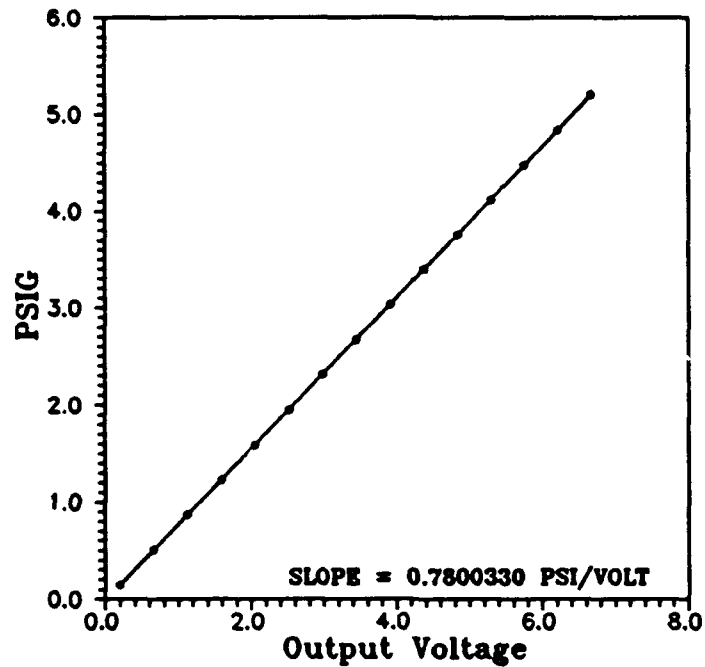


Figure A.14 Calibration Curve for Pressure Transducer Serial Number 79BF

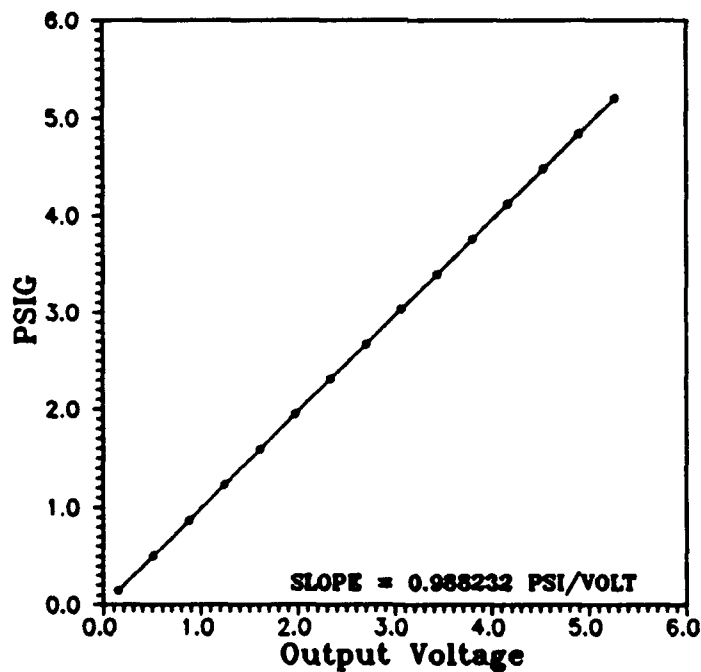


Figure A.15 Calibration Curve for Pressure Transducer Serial Number MO38

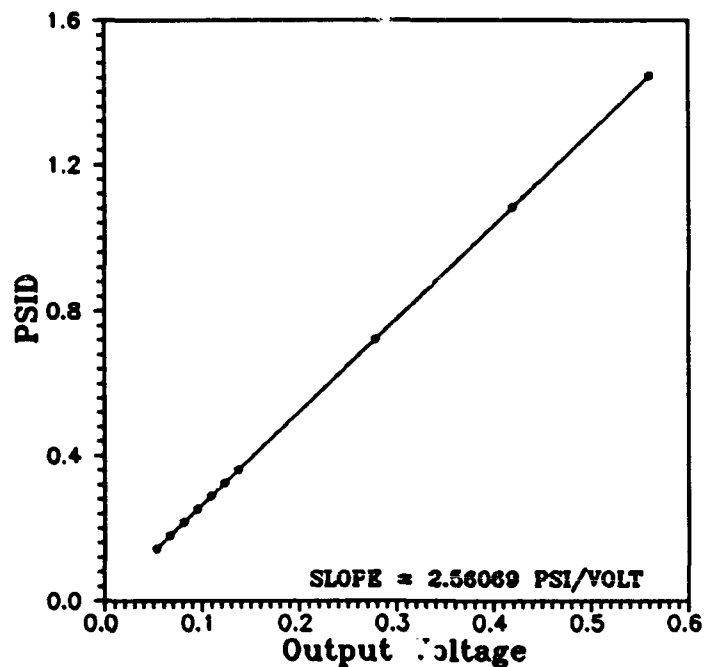


Figure A.16 Calibration Curve for Pressure Transducer Serial Number TCPT69

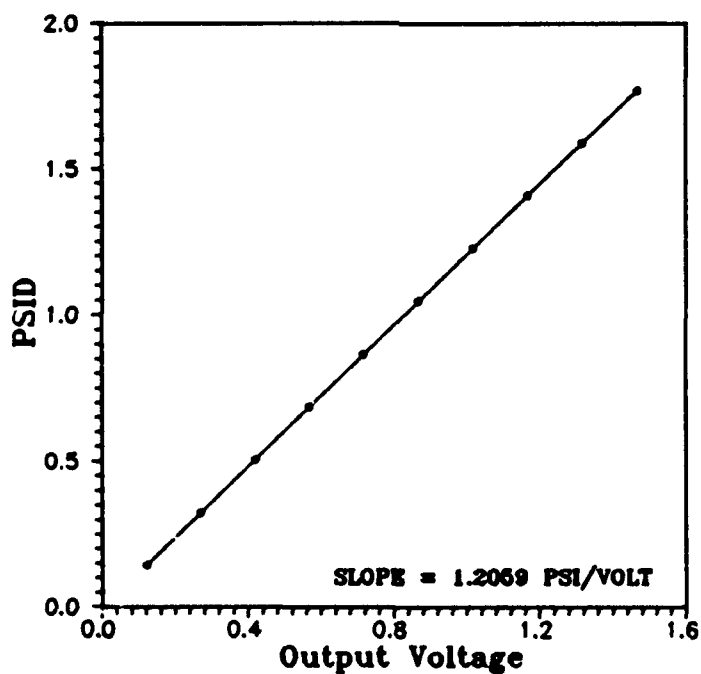


Figure A.17 Calibration Curve for Pressure Transducer Serial Number 1472

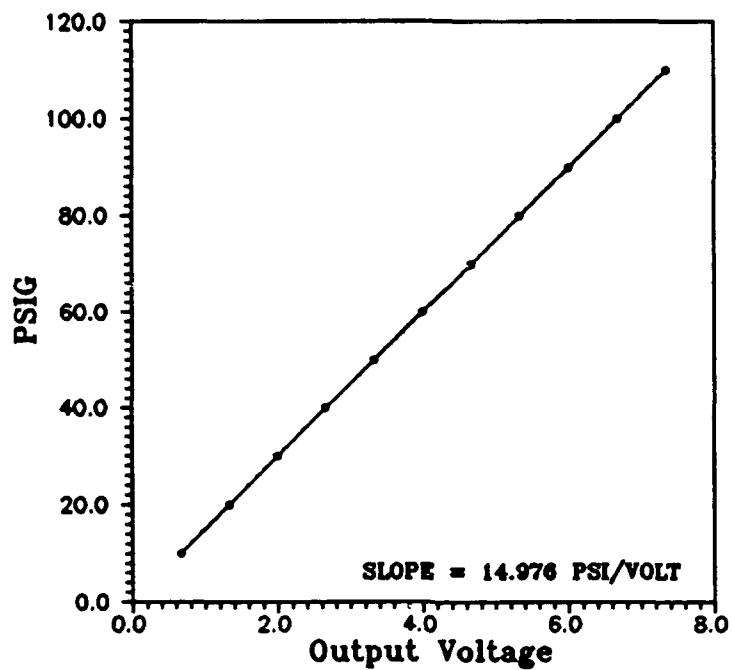


Figure A.18 Calibration Curve for Pressure Transducer Serial Number 63DL

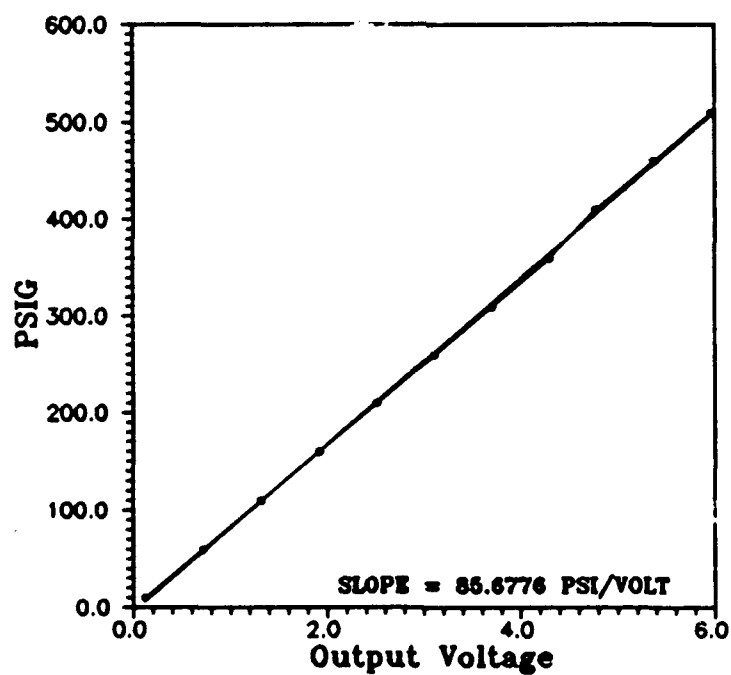


Figure A.19 Calibration Curve for Pressure Transducer Serial Number 43YB

Appendix B: Data Acquisition Software

The two major programs which control pre-run acquisition and post-run reduction of data were written in Microsoft GW-BASIC.

PRERUN.BAS

```
10 REM Program PRERUN.BAS
20 REM
30 REM Written by: Curt D. Botts
40 REM This program queries the user for pre-run information necessary for
50 REM post data acquisition calculations. This program should be run and
60 REM information provided as close as possible to actual data acquisition.
70 REM Each time this program is run a COUNTER file is accessed and the run
80 REM number is incremented. An output file containing the following inputs
90 REM is created with a "PRE(run number).DAT" filename format. This output
100 REM file will be accessed during the POSTRUN data reduction.
110 REM
120 REM 1) The Helium Line Temperature - this value is the degrees
130 REM Fahrenheit displayed on the right hand Microstar F
140 REM digital display. The line should be pressurized
150 REM with helium prior to recording.
160 REM
170 REM 2) The Air Line Temperature - similarly, this value is read
180 REM off the left hand Microstar F digital display. The
190 REM air line is always pressurized with 100 psia air at
200 REM the thermocouple location.
210 REM
220 REM 3) Atmospheric pressure - this value, used for transducer
230 REM pressure calculations on any transducer which is not
240 REM referenced to vacuum, can be read off any RELIABLE
250 REM source (i.e. the MKS PVS-2 Portable Vacuum Standard,
260 REM or the Room 148 wall barometer if it has been calibrated).
270 REM
280 REM 4) The Vacuum Reference Pressure - this is the vacuum reference
290 REM pressure applied to the reference port of transducers placed
300 REM in the test section area. It is read off the 20 mm Hg range
310 REM vacuum gauge which reflects vacuum pressure at the tips
320 REM of the vacuum reference tubing (not the vacuum pump).
330 REM
340 REM 5) Helium Line 2nd Dome Pressure - this is the pressure setting in
350 REM psig for the particular run of the 2nd Grove dome regulator
360 REM gauge located on the helium farm.
370 REM
380 REM 6) Diffuser Throat Diameter - this is the measurement in inches
390 REM of the supersonic diffuser throat diameter.
400 REM
410 SCREEN 9: COLOR 10,1:CLS 0:PRINT:PRINT
420 PRINT SPC(28) "PRE-RUN INPUTS PROGRAM"
430 PRINT SPC(27) "-----":PRINT:PRINT:PRINT
440 COLOR 7,1,4
460 COUNTER$ = "D:\CB\DATAFILES\COUNTER.DAT"
470 OPEN COUNTER$ FOR INPUT AS #1
480 INPUT#1,COUNTX
490 CLOSE #1
500 COUNTX = COUNTX+1
```

```

510 OPEN COUNT$ FOR OUTPUT AS #1
520 WRITE#1,COUNT$
530 RUNNUM% = COUNT$
540 CLOSE #1
550 PRINT SPC(15) "PLEASE ENTER THE FOLLOWING PRE-RUN #";RUNNUM%;" INPUTS:"
560 PRINT
570 RUNNUM$=STR$(RUNNUM%)
580 N = LEN(RUNNUM$)
590 INPUT "          Helium Line Temperature in degrees F: ",HETEMP!
600 HETEMP!=HETEMP!+459.67 'Convert to degrees R
610 INPUT "          Air Line Temperature in degrees F: ",AIRTEMP!
620 AIRTEMP!=AIRTEMP!+459.67 'Convert to degrees R
630 INPUT "          Atmospheric Pressure in inches of Hg: ",PATM!
640 PATM!=PATM!*.49124 'Convert to psia
650 INPUT "          Vacuum Reference Pressure in mm Hg: ",PREF!
660 PREF!=PREF!*.01933 'Convert to psia
670 INPUT "          Helium Line 2nd Dome Pressure in psig: ",DOME2PRESS!
680 INPUT "          Diffuser Throat Diameter in inches: ",DIFFDIA!
690 PRERUNS = "D:\CB\DATAFILS\PRE" + RIGHT$(RUNNUM$,N-1) + ".DAT"
700 OPEN PRERUNS FOR OUTPUT AS #1
710 WRITE #1,HETEMP!,AIRTEMP!,PATM!,DOME2PRESS!,DIFFDIA!
720 CLOSE #1
730 COLOR 10,1:CLS 0:PRINT:PRINT:PRINT:PRINT:PRINT:PRINT:PRINT:PRINT:
740 INPUT" PRESS [ENTER] TO EXIT. THEN BEGIN NICOLET 500 DATA ACQUISITION PROGRAM",DUMMYS
750 COLOR 7,1:CLS 0
760 SYSTEM
770 END

```

POSTRUN.BAS

```

10 ' PROGRAM POSTRUN.BAS
20 '
30 ' Written by: Curt D. Botts
40 ' This program reduces waveform data saved in Nicolet .WFT files. Two output
50 ' files are created for each channel for each run. A "(run number)00(channel number).DAT"
60 ' file is compatible with the GRAPHER program for creating pressure versus time graphs. A
70 ' "(run number)OUT.DAT" file contains information on a single run including numerical output
80 ' of pressures, mass flows, gamma value, and exit Mach number at time intervals during a run.
90 '
100 OPTION BASE 1
110 DIM SLOPE1(20),PRESS1(20,101),MDOTAIR1(101),MDOTHELI(101),GAMMA1(101),HOLD1(20),MACHE1(101)
120 ON ERROR GOTO 140
130 GOTO 240
140 A=ERR:B=ERL
150 SCREEN 0:COLOR 28,1:CLS 0:PRINT:PRINT:PRINT
160 PRINT SPC(19) "ERROR NUMBER ";A;"OCCURRED AT LINE";B
170 COLOR 7,1
180 PLAY "O3":PLAY"L4":PLAY "C":PLAY"L6":PLAY "C":PLAY"L8":PLAY "C":PLAY"L4":PLAY "C"
190 PLAY"L4":PLAY"E-":PLAY"L6":PLAY"D":PLAY"C":PLAY"C":PLAY"L4":PLAY"O2"
200 PLAY"B":PLAY"O3":PLAY"L1":PLAY"C"
210 GOTO 2250
220 '
230 REM Input transducer calibration slopes.
240 DATA 0.87693,0.592344,0.82331,2.49835,17.1952,0.924565,0.977901,0.700219
250 DATA 0.931072,0.897628,0.782386,0.437291,0.786606,0.7800330,0.988232,2.56069

```



```

910      CLOSE #1
920 '
930 REM Retrieve zero voltage values from ZERO01A.WFT through ZERO05D.WFT
940 REM data files by first converting them to .FLT files via the WFT2FLT.EXE
950 REM program. This program reads the .WFT binary data and creates a
960 REM 2 column (volts,time) .FLT file. The average over all data points
970 REM per channel becomes that channel's zero voltage.
980     ZEROS="D:\CB\DATAFILES\ZERO0"+RIGHT$(CHANNEL$,2)
990     SHELL "D:\CB\DATAFILES\WFT2FLT "+ZEROS+".WFT">JUNKOUT"
1000     OPEN ZEROS+".FLT" FOR INPUT AS #1
1010 REM This finds the first data point.
1020     FOR JX=1 TO 20
1030         INPUT #1,CHECK1
1040         IF CHECK1<>.06 THEN HOLD1(JX)=CHECK1
1050         IF CHECK1=.06 GOTO 1090
1060     NEXT JX
1070     PRINT "                ERROR IN READING DATA FILE ";ZEROS;".FLT"
1080     GOTO 180
1090     VOLTSUM1=HOLD1(JX-1)+HOLD1(JX-3)
1100     FOR JX=1 TO 998
1110         INPUT #1,VOLT1,SECS1
1120         VOLTSUM1=VOLTSUM1+VOLT1
1130     NEXT JX
1140     ZEROVOLT1=VOLTSUM1/10001
1150     CLOSE#1
1160 '
1170 REM Convert .WFT file to .FLT file via the Nicolet WFT2FLT.EXE program.
1180 REM This reads the .WFT binary data and creates a 2 column (volts,secs)
1190 REM .FLT file.
1200     SHELL "D:\CB\DATAFILES\WFT2FLT "+DATAFILES$+">JUNKOUT"
1210     DATAFILES$="D:\CB\DATAFILES\"+RUNNUM$+"00"+RIGHT$(CHANNEL$,2)
1220 REM To save disk space write over old .FLT file.
1230     NAME DATAFILES$+".FLT" AS "D:\CB\DATAFILES\FLTHOLD.DAT"
1240     OPEN "D:\CB\DATAFILES\FLTHOLD.DAT" FOR INPUT AS #1
1250 REM Open .DAT file to store pressure vs. time data which is accessible
1260 REM from GRAPHER.
1270     OPEN DATAFILES$+".DAT" FOR APPEND AS #2
1280 REM This finds the first data point.
1290     FOR JX=1 TO 10
1300         INPUT #1,CHECK1
1310         IF CHECK1<>.001 THEN LAST1=CHECK1
1320         IF CHECK1=.001 GOTO 1380
1330     NEXT JX
1340     PRINT "                ERROR IN READING DATA FILE ";DATAFILES$;".DAT"
1350     GOTO 2250
1360 '
1370 REM Calculate the pressure at each 10th time point and store in array PRESS(channel,time).
1380     NX=0:CX=1:MX=0
1390     FOR JX=1 TO 1000
1400         NX=NX+1
1410         IF JX=1 THEN VOLT1=LAST1:SECS1=CHECK1:GOTO 1450
1420         INPUT #1,VOLT1,SECS1
1430         IF JX=1000 GOTO 1450
1440         IF NX<>10 GOTO 1540
1450         MX=MX+1
1460         DELVOLT1=ABS(VOLT1-ZEROVOLT1)
1470         PRESS1(IX,MX)=DELVOLT1*SLOPE1(IX)+PREF1
1480 REM Except those referenced to atmosphere and differentials without reference.
1490         IF (KX=4) AND (LX=68) THEN PRESS1(IX,MX)=DELVOLT1*SLOPE1(IX)
1500         IF (KX=5) AND (LX=65) THEN PRESS1(IX,MX)=DELVOLT1*SLOPE1(IX)
1510         IF (KX=5) AND (LX=66) THEN PRESS1(IX,MX)=PRESS1(IX,MX)+PATM1
1520         NX=0
1530         WRITE#2,SECS1,PRESS1(IX,MX)
1540     NEXT JX
1550     CLOSE #1:CLOSE #2:SHELL "DEL D:\CB\DATAFILES\FLTHOLD.DAT"
1560     COLOR 2,1:PRINT"    COMPLETED":COLOR 7,1
1570     NEXT LX

```

```

1580 NEXT KX
1590 '
1600 GOSUB 2260 'Calculate the air mass flow rate.
1610 GOSUB 2420 'Calculate the helium mass flow rate.
1620 '
1630 REM Calculate the mixture gamma value and the nozzle exit Mach number.
1640 REM Write to GRAPHER compatible files.
1650 OPEN "d:\cb\datafiles\"+RUNNUMS+"gamma.dat" FOR APPEND AS #1
1660 OPEN "d:\cb\datafiles\"+RUNNUMS+"mache.dat" FOR APPEND AS #2
1670 FOR CX=1 TO 100
1680
GAMMA1(CX)=(MDOTAIR1(CX)*CPAIR1+MDOTHELI(CX)*CPHELI1)/(MDOTAIR1(CX)*CVAIR1+MDOTHELI(CX)*CVHELI1)
1690 MACHE1(CX)=SQRT(21/(GAMMA1(CX)-1))*(((PRESS1(5,CX)/PRESS1(15,CX))^(11-11/GAMMA1(CX)))-1))
1700 PRINT#1,GAMMA1(CX),CSNG(CX-1)/101
1710 PRINT#2,MACHE1(CX),CSNG(CX-1)/101
1720 NEXT CX
1730 CLOSE#1:CLOSE#2
1740 '
1750 REM Create output data file for this run.
1760 OPEN "A",#1,"D:\CB\DATAFILES\"+RUNNUMS+"OUT.DAT"
1770 PRINT#1,SPC(28) "RUN NUMBER ";RUNNUMS;" DATA":PRINT#1,"":PRINT#1,""
1780 PRINT#1," Date: ";
1790 IF MONTH<10 THEN PRINT#1,USING "0#/" ;MONTH;:GOTO 1810
1800 PRINT#1,USING "##/" ;MONTH;:GOTO 1810
1810 IF DAY<10 THEN PRINT#1,USING "0#/" ;DAY;:GOTO 1830
1820 PRINT#1,USING "##/" ;DAY;
1830 PRINT#1,USING "##" ;YEAR
1840 HOURS=SECONDS/3600000:IHOURS=INT(HOURS)
1850 MINUTES=(HOURS-IHOURS)*60:IMINUTES=INT(MINUTES)
1860 SECONDS=(MINUTES-IMINUTES)*60
1870 PRINT#1," Time: ";
1880 IF IHOURS<10 THEN PRINT#1,USING "0#:" ;IHOURS;:GOTO 1900
1890 PRINT#1,USING "##:" ;IHOURS;
1900 IF IMINUTES<10 THEN PRINT#1,USING "0#:" ;IMINUTES;:GOTO 1920
1910 PRINT#1,USING "##:" ;IMINUTES;
1920 IF SECONDS<10 THEN PRINT#1,USING "0#." ;SECONDS;:GOTO 1940
1930 PRINT#1,USING "##." ;SECONDS
1940 PRINT#1,USING " Atmospheric pressure: ##.## psia";PATM1
1950 PRINT#1,USING " Reference vacuum pressure: ##.## psia";PREF1
1960 PRINT#1,USING " Helium temperature: ##.## deg F";HETEMP1-459.67
1970 PRINT#1,USING " Air temperature: ##.## deg F";AIRTEMP1-459.67
1980 PRINT#1,USING " Helium 2nd dome pressure: ##.## psig";DOME2PRESS1
1990 PRINT#1,USING " Diffuser throat diameter: ##.### inch";DIFFDIA1
2000 PRINT#1,""
2010 FOR JX=1 TO 100
2020 PRINT#1,"
2030 PRINT#1,USING" Time=##.## sec";CSNG(JX-1)/101:PRINT#1,""
2040 PRINT#1," psia at position#:"
2050 PRINT#1," -----"
2060 PRINT#1,USING" 1) ###.### 12) ###.### ";PRESS1(1,JX),PRESS1(9,JX)
2070 PRINT#1,USING" 2) ###.### 13) ###.### ";PRESS1(2,JX),PRESS1(10,JX)
2080 PRINT#1,USING" 3) ###.### 14) ###.### Air mass flow rate=##.###
lbm/s";PRESS1(3,JX),PRESS1(11,JX),MDOTAIR1(JX)
2090 PRINT#1,USING" 5) ###.### 15) ###.### Helium mass flow rate=##.###
lbm/s";PRESS1(4,JX),PRESS1(12,JX),MDOTHELI1(JX)
2100 PRINT#1,USING" 6) ###.### 16) ###.### Mixture
gamma=##.###";PRESS1(5,JX),PRESS1(13,JX),GAMMA1(JX)
2110 PRINT#1,USING" 9) ###.### 17) ###.### ";PRESS1(6,JX),PRESS1(14,JX)
2120 PRINT#1,USING" 10) ###.### 18) ###.### Nozzle exit
Mach=##.###";PRESS1(7,JX),PRESS1(15,JX),MACHE1(JX)
2130 PRINT#1,USING" 11) ###.### 31) ###.### ";PRESS1(8,JX),PRESS1(18,JX)
2140 NEXT JX
2150 CLOSE #1
2160 PLAY"MB":PLAY"L4":PLAY"O3":PLAY"C":PLAY"D":PLAY"C":PLAY"D":PLAY"C":PLAY"D"
2170 IF CHOICE%1 GOTO 2190 ELSE NEXT RUNNUMX
2180 GOTO 2230
2190 INPUT" WOULD YOU LIKE TO REDUCE ANOTHER RUN";ANSWERS

```

```

2200 IF ANSWER$="YES" OR ANSWER$="yes" OR ANSWER$="Y" OR ANSWER$="y" GOTO 460
2210 IF ANSWER$="NO" OR ANSWER$="no" OR ANSWER$="N" OR ANSWER$="n" GOTO 2230
2220 PRINT"
2230 COLOR 7,1
2240 SYSTEM
2250 END

```

```

2260 REM Mass flow rate calculation through air orifice meter.
2270 R1=1717.59 'air gas constant (sq.ft/sq.sec-deg R)
2280 K1=1.4 'air ratio of specific heats
2290 BETA1=.2666667 'ratio of orifice to pipe diameters
2300 FOR MX=1 TO 100
2310 IF PRESS1(17,MX)<>0! GOTO 2330
2320 PRINT:PRINT SPC(18) "BAD RUN! FLOW DID NOT OCCUR AT TRIGGER!":RETURN
2330 RATIO1=(PRESS1(18,MX)-PRESS1(17,MX))/PRESS1(18,MX)
2340 IF RATIO1=1! THEN MDOTAIR1(MX)=0! GOTO 2400
2350 PART11=RATIO1^(21/K1)*K1/(K1-11)*(11-(RATIO1^((K1-11)/K1)))/(11-RATIO1)
2360 PART21=PART11*(11-BETA1^41)/(11-BETA1^41*RATIO1^(21/K1))
2370 Y1=SQR(PART21)
2380 PART11=SQR(PRESS1(18,MX)/(R1*AIRTEMP1)*PRESS1(17,MX))
2390 MDOTAIR1(MX)=13.760371#*Y1*PART11
2400 NEXT MX
2410 RETURN

```

```

2420 REM Mass flow calculation through Helium venturi meter.
2430 R#12427.9291# 'helium gas constant (sq.ft/sq.sec-deg R)
2440 K1=1.666667 'helium ratio of specific heats
2450 BETA1=.59809 'ratio of throat to pipe diameters
2460 FOR MX=1 TO 100
2470 IF PRESS1(16,MX)<>0! GOTO 2430
2480 PRINT:PRINT SPC(18) "BAD RUN! FLOW DID NOT OCCUR AT TRIGGER!":RETURN
2490 RATIO1=(PRESS1(19,MX)-PRESS1(16,MX))/PRESS1(19,MX)
2500 IF RATIO1=1! THEN MDOTHEL1(MX)=0! GOTO 2570
2510 IF DOME2PRESS1=0! THEN MDOTHEL1(MX)=0! GOTO 2570
2520 PART11=RATIO1^(21/K1)*K1/(K1-11)*(11-(RATIO1^((K1-11)/K1)))/(11-RATIO1)
2530 PART21=PART11*(11-BETA1^41)/(11-BETA1^41*RATIO1^(21/K1))
2540 Y1=SQR(PART21)
2550 PART11=SQR((PRESS1(19,MX)/(R1*HETEMP1))*PRESS1(16,MX))
2560 MDOTHEL1(MX)=9.5272834#*Y1*PART11
2570 NEXT MX
2580 RETURN

```

Bibliography

1. "Alpha Laser Completes Second of Four Ground Tests," Aviation Week & Space Technology, 128: 23 (January 11, 1988).
2. Patterson, Kerry E., Jad Batteh and S. Howie. "Simple Model for Base Pressure Effects in Source Flow Chemical Lasers," AIAA Aerospace Sciences Meeting. Paper No. 82-0400. Orlando, Florida: American Institute of Aeronautics and Astronautics, January 1982.
3. Lankford, D. W. and Rapaganani, N. L. "Modeling of Cavity Flows with Large Base Relief," International Symposium on Gas-Flow and Chemical Lasers. 343-347. Washington: Hemisphere Publications, 1979.
4. Stiglich, Capt Stephen W. Experimental Investigation of A Chemical Laser Cavity Flowfield. MS thesis, AFIT/GAE/ENY/89D-36. School of Engineering, Air Force Institute of Technology (AU), Wright-Patterson AFB OH, December 1989.
5. Wark, Kenneth. Thermodynamics. New York: McGraw-Hill Book Company, 1977.
6. Ames Research Committee. Fluid Meters, Their Theory and Application (Sixth Edition). 47-65. The American Society of Mechanical Engineers, 1971.
7. Shapiro, Ascher, H. The Dynamics and Thermodynamics of Compressible Fluid Flow. New York: John Wiley and Sons, Inc., 1953.
8. Zakanycz, Stephen. Turbulence and the Mixing of Binary Gases. PhD dissertation. Ohio State University, OH, 1971.
9. Air Force Weapons Laboratory, Air Force System Command. Contract F29601-80-C-0040 with the TRW Corporation. Drawing X430038, Sheet 2.
10. AMETEK Mansfield and Green Division. Handbook Operating and Service Instructions. Form No. 75-109 (Rev. 4). AMETEK Mansfield and Green Division, Largo, FL, June 1984.

11. Holder, D. W. and North, R. J. AGARDograph 23, Optical Methods for Examining the Flow in High-speed Wind Tunnels, Part I Schlieren Methods. North Atlantic Treaty Organization, Advisory Group for Aeronautical Research and Development, 1956.
12. Nicolet Instrument Corporation. System 500 Data Acquisition System Operation Manual. Part Number 269-908700, Nicolet Instrument Corporation, Madison, WI, 1989.
13. Microsoft Corporation. Microsoft Windows User's Guide. Microsoft Corporation, 1985-1990.
14. Hess, Capt George M., Jr. An Evaluation of the Performance of Two, Small, Two-Dimensional Nozzles. MS thesis, AFIT/GAM/ME/69-6. School of Engineering, Air Force Institute of Technology (AU), Wright-Patterson AFB OH, March 1969.
15. Gross, R. W. F. and Bott, J. F. Handbook of Chemical Lasers. New York: John Wiley & Sons, 1976.

Vita

Captain Curt D. Botts was born on 1 May 1957 in Oklahoma City, Oklahoma. He graduated from Benson Union High School in Benson, Arizona in 1975 and enlisted in the U.S. Navy in 1976. He married Nancy G. (Anglin) and has three children, Courtney, Eryc, and Aubrey. After four years in the Navy he began work on a Bachelor of Science degree in Aerospace Engineering at the University of Arizona in 1980. He transferred to North Carolina State University in 1981 and joined the Air Force College Senior Engineer Program (CSEP) in 1984. Following graduation, he attended Officer Training School and was commissioned in August of 1985. His first duty station was the Inertial Upper Stages (IUS) System Program Office at Space Division where he served as a Space Shuttle/IUS Launch Operations Manager for four years. Captain Botts entered the School of Engineering, Air Force Institute of Technology in May 1989.

Permanent Address: 4965 Paseo Manolet
Sierra Vista, Arizona 85636

1 December 1990 Master's Thesis

Effects of Specific Heat Ratio on a
Simulated Chemical Laser Flow

Curt D. Botts, B.S., Capt, USAF

School of Engineering AFIT/ENY
Air Force Institute of Technology (AU)
Wright-Patterson AFB, OH 45433-6583

AFIT/GAE/ENY/90D-3

Air Force Weapons Laboratory AFWL/ARDK
Kirtland AFB, NM 87117

Thesis Advisor: William C. Elrod, Professor
Department of Aeronautics and Astronautics

Unclassified/Unlimited

Mixing of primary cold flow air and secondary helium to control the ratio of specific heats for the medium flowing through a simulated chemical laser nozzle/lasing cavity was accomplished. The effects of a range of mixture specific heat ratios on flowfield behavior were examined using static pressure ports in the test cavity. Schlieren photography and high speed filming aided description of the flow dynamics. Results indicated that boundary layer effects became evident in the nozzles as specific heat ratios increased. Large pressure fluctuations were observed in the cavity when helium was introduced into the flow to raise the specific heat ratio. This unstable behavior was attributed to the helium mass flow into the mixer and the mixer design itself. Use of the air/helium mixer brought about the pressure fluctuations earlier in a test run than with the mixer removed under the same conditions. Favorable pressure conditions for lasing were achieved for at least two seconds for the supersonic nozzles' design specific heat ratio of 1.51. Adverse pressure behavior was also attributed to three dimensional viscous effects along the cavity walls.

Chemical Lasers Laser Cavities Gas Dynamics
Flow Fields

100

Unclassified

Unclassified

Unclassified